NPS ARCHIVE
1963
LEVIN, R.

Library
U. S. Naval Postgraduate School
Monterey, California

DUDLEY KNOX LIBRARY
NAVAL POSTGRADUATE SCHOOL
MONTEREY CA 93943-5101

NORTHWESTERN UNIVERSITY

KINETICS OF OXIDATION OF IRON-CHROMIUM ALLOYS AND THE TRANSPORT PROPERTIES OF THE OXIDES IN CARBON DIOXIDE-CARBON MONOXIDE MIXTURES

A DISSERTATION

SUBMITTED TO THE GRADUATE SCHOOL

IN PARTIAL FULFILLMENT OF THE REQUIREMENTS

for the degree

DOCTOR OF PHILOSOPHY

Field of Materials Science

by

ROGER LEE LEVIN

Evanston, Illinois

June 1963

NPS Archive
1963
Levin, R.

Thesis
L54

Library
U. S. Naval Postgraduate School
Monterey, California

ABSTRACT

The oxidation of iron-chromium alloys containing 0.20, 0.88, 1.70, 5.70, 7.55 and 18.21 wt.% Cr has been studied in carbon dioxide-carbon monoxide mixtures over the temperature range 800°-1100°C under conditions where wüstite is the only stable iron oxide. The experimental results, obtained from a continuous recording of the gain in weight by a semi-micro, automatic recording balance, show that all of the alloys oxidize in CO_2-CO mixtures with the same sequence of mechanisms. The first stage of the reaction is one of linear oxidation where the rate controlling process is a phase-boundary reaction at the wüstite/gas interface which is determined to be the adsorption of CO_2 below about 950°C and the dissociation of CO_2 into CO and adsorbed oxygen atoms or ions above this temperature. The second stage of the reaction is one of parabolic oxidation kinetics where diffusion of the metal ions and electrons through the scale is the rate-determining step. The oxide thickness at which the kinetics transform from linear to parabolic is dependent upon chromium content in the wüstite and upon temperature.

The effect of soluble chromium in the wüstite lattice is to cause an increase in the cation vacancy concentration which is manifested as an increase in the rate of parabolic oxidation of the Fe-Cr alloys over that of pure iron oxidized under the same conditions. The rate of oxidation of Fe-Cr alloys is shown also to be many times more rapid in CO_2-CO mixtures than in oxygen.

Lattice parameter and electrical conductivity measurements of pure and doped wüstite have been performed to confirm the effect of soluble chromium in increasing the vacancy concentration in wüstite. From the conductivity measurements, values of the enthalpy of movement of the electron holes and the enthalpy of formation of the ionic and electronic defects have been determined. It has been possible also to determine certain solubility limits of chromium in wüstite.

Finally, from reduction and oxidation experiments on pure and doped wüstite over the temperature range 900°-1100°C, the chemical diffusion coefficients of iron in wüstite have been determined from an integrated form of the solution of Fick's law. The chemical diffusion coefficients, the value of D obtained for the propagation of a concentration gradient through samples of pure wüstite and chromium-doped wüstite are compared with the self-diffusion coefficients for iron in wüstite.

TABLE OF CONTENTS

		Page
I.	INTRODUCTION	1
	A. The Defect Structure of Oxides	1
	1. Atomic Defects	2
	2. Electronic Defects	5
	3. The Effect of Oxygen Partial Pressure and of Solute Foreign Atoms on the Defect Structure of Oxides	8
	B. The Oxides Formed on Pure Iron	12
	1. The Oxidation of Iron in Oxygen-rich Atmospheres	13
	2. The Oxidation of Iron in Low Oxygen Pressures	15
	3. Studies of Diffusion in Wüstite	18
	C. The Oxidation of Iron-Chromium Alloys in Oxygen-rich Atmospheres	20
II.	EXPERIMENTAL OBJECTIVES	27
	A. The Oxidation of Iron-Chromium Alloys in Carbon Dioxide - Carbon Monoxide Mixtures	28
	1. Linear Oxidation Kinetics	29
	2. Parabolic Oxidation Kinetics	31
	3. Temperature and Pressure Dependence of Oxidation Rates	32
	4. Transition from Linear to Parabolic Oxidation Kinetics	34
	B. X-Ray Diffraction Studies of Pure and Doped Wüstite	36
	C. The Conductivity of Pure and Doped Wüstite	37
	1. Temperature and Pressure Dependence of Electrical Conductivity	37

Page

D. Reduction and Oxidation Studies of Pure and Doped Wüstite 44

III EXPERIMENTAL PROCEDURE. 45

A. The Oxidation of the Alloys 45

1. Specimen Analysis and Preparation 45

2. The Oxidation Apparatus 47

3. The CO_2-CO Gas Control System 49

4. Temperature Control 50

B. X-Ray Analysis of Pure and Doped Wüstite. 51

C. Conductivity Measurements 53

1. Specimen Preparation. 53

2. Apparatus 54

D. The Reduction and Oxidation of Pure and Doped Wüstite 56

1. Specimen Preparation. 56

2. Apparatus and Procedure 57

E. Metallographic Examinations 58

IV EXPERIMENTAL RESULTS AND DISCUSSIONS. 59

A. The Oxidation of Iron-Chromium Alloys 59

1. Oxidation of the 0.20 wt.% Cr-Fe Alloy. 62

a. Linear Kinetics 62

b. Parabolic Kinetics. 65

(1) Temperature Dependence 65

(2) Pressure Dependence. 67

2. Oxidation of the 0.88 and 1.7% Cr-Fe Alloys. . . 71

a. Linear Kinetics 71

Page

a. Parabolic Kinetics 72

3. Oxidation of the 5.70% Cr-Fe Alloy 73

4. Oxidation of the 7.55 and 18.21% Cr-Fe Alloy . . . 74

5. The Transition from Linear to Parabolic Kinetics . 75

6. Discussion and Analysis. 77

a. Linear Kinetics. 77

b. Parabolic Kinetics 81

c. The Mechanism of Oxidation of the Alloys when a Multi-layered Scale is Formed. 87

B. X-Ray Analysis of Pure and Doped Wüstite 89

C. The Electrical Conductivity of Pure and Doped Wüstite. 93

1. Pressure Dependence. 93

2. Temperature Dependence 94

3. Comparison with Linear Oxidation 98

D. Diffusion Coefficients from the Reduction and Oxidation of Wüstite 98

1. Pure Wüstite 98

2. Chromium-doped Wüstite 102

3. Discussion of the Results. 103

V DISCUSSION OF THE ERRORS 107

A. The Oxidation Studies. 107

B. X-Ray Studies. 108

C. Conductivity Studies 109

VI SUMMARY AND CONCLUSIONS. 110

Page

ACKNOWLEDGMENTS 113

BIBLIOGRAPHY. 114

TABLES OF DATA. 119

FIGURES

VITA

I. INTRODUCTION

A. The Defect Structure of Oxides

Fundamental to the understanding of the process of oxidation of metals is a complete knowledge of the oxide layer which forms, generally as a protective layer, between the reacting metal and the oxidizing atmosphere. It is clear that the rate of oxidation of a metal is dependent not only upon the effective oxidizing potential of the atmosphere but also, to a larger extent, upon the defect structure of the oxide. Unless the oxide is volatile, as in the case of the oxidation of germanium above 575°C and molybdenum above 795°C, or unless the oxide layer continuously cracks or spalls off, e.g. in the high-temperature oxidation of Zr, U and Ti, the reaction between the metal and the oxygen in the atmosphere will continue only if one, or both, of the species is able to diffuse through this protective layer. This migration of the metallic cations and/or the oxygen anions through the ionic oxide layer can occur only if deviations from the perfect lattice exist. Inasmuch as the equilibrium concentration of defects in a solid at any temperature T is determined by the minimum value of the Helmholtz free energy at this temperature, first Frenkel,[1] and shortly thereafter Schottky and Wagner,[2] showed that lattice imperfections could be thermodynamically stable in solids at temperatures above the absolute zero. In a discussion of the crystalline point defects which can exist in oxides, it is convenient to divide them into two groups: (1) atomic defects which include vacant lattice sites, interstitials, and foreign

atoms, and (2) electronic defects, the excess conduction electrons and/or holes which are responsible for the electrical conduction in semiconductors. Because of the importance of the effect of foreign atoms upon such processes as the oxidation rate, diffusion, and electrical conductivity in the semi-conducting oxides, this effect will be discussed separately. Other lattice defects such as phonons, excitons, and dislocations will be considered as secondary in this study and will not be considered further.

1. Atomic Defects--For a stoichiometric oxide a simple relationship must exist between the concentration of metal cations and the oxygen ions in the crystal. For this reason any defects which occur must occur in pairs such that the remaining metal/oxygen ratio remains fixed. The five basic types of defects in stoichiometric crystals are:

(a) Schottky-type defects which consist of concentrations of vacant sites on the M sublattice ($\equiv V_M$) and on the X sublattice ($\equiv V_X$), or Example: NaCl

(b) equal concentrations of M and X interstitials ($\equiv M_i$, X_i) Example: CaF_2

(c) Frenkel-type defects on the M sublattice which consists of equal concentrations of M interstitials and vacancies. Example: AgCl

(d) Frenkel-type defects on the X sublattice. Example: $PbCl_2$

(e) Substitutional-type defects with equal concentrations of

M ions on X sites and X ions on M sites.

Example: None known.

A pure stoichiometric crystal would fall entirely in one of the above types would exhibit purely ionic conductivity. Crystals containing a contribution from both of the above types (mixed conductors) have two or more of the types of defect listed under 1. Fortunately, for any given crystal the number of types of different defects are limited due to the differences in the energies of formation of the defects.

When the defects are so very dilute as to be considered as not interacting to any large extent, we can write an equilibrium constant, K, for the reaction of the defects to form pairs (associated or unbound) and the law of mass action to relate the concentrations of the defects. As an example, in an ionic crystal containing Schottky pairs (see Kröger [1] for a discussion of defect chemistry), it is necessary only to consider

$$0 = \sum_{(i,k)} \nu_{(i,k)} \mu_{(i,k)} \qquad (1)$$

where

$$K = \frac{\prod_{(i,k)} a_{(i,k)}^{\nu_{(i,k)}}}{\prod_{(i,k)} a_{(i,k)}^{\nu_{(i,k)}}} \qquad (2)$$

In the present work, we shall assume that the activity coefficients, $\gamma_{(i,k)} = 1$, and therefore K is used rather than K_a. The change in the number of ions on interstitial sites is neglected.

$$M_{(i-s)} \quad X_{(i-s)}$$

and

$$V_M = K''[V_M]$$

$$V_X = K''[V_X]$$

hence

$$K_D = [V_M] \cdot [V_X] \qquad (3)$$

and since the equilibrium number of defects depends exponentially upon the temperature, one may write

$$K_s = [V_M] \cdot [V_X] = k_s' \exp(-E_s/RT) \qquad (4)$$

Where K_s is the Schottky constant, k_s' is the ratio of reaction rates and E_s is the increase in energy when the crystal undergoes by the introduction of Schottky defects. Similar equations can be written for the other type of defects.

Most metal oxides exhibit non-stoichiometry and the deviation from stoichiometry is due to defect formation in that a unit volume of the crystal remains electrically neutral. Whereas the Frenkel and Schottky-type defects discussed above exist only in crystals where the formation of an electron-defect (electron or hole) would require extraordinary energies such as metal oxides or semiconductors, the stoichiometric materials. In the case of ionic crystals and solutions, the effect on the total

gap, E_g, from a filled valence band. Under these conditions the crystal is an insulator and will remain so unless an electron can be promoted into the conduction band or, alternatively, an electron can be removed from the filled band leaving behind an electron hole.

Intrinsic conductivity occurs when sufficient energy, e.g. thermal energy, is imparted to the crystal to "excite" an electron from the valence band across the energy gap into the conduction band. When these electronic defects exist in dilute concentrations, one can apply the law of mass action by treating them as chemical constituents, where

$$null = \oplus + \ominus - E_g \tag{5}$$

and

$$K = \oplus \cdot \ominus = e^{-E_g/kT} \quad (E_g \gg kT) \tag{6}$$

Extrinsic conductivity also occurs in crystals in which the valence band is separated from the conduction band by a forbidden energy gap. In an ionic crystal containing excess negative ions, the excess electron can be considered as being near the extra anions in regard upon size. These electron defects constitute filled impurity levels near energy levels which lie within the gap between the valence and conduction bands, and the distribution of electrons between these impurity levels and the conduction band is determined by quantum statistics. (Figure 1A) where

$$[B] = K_2 \exp(-E_2/kT) \qquad (7)$$

Similarly, for a hypothetical nickel-deficient oxide containing cation interstitials or cation vacancies, two cations must be oxidized to the next higher valence for every extra oxygen ion or vacancy incorporated into the lattice. These centers of higher valency constitute empty impurity levels, or trapped positive holes, within the energy gap, (Figure 1) and again the concentration of mobile positive holes in the second valence band or the ground is represented by a Boltzmann-type distribution where

$$\oplus = K_2 \exp(-E_2/kT) \qquad (8)$$

Figure 1. Hypothetical electronic energy band schematic for (A) undoped or cation-deficient oxide existing as (B) cation excess, and (C) cation rich.

change in the magnitude of electronic conductivity.

The creation of defects in wüstite, a p-type semiconductor which is always metal deficient with cation vacancies, can be described by

$$2Fe^{++} + 1/2\,O_2 = 2Fe^{+++} + V_{Fe} + O^{=} \qquad (9)$$

or

$$Fe + 1/2\,O_2 = Fe_{Fe} + V_{Fe}^{=} + 2\,\oplus \qquad (10)$$

Equation (9) is written in the chemical notation which shows that by increasing the oxygen pressure one would increase the oxygen/iron ratio by creating more iron ion vacancies, and the charge balance would be maintained by the two additional trivalent iron ions for every vacancy. This extra charge may migrate from one cation to another. Equation (10) is the same reaction written in the physical sense where the creation of vacancy is assumed to acquire an effective double negative charge relative to a neutral lattice, and two quasi-free electron holes are created. Regardless of the way written, both reactions will contribute to an increase in the cation diffusion coefficient and the electronic conductivity.

Seyb,[7] by analyzing the data of Darken and Gurry,[8] had shown that the law of mass action is valid for the formation of wüstite, thus the equilibrium constant can be written for reaction (10) at any given temperature as

$$K = \frac{[V_{Fe}^{=}]\cdot[\oplus]^2}{P_{O_2}^{1/2}} \qquad (11)$$

Since two quasi-free electron holes are created for every cation vacancy, and since the intrinsic hole concentration is considered to be small, when the holes and vacancies are dissociated, we can write

$$[\oplus] = 2[V''_{Fe}] \tag{12}$$

Substituting (12) into (11) we obtain for the concentration of holes

$$[\oplus] = (2K)^{1/3} P_{O_2}^{1/6} \tag{13}$$

and for the concentration of vacancies

$$[V''_{Fe}] = \left(\frac{K}{2}\right)^{1/3} P_{O_2}^{1/6} \tag{14}$$

Thus, at any specific temperature, an increase in the equilibrium partial pressure of oxygen over wüstite will increase the oxygen content (x) and the hole and vacancy concentrations in both the oxygen and cation sublattices.

The relationship can be combined with the well-established parabolic rate law for oxidation of iron, $x^2 = k_p t$, to yield the hole concentration as a function of oxygen pressure and time. This procedure has been carried out by Hauffe and Pfeiffer[12] who have confirmed the one-sixth dependence. Similar increases in the oxidation rate of iron at increasing oxygen pressures have been observed by Pettit and Wagner[11] where the rate of diffusion of iron cations through wüstite layer was the rate-determining step.

In addition to the effect of the oxygen partial pressure in the defect structure of an oxide, impurity atoms, particularly those of a different valence, affect the concentration of defects and, hence, the rate of diffusion, solid-state oxidation reactions, and the conductivity. If, for example, a small amount of chromium is dissolved into the wüstite lattice according to the defect equation

$$3Fe + Cr_2O_3 \rightarrow 2Cr^{+}_{(Fe)} + 3FeO + V^{=}_{Fe} \qquad (15)$$

where $Cr^{+}_{(Fe)}$ is a mole of chromium ions on a divalent iron site, one would expect that the increase in V_{Fe} would result in an increase in the rate of oxidation of the doped-iron. Similarly, any monovalent ion incorporated into the wüstite lattice would cause a decrease in the vacancy concentration and, hence, a reduction in the rate of oxidation. Experiments have demonstrated, in accord with expectation, a marked effect of monovalent and trivalent additives on the oxidation rate of zinc[12] and nickel.[13]

If in equation (14) we substitute for the equilibrium constant, K, its temperature and oxygen pressure,

$$\sigma = [V_{Fe}] \cdot \Theta \qquad (16)$$

then, any change which would affect the vacancy concentration should cause a corresponding change in electronic conductivity. This change has been observed for lithium[14] and chromium[15] doped nickel oxide.

B. The Oxides Formed on Pure Iron

Excellent examples of nonstoichiometric oxides are provided in the iron-oxygen binary system shown in Figure 2. Iron has two valence states, the divalent and trivalent, and forms three oxides, FeO (Wüstite), Fe_3O_4 (magnetite) and Fe_2O_3 (hematite).

The compound Fe_2O_3 has very narrow composition limits and normally it does not exist exactly at the stoichiometric ratio, but contains an excess of iron probably corresponding to oxygen ion vacancies. Diffusion studies have indicated that the mechanism of material transport across this oxide during the oxidation of iron is accomplished by the diffusion of oxygen.[7] Hematite exists in two forms: α-Fe_2O_3 which has the corrundum structure, the symmetry being rhombohedral, and γ-Fe_2O_3 which is a cubic, ferromagnetic structure which is unstable and never observed in the oxide scales formed on iron at high temperatures.

Magnetite, Fe_3O_4, possesses the cubic, inverse spinel structure in which the oxygen ions have a cubic, close-packed arrangement. In the unit cell of this structure, eight trivalent cations occupy the tetrahedral sites and sixteen cations are on the octahedral positions randomly distributed as eight Fe^{++} and eight Fe^{+++}. The deviation from stoichiometry exists as metal deficit with cation vacancies, and the mechanism of material transport during oxidation has been shown to be predominately diffusion of iron.[7,16]

Wüstite, "FeO," the lowest of the oxides, has a NaCl type cubic structure formed by close-packing of the large oxygen ions with the

smaller iron ions arranged in the interstices. The ionic radius of Fe^{++} is about 0.76 Å, that of Fe^{+++} about 0.64 Å and that of $O^{=}$ is about 1.4 Å.[7] As shown by a number of investigators, the most widely accepted work [illegible] Darken and Gurry,[2] wüstite exists as a thermodynamically stable, single-phase structure over a wide range of compositions which does not include the stoichiometric compound FeO. Wüstite is a metal deficient compound with vacancies in iron lattice sites with the maximum iron content corresponding to $Fe_{0.953}O$ coexisting with metallic iron and with $Fe_{0.882}O$ according to Darken and Gurry.[2] Their investigation [illegible] the interchange of oxygen between gas phase and wüstite is determined by the manometric technique using the equilibrium $CO_2 + Fe \rightleftharpoons CO + FeO$. Similar studies have been conducted on the rate of diffusion of oxygen in and wüstite [illegible] Fe-O system is [illegible] Fe-O [illegible] Fe-O [illegible] Fe-O

the intermediate layer is Fe_3O_4 (magnetite), and the outer layer is Fe_2O_3 (hematite). When iron oxidized under the same conditions, but below 570°C, the metal-oxide layer sequence is $Fe/Fe_3O_4/Fe_2O_3$. This can be seen readily from Figures 2 and 3. Fig. 2 is a schematic phase diagram in terms of temperature versus metal/oxygen system equilibrium oxygen pressure, respectively. Engell[2] has shown that the relative thicknesses of hematite, magnetite and wüstite remain constant at about 1, 9 and 90 per cent, respectively, of the total thickness of the oxide layer over the range 570° to 1000°C. Caplan et al.[21] studied the oxidation of relatively pure iron ("Ferrox") in pure dry oxygen over the temperature range 200° to 1200°C. Between 400° and 570°C the isothermal growth of the FeO layer followed the parabolic law with the overall rate being determined by the rate of growth of the magnetite layer which remained nearly constant in thickness. Above 570°C, however, the FeO layer grew at a rate comparable to that of Fe_3O_4, and because of this rapid growth the rate of oxidation increased by two orders of magnitude. Since the FeO layer was the predominant layer above 570°C, the growth rate was controlled by the diffusion of iron ions and electrons in the FeO lattice. The wüstite layer was formed at the oxide/gas interface by the reaction of iron ions with oxygen. The growth of the Fe_3O_4 layer was controlled by the diffusion of iron ions and electrons in the FeO lattice. The Fe_2O_3 layer was formed at the oxide/gas interface by the reaction of iron ions with oxygen. The growth of the Fe_3O_4 layer was controlled by the diffusion of iron ions and electrons in the FeO lattice. The Fe_2O_3 layer was formed at the oxide/gas interface by the reaction of iron ions with oxygen.

570°C but above this temperature the rate curve decreased with increasing temperature. This deviation was caused by the complications which arise in the formation of the multi-layered scale $FeO/Fe_3O_4/Fe_2O_3$. On the other hand, Padalssi[20] reports an activation energy of 45.5 Kcal/mole for the formation of the total scale in air over the range 700-1200°C.

2. The Oxidation of Iron in Low Oxygen Pressures--A more fundamental problem, necessary for a better understanding of the true mechanism of oxidation of a metal, is an oxidation study under conditions where only one oxide is formed. Such an investigation is the oxidation of iron in carbon dioxide--carbon monoxide mixtures or in hydrogen--water vapor atmospheres where the effective oxygen pressure is below the decomposition pressures of hematite and magnetite, and where wüstite is the only oxide formed. From Figures 3 and 4 one can see that by a suitable choice of experimental conditions, i.e., proper ratios of CO_2-CO or H_2O-H_2 as the oxidizing atmospheres, wüstite will be the only oxide formed at high temperatures. For example, at the phase boundary where FeO is in equilibrium with iron, the equilibrium pressure of oxygen is 1.24×10^{-15} atm. where $CO_2/CO = 0.396$ or $N_{CO_2} = 0.28$, where N_{CO_2} designates the mole fraction of CO_2 in the CO_2-CO atmosphere. This pressure is the minimum needed to oxidize iron at 1000°C. At the opposite side of the phase field, the equilibrium pressure between FeO-Fe_3O_4 is 1.69×10^{-13} atm. where $CO_2/CO = 4.62$ or $N_{CO_2} = 0.82$. Thus we see that CO_2-CO (or H_2O-H_2) mixtures provide a convenient gaseous atmosphere

with which very low effective oxygen partial pressures can be obtained while still working at 1 atm. total pressure.

The first published work on the oxidation of iron in low oxygen pressure atmospheres is apparently that of Fischbeck, Neudeubel and Sulzer[22] who demonstrated that the oxidation of iron in CO_2, H_2O, and NO obeyed a linear relationship at high temperatures. Somewhat later Bénard and Talbot[23] reported that the initial stages of oxidation of iron in oxygen were also linear. In both investigations it was observed that the Arrhenius temperature coefficients of the linear reaction rates changed at the alpha to gamma transition of iron and because of this they both concluded that the rate controlling step of the oxidation reaction was the movement of iron across the metal/oxide interface. Other recent studies on the oxidation of iron in low oxygen pressure atmospheres have been done by Hauffe and Pfeiffer,[10,24] Smeltzer,[25] Wagner et al.,[26] and Pettit.[27] Hauffe and Pfeiffer questioned the rate-controlling reaction at the iron/oxide interface, and based upon their findings that the oxidation of iron to wüstite may be linear or parabolic depending upon the pressure of the gas and the temperature, they proposed that the linear rate of oxidation is controlled by a chemisorption reaction at the wüstite/gas interface. Wagner et al., have shown that the oxidation rate of iron to wüstite at temperatures 925° to 1075°C is a linear function of the mole fraction of CO_2 in the gas phase and also a linear function of the sum of the partial pressures of CO_2 and CO between .34 and 1.0 atm. pressure. Their data confirms that the rate determining step for the oxidation reaction

$$xFe + CO_2 = Fe_xO + CO \qquad (17)$$

is the dissociation of carbon dioxide into carbon monoxide and chemisorbed oxygen atoms or ions. Smeltzer in oxidation studies from 590° to 1100°C attributed the different rates of oxidation of alpha and gamma to the effect of oxide orientation on the chemisorption reactions

$$CO_2 = CO + O^-_{ads} + \oplus \qquad (18a)$$

and

$$Fe + O^-_{ads} = FeO + V^-_{Fe} \qquad (18b)$$

This is understandable when one considers that during the initial stages of the oxidation of iron in low oxygen pressure atmospheres the nucleation of the oxide will not necessarily be random and uniform over all the various exposed iron crystal orientations. Gulbransen and co-workers[28,29] have shown that on a clean iron surface in H_2-H_2O mixtures at 750°C wüstite nucleation occurs on certain preferred sites and favorably oriented nuclei grow faster than other less favorably oriented oxide nuclei. It has also been shown[30] that in a 50% H_2O-50% H_2 mixture the rate of oxidation of iron at 286°C is most rapid on (100) planes and decreases in the order (111), and (110). Gwathmey et al.[31] confirmed this by showing that between 250° and 550°C in oxygen pressures of 10 to 760 m.m. Hg, the relative rate of oxide growth on the (100), (111), (110) and (320) decrease in this order. Hardie[32] also found that the number of nuclei per unit surface area increased from

1 on the (110) planes to 10 on the (111), and to 100 on the (100) planes of α-Fe during oxidation in oxygen at 10^{-4} m.m. Hg at 850°C. For the case of wüstite formation on α-Fe, Mehl and McCandless[30] found that (100) plane of FeO lies parallel to the (100) plane of α-Fe while the <100> direction of FeO lies parallel to the <110> direction of α-Fe. Bardolle and Benard[33] also observed this same epitaxial relationship between wüstite and α-Fe. In a study of the formation of oxide nuclei on γ-Fe, Bardolle has proposed that the epitaxial relationships differ between α-Fe/FeO and γ-Fe/FeO. It has not been experimentally verified, but he proposes that the basal plane of wüstite, (100), is parallel to the (111) plane of γ-Fe, the surface of largest density of atomic iron.

For thick wüstite scales the oxidation rate law is parabolic where the rate controlling step of the reaction is the diffusion of iron ions and electrons outward to the oxide/gas interface. Under these conditions where diffusion is rate-controlling, the rate of oxidation of iron in low-oxygen pressure atmospheres is determined by the gradient across the wüstite scale where the wüstite at the Fe/FeO interface is in equilibrium with the iron while the wüstite at the FeO/gas interface is that in equilibrium with the p_{O_2} in the gas phase.

3. Studies of Diffusion in Wüstite--With few exceptions diffusion measurements can be described by an Arrhenius type equation as

$$D = D_o \exp(-Q/RT) \qquad (19)$$

where D_o is the pre-exponential factor which contains the entropy terms, Q is the experimentally determined activation energy for the process which contain the enthalpy terms. R is the gas constant and T is the absolute temperature.

The rates of self-diffusion of Fe^{55} in wüstite of various compositions, prepared by the oxidation of iron in H_2O-H_2 mixtures, have been measured by Himmel, Mehl and Birchenall[9] by employing the decrease in surface activity technique. For wüstite of the composition $Fe_{0.957}O$ (76.00 wt % Fe), the temperature dependence of the self diffusion coefficient was given as

$$D^*_{Fe} = 0.118 \exp(-29{,}700/RT) \qquad (19a)$$

However, they also observed an anomalous decrease in the activation energy for diffusion in wüstite samples with decreasing vacancy concentration, such that for $Fe_{0.946}O$ (76.75 wt % Fe), the activation energy is found to be 22,100 cal/mole. They also observed that the composition dependence for diffusion of iron in Fe_xO decreases with decreasing temperature. From their data it is seen that the dependence of D on oxygen pressure varies from approximately the 1/4 power at 983°C to the 1/6 power at 897° and 800°C. They did not discuss the significance of this data. The self-diffusion of iron in wüstite of the single composition $Fe_{0.920}O$ (76.20 % Fe) has also been measured by Carter and Richardson,[34] by the sectioning method, and they obtained the relation

$$D^{*}_{Fe} = 0.014 \exp(-30{,}200/RT)$$

which is in excellent agreement with the data of Birchenall et al. for the most oxygen-rich wüstites.

Engell[35] has measured the concentration of vacancies in wüstite of different compositions by an electrochemical method. By assuming that the self-diffusion of iron depends exclusively on the place exchange between iron ions on lattice sites and iron ion vacancies, he has been able to use an equation derived by C. Wagner,[36] and the values of D^{*}_{Fe} of Birchenall et al.,[9] to calculate the self-diffusion of the vacancies, $D_{V^{=}_{Fe}}$, in wüstite. He found that at 983° and 897°C there was no recognizable dependence of the diffusion coefficient on the vacancy concentration, while at 800°C the $D_{V^{=}_{Fe}}$ decreases slightly with increasing vacancy concentration.

C. The Oxidation of Iron-Chromium Alloys in Oxygen-rich Atmospheres

Before one can thoroughly understand the mechanism of oxidation of an alloy, one must understand the mechanism of oxidation of the pure metal constituents, and although pure iron cannot be considered as a material for use at high temperatures, it is the base metal in all oxidation resistant stainless steels. For this reason, the oxidation of pure iron has been discussed briefly, and the numerous detailed studies of its oxidation have provided the basis for a better understanding of the complex mechanism of iron alloy oxidation. In these studies the various oxide layers have been identified and the

mechanism of material transport across these various layers has been determined. In addition the rate of oxidation of pure iron as a function of the variables temperature and effective oxygen pressure in determining the rate controlling step and the role of crystal orientation have been studied.

For this same reason, before a discussion of the present work on the mechanism of oxidation of iron-chromium alloys in CO_2-CO mixtures is undertaken, the existing works on the oxidation of these iron alloys in air and other oxygen-rich atmospheres are considered briefly.

The thermodynamic conditions for oxidation of a metal can be inferred from a diagram of the equilibrium oxygen pressure over the metal/oxide system as a function of temperature. From the reaction

$$\text{metal} + O_2 = \text{oxide}$$

one can obtain the equilibrium constant, K, when both the metal and oxide occur as pure, separate phases, and from the expression $\Delta G^\circ = -RT \ln K$, it follows that

$$\Delta G^\circ = RT \ln p_{O_2}$$

where ΔG° is the change in free energy of the system which occurs during the oxidation reaction when the components are in the standard state. If the partial pressure of oxygen in the gaseous atmosphere exceeds this equilibrium value the metal will oxidize, and if it is less than the equilibrium value, the oxide will dissociate.

In Figure 4 are shown values of the oxidation potential, ΔG°,

over a range of temperatures for the oxides of iron and chromium, and for several other metals generally found in commercial stainless steels. Also shown for convenience are lines of constant p_{O_2} for various CO_2-CO mixtures and for p_{O_2} = 0.01 atm. Although these values of ΔG° are valid only for the oxidation of pure metals, one should not be too far wrong in using it to predict oxide formations on alloys provided the activities of the constituents do not deviate too far from unity.

Thus the equilibrium oxygen potentials shown in Figure 4 are a measure of the relative affinities for oxygen of the various metals and oxides. The more noble the metal, the higher is this equilibrium partial pressure of oxygen and the lower the oxidation potential. The layered scale structure formed on iron oxidized in oxygen above 560°C can readily be seen to be $Fe_2O_3/Fe_3O_4/FeO/Fe$ as mentioned earlier.

From Figure 4 only an indication of the sequence of oxide layers formed on a metal or alloy is obtained, but it provides no guidance regarding their rate of formation. The rate of oxidation of a metal is dependent more upon the structure of the growing oxide, and the ease of material transport across this layer, than upon the oxygen affinity of the metal. For example, ΔG° for the oxidation of chromium is much less than that for the oxidation of iron, i.e., chromium has a greater affinity for oxygen yet, under the same conditions, iron will oxidize many times faster than chromium. In oxygen rich atmospheres at high temperatures both metals oxidize according to the parabolic

law

$$\left(\frac{\Delta m}{A}\right)^2 = K_p \cdot t \qquad (2)$$

where $\Delta m/A$ is the weight gain per unit area, K_p is the parabolic oxidation rate constant, and t is the time. In Table I are listed the parabolic rate constants for the oxidation of iron and chromium in pure oxygen at various temperatures. It is seen that the oxidation rate of chromium is at the most only $1/10^6$ that of iron. Both metals oxidize by the outward migration of cations and electrons via cation vacancies (p-type oxides), however, Cr_2O_3 possesses the corrundum structure (as α-Fe_2O_3) while FeO is cubic. The relative rate of movement of these cations through their respective oxides can be determined by comparing the self-diffusion of Cr in Cr_2O_3 from the work of Hagel and Seybolt[37] with that of iron mentioned in Section B-3.

$$D^*_{Cr(\text{in } Cr_2O_3)}/D^*_{Fe(\text{in FeO})} = \frac{0.137 \exp(-61{,}100/RT)}{0.118 \exp(-29{,}700/RT)} \approx 10^{-7}$$

The extremely good high-temperature oxidation resistance of Fe-Cr alloys in oxygen-rich atmospheres is due to the selective oxidation of chromium and the high resistance to cation diffusion of these chromium-rich oxides.

Although the oxygen potential diagram is helpful when one attempts to determine the oxidation products on an Fe-Cr alloy, a necessary pre-requisite for understanding the kinetic behavior of these alloys of different composition in oxygen at high temperatures

is the Fe-Cr-O phase diagram. The first attempt at establishing such a diagram was by Yearin, Randell and Longo[38] and more recently and more accurately by Seybolt.[39] This Fe-Cr-O diagram which is reported applicable with only minor changes over the temperature range 600° to 1300°C is shown as Figure 5.

Numerous investigators have studied the oxidation of iron-chromium alloys in an effort to determine the mechanism of oxidation and the role of the alloy additions in forming adherent, protective oxide layers in corrosive atmospheres at high temperatures. The oxides formed on these alloys, which contain less than 13% Cr, in air or oxygen are all structurally related to the oxides formed on iron and are solid solutions of Cr_2O_3 and the three iron oxides. As seen from Figure 5, hematite and chromic oxide form a complete solid solution, while magnetite dissolves chromium up to the stoichiometric iron chromite composition at S_3 ($FeCr_2O_4$). Birchenall et al.[40] in a study of the oxidation of iron containing 0.2 to 10 per cent chromium in oxygen from 750° to 1025°C found that wüstite was not an oxidation product to any extent on any of these alloys, but instead, it was replaced by a spinel oxide which Seybolt has shown to have a composition lying between S_1 ($Fe_{1.5}Cr_{1.5}O_4$) and S_3 ($FeCr_2O_4$). Brabers and Birchenall[41] also showed that the wüstite phase could be reduced and eventually eliminated in Fe-Ni alloys when the nickel content was increased from 30 to 50 wt. per cent. Since on pure iron the rate of growth of wüstite is about 20 times faster than magnetite, any alloy addition which will cause a decrease or elimination of the wüstite

phase will result in a spinel oxide phase (magnetite + alloy), in which the cation diffusion is slow, and hence, the oxide layer is very protective. Chromium is a particularly good additive for oxidation resistance because very small additions appear to suppress completely the fast growing wüstite phase when the oxidation is carried out in oxygen. Because the equilibrium oxygen pressure of the spinels of high chromium content is lower than the spinels low in chromium, the conditions of an oxygen pressure gradient across the oxide will cause the high chromium spinels to form at the inner side of the scale, and a composition gradient will exist from the limits $FeCr_2O_4$ to Fe_3O_4. This has been observed by McCulloch, Fontana and Beck[42] in a study of the oxidation of stainless steels in O_2-N_2 mixtures at 815° to 980°C. In a study on the oxidation resistance of commercial steels containing 12, 16, and 27 per cent Cr in air from 870° to 1100°C, Caplan and Cohen[43] observed that chromite, Cr_2O_3 was always the innermost oxide in contact with the metal. On the other hand, Moreau[44] reports finding stable wüstite next to the metal on a wide range of Fe-Cr alloys (2.6, 8, 18, 23 and 30% Cr) oxidized at 800° to 1250°C in air. He finds particles of iron chromite, $FeCr_2O_4$, dispersed in the wüstite. The intermediate layer he reports as a spinel with chromium content decreasing to Fe_3O_4 and an outer layer of α-Fe_2O_3.

The oxide formed on Fe-Cr alloys containing greater than about 13% Cr has been shown[39] to be essentially Cr_2O_3, a rhombohedral-type oxide, which was shown above to be quite impervious. The role of chromium additions on the oxidation resistance of Fe-Cr alloys is

illustrated in Figure 6 from the work of Yearin et al.[38] for specimens exposed to oxygen at high temperatures for various lengths of times. Above about 15% Cr the degree of attack is seen to be reduced sharply.

As a summary, models for the oxide scales formed on pure iron, pure chromium, and Fe-Cr alloys containing less than and greater than 13 per cent Cr oxidized in oxygen above 570°C are shown in Figure 7.

II. EXPERIMENTAL OBJECTIVES

The mechanism of oxidation of Fe-Cr alloys at high temperatures in air or oxygen and the role of chromium-rich, multi-layered oxides in imparting good oxidation resistance to these alloys are relatively well-understood. However, data on the oxidation characteristic and degree of resistance to attack on these same alloys at high temperatures but under very low effective oxygen pressures is meagre and the mechanism is unknown. The need for such information exists whenever stainless steels are used in such low oxygen pressures atmospheres as H_2O, H_2-H_2O mixtures, CO_2 or CO-CO_2 mixtures. These atmospheres may approximate those found under such practical conditions as in steam turbines, internal combustion engines, gas-cooled nuclear reactors, or in atmospheres encountered in space flights such as around the planet Venus where the gaseous atmosphere is reported to consist of very large amounts of carbon dioxide.

The purpose of this investigation is to study the mechanism of oxidation of Fe-Cr alloys in carbon dioxide-carbon monoxide mixtures over the temperature range 800° to 1100° C where the effective oxygen partial pressure is below the decomposition pressures of hematite and magnetite, and wüstite is the only iron oxide formed.

In addition to the study of the change in the rate of oxidation of Fe-Cr alloys when the higher oxides are not stable, the variables affecting the transition from one rate-controlling step (a phase boundary reaction) to another rate-controlling step (diffusion of ions

and electrons) will be investigated. It is desired also to study further the linear and parabolic oxidation mechanisms with a determination of the effect of a polyvalent impurity on the oxidation of iron in CO_2-CO atmospheres where wüstite is the only iron oxide formed. Chromium has been selected as a trivalent impurity on the basis of its solubility in wüstite[38,39] and in iron. In the case of small chromium additions (≤ 1 atom % Cr), the corresponding defect equation is to be expected

$$3Fe + Cr_2O_3 = 2Cr^{+}_{(Fe)} + 3FeO + V''_{Fe} \qquad (21)$$

To study and characterize further the oxide or oxides formed, the oxidation data will be supplemented with diffusion coefficients, obtained from oxidation-reduction studies of pure and doped wüstite, conductivity data, and lattice parameters. The results of the Fe-Cr oxidation in CO_2-CO mixtures will be compared to the existing data in the literature for the oxidation of pure iron under the same conditions and for the oxidation of similar Fe-Cr alloys in oxygen-rich atmospheres. When data is not available for pure iron or for pure wüstite for comparison, this work will also be performed.

A. The Oxidation of Iron-Chromium Alloys in Carbon Dioxide-Carbon Monoxide Mixtures

The limits of existence of the stable wüstite phase field in various CO_2-CO mixtures, as determined by Darken and Gurry,[8] are shown in Figure 8. The partial pressure of oxygen is given by

$$p_{O_2} = \left(\frac{p_{CO_2}}{p_{CO}}\right)^2 \cdot K \qquad (22)$$

where K is the temperature dependent equilibrium constant for the reaction

$$2CO_2 = 2CO + O_2 \qquad (23)$$

1. Linear Oxidation Kinetics--As was mentioned earlier, iron oxidized under the above atmosphere has been observed to follow initially the linear rate law defined as

$$\frac{d(\Delta x)}{dt} = K_L \qquad (24a)$$

or

$$\Delta x = K_L t \qquad (24b)$$

where Δx is the increase in thickness of the wüstite layer, t is the time, and K_L is the linear oxidation rate constant. This equation states that the reaction rate is constant with time and independent of the film thickness.

Experimentally it is more convenient to measure the increase in thickness as $(\Delta m/A)$ where Δm is the weight gained and A is the original area of the metal specimen. The two quantities are proportional since

$$\frac{\Delta m}{A} = \Delta x \cdot \frac{M_{oxygen}}{M_{FeO}} \cdot \rho_{FeO} \qquad (25)$$

where M_{oxygen} and M_{FeO} are the molecular weights of the species and

$$p_{O_2} = \left(\frac{p_{CO_2}}{p_{CO}}\right)^2 \cdot K \tag{22}$$

where K is the temperature dependent equilibrium constant for the reaction

$$2CO_2 = 2CO + O_2 \tag{23}$$

1. Linear Oxidation Kinetics--As was mentioned earlier, iron oxidized under the above atmosphere has been observed to follow initially the linear rate law defined as

$$\frac{d(\Delta x)}{dt} = K_L \tag{24a}$$

or

$$\Delta x = K_L t \tag{24b}$$

where Δx is the increase in thickness of the wüstite layer, t is the time, and K_L is the linear oxidation rate constant. This equation states that the reaction rate is constant with time and independent of the film thickness.

Experimentally it is more convenient to measure the increase in thickness as $(\Delta m/A)$ where Δm is the weight gained and A is the original area of the metal specimen. The two quantities are proportional since

$$\frac{\Delta m}{A} = \Delta x \cdot \frac{M_{oxygen}}{M_{FeO}} \cdot \rho_{FeO} \tag{25}$$

where M_{oxygen} and M_{FeO} are the molecular weights of the species and

ρ_{FeO} is the density of wüstite which varies with composition.

The rate laws are of practical importance because they provide concise expressions for the type of reaction, and one may apply them to calculate the amount of oxidation to be expected under a given set of conditions. When linear kinetics are observed for the formation of a protective oxide and the oxide is dense and adherent and is not volatile, then a phase boundary reaction must necessarily be the rate-determining step, which has been shown[26,27] to be the dissociation of CO_2 into CO and adsorbed oxygen atoms or ions. From the results of Kobayashi and Wagner[45] for the dissociation of H_2S on the surface of Ag_2S, the rate of dissociation of CO_2 on wüstite should depend not only on the composition of the gas phase, but also on the concentration of excess electron holes in the wüstite solid phase. During the linear oxidation of pure iron, the electron hole concentration in wüstite is fixed as that in equilibrium with metallic iron. However, if chromium is added, in accordance with equation (21), the concentration of cation vacancies is increased, and from equation (11) we can see that at constant oxygen pressure, if V''_{Fe} increases, $\oplus$ must accordingly decrease. If the equation

$$\Theta \cdot \oplus = K$$

is valid, then from the reactions

$$CO_{2_{ads.}} = CO_{ads.} + 1/2\ O_{2_{ads}}$$

$$1/2\ O_{2_{ads.}} = O^{=}_{ads.} + 2\oplus$$

one would expect that as the concentration of excess electron holes is decreased (or Θ increased) by the addition of chromium, the rate of adsorption and incorporation of oxygen ions into the wüstite lattice should be increased, if chemisorption is the rate determining step. The validity of the above reactions should be reflected as an increase in the linear oxidation kinetics for the chromium-doped iron.

2. Parabolic Oxidation Kinetics--When the wüstite forms as a compact oxide layer and diffusion of ions and electrons through this layer becomes rate determining the kinetics may be described in terms of the parabolic rate equation

$$\frac{d\left(\frac{\Delta m}{A}\right)}{dt} = \frac{K_p'}{(\Delta m/A)} \qquad (26a)$$

where the increase in thickness with respect to time is inversely proportional to the thickness.[46] Integration of this rate law yields

$$(\Delta m/A)^2 = K_p\, t \qquad (26b)$$

where K_p is the parabolic oxidation rate constant.

The parabolic kinetics are followed because the rate of diffusion of iron ions via the vacancy mechanism becomes slower than the rate of dissociation of CO_2 and/or adsorption of oxygen atoms or ions on the surface. From equation (21) it is seen that the incorporation

of chromium should lead to an increase in the cation vacancy concentration, hence the rate of oxidation should be increased in the parabolic range until a new oxide is formed. Such rate increases have been demonstrated by Wagner and Zimens[13] for the oxidation of chromium-nickel alloys (0.3 to 3.0% Cr) in oxygen at 1[illegible]°C, and by Pettit[27] for the oxidation of cobalt containing 0.6 at.% manganese in pure carbon dioxide.

3. Temperature and Pressure Dependence of Oxidation Rates--When diffusion is the rate-controlling step in an oxidation process, one would expect that the temperature dependence of the parabolic rate constant should follow an Arrhenius-type equation, similar to Eq. (19), of the type

$$K_p = A \exp(-Q/RT) \tag{27}$$

This was first shown by Dunn[47] in 1926. Mott[48] has related the parabolic oxidation rate constant to diffusion theory by showing that

$$K_p = B D_v' (V_g - V_m) \tag{28}$$

where D_v is the diffusion coefficient of the vacancies, B is a constant, and V_g and V_m are the vacancy concentrations at the gas/oxide and metal/oxide interfaces, respectively. If V_g is much larger than V_m, then $V_g \simeq [V_{Fe}^{=}]$ and upon substituting Equation (14) into (28) we obtain

$$K_p = C D_v' K^{1/3} p_{O_2}^{1/6} \tag{29}$$

From Eyring's theory of absolute reaction rates[49]

$$D_V'' = C' \exp(-\Delta H_m''/RT) \exp(\Delta S_m''/R) \quad (30)$$

where $\Delta H_m''$ and $\Delta S_m''$ are the enthalpy and entropy of movement of the metal ions into vacancies and C' is a constant. ΔH_m and ΔS_m are activated quantities related to an equilibrium existing between the reactants and the activated complex. Because K in Eq. (29) is the equilibrium constant for the reaction

$$Fe + 1/2\ O_2 = FeO + V_{Fe}'' + 2\oplus \quad (31)$$

and because $\Delta G = -RT \ln K$ (32)

and $\Delta G = \Delta H - T\Delta S$ (33)

then $K = \exp(-\Delta H_f/RT) \exp(\Delta S_f/R)$ (34)

where ΔH_f and ΔS_f are the enthalpy and entropy of formation for one mole of reaction which gives two moles of holes. These are activated quantities. Substituting Equations (30) and (34) into (29) yields:

$$h_f = C'' P_{O_2}^{1/6} \exp\left[-\left(\Delta H_m'' + \frac{\Delta H_f}{3}\right)/RT\right] \exp\left[\left(\Delta S_m'' + \frac{\Delta S_f}{3}\right)/R\right] \quad (35)$$

Thus it is seen that h_f varies as $P_{O_2}^{1/n}$ where in the case of oxidation of FeO, $n = 6$. This was derived by assuming complete dissociation of the reaction holes and the vacancies. If $n \neq 6$, then this assumption would be incorrect. Also, by obtaining h_f from oxidizing experiments,

under certain fixed conditions, one should be able to get values of ΔH_m^* and ΔH_f. Birchenall[50] has stated that when self-diffusion measurements are conducted on specimens of constant composition, the activation energy should reflect only the energy necessary to move the ionic or electronic defects, whichever is the more difficult. When constant pressure of one of the components is used, the ionic and electronic defects should vary with the temperature, and therefore, the activation energy should include the enthalpy of formation as well as the enthalpy of motion.

4. Transition from Linear to Parabolic Oxidation Kinetics--As mentioned previously, when the oxide attains a certain thickness such that the diffusion of ions and electrons becomes the rate determining step, the kinetics change from linear to parabolic. An example of this is shown by the oxidation curve in Figure 9. The parabolic portion of the curve can then be described by

$$(\Delta m/A)^2 = K_p (t-t_p) \tag{36}$$

where t_p is the time when the parabolic curve is extrapolated back to zero gain in weight. Thus, it is seen that the transition thickness, $(\Delta m/A)_{tr.}$, is the thickness at the point where the linear curve and the parabolic curve are tangent, i.e., where the slopes of the two curves are equal. If the two rate laws are differentiated and the slopes are equated, we get

$$d\left(\frac{\Delta m}{A}\right) = K_L dt \tag{37a}$$

$$2\left(\frac{\Delta m}{A}\right) d\left(\frac{\Delta m}{A}\right) = K_p\, dt \qquad (37b)$$

or

$$\frac{d\left(\frac{\Delta m}{A}\right)}{dt} = K_L = \frac{K_p}{2\left(\frac{\Delta m}{A}\right)}$$

and

$$\left(\frac{\Delta m}{A}\right)_{transition} = \frac{K_p}{2K_L} \qquad (37c)$$

In actuality, $(\Delta m/A)_{tr.}$ probably is not a fixed oxide thickness, but rather, the transition from linear to parabolic kinetics occurs over a small range of thicknesses. However in order to compare the experimental value with the calculated value, the average of the thickness when the reaction is no longer linear, and when the reaction becomes parabolic, will be used. The values of $(\Delta m/A)_{tr.}$ for Fe-Cr alloys will be compared with those obtained from the oxidation of pure iron.

The transition thickness is also a function of temperature where

$$K_p = A \exp\left(-E_p/RT\right) \qquad (38c)$$

and

$$K_L = B \exp\left(-E_L/RT\right) \qquad (38c)$$

Hence, substitution into equation (37c) gives

$$\left(\frac{\Delta m}{A}\right)_{tr.} = C \exp\left[-(E_p - E_L)/RT\right] \qquad (38c)$$

Thus, it is seen that a plot of the logarithm of the transition

thickness versus reciprocal temperature gives a curve whose slope is the difference of those obtained from the parabolic and linear data, and any changes affecting the linear and parabolic mechanisms should be manifested also in the transition thickness.

B. X-Ray Diffraction Studies of Pure and Doped Wüstite

Several investigators have made room-temperature lattice parameter measurements on wüstite as a function of composition. Perhaps the most acceptable have been those of Jette and Foote[18] who used these measurements to determine the phase limits of wüstite. Willis and Rooksby[51] and Bénard[52] have also measured the lattice parameters of wüstite at room temperature, but their values of a_o are considerably different from those of Jette and Foote.

Because the wüstite used in the above experiments were prepared from relatively impure iron, and because of the discordant values reported by the different investigators, it was felt that lattice parameter measurements should be obtained first on very pure wüstite. The values of a_o have been extended to the limits of the stable wüstite phase field as determined by Darken and Gurry,[8] which include a larger range of existence than that found by Jette and Foote.

In order to characterize further the oxide scale formed on Fe-Cr alloys and to study the effect of a trivalent impurity ion in wüstite, lattice parameter measurements of doped wüstite equilibrated at various compositions also have been obtained at room temperature.

C. The Conductivity of Pure and Doped Wüstite

In an attempt to determine the effect of chromium on the oxidation properties of Fe-Cr alloys during both the initially linear range and subsequent parabolic range, conductivity measurements have been made on both pure and doped wüstites. Conductivity measurements should yield an indication of the relative concentrations of holes in doped wüstite as compared to pure wüstite and thus the magnitude of the values of the electrical conductivity in these different oxides should be particularly helpful in determining whether the rate determining step, during the initially linear oxidation reaction, is the dissociation and/or adsorption of CO_2 into CO and oxygen atoms or ions. If the effect of chromium is as given by Equation (21), one would expect that under the same conditions of temperature and oxygen pressure, the impure wüstite should exhibit the lower conductivity. This has been shown by Hauffe and Block[53] for nickel oxide containing dissolved chromium oxide.

1. Temperature and Pressure Dependence of Electrical Conductivity--The conductivity of wüstite has received surprisingly little attention. Wagner and Koch[54] have reported that the conductivity of wüstite increases at 800°, 900° and at 1000°C approximately according to the 1/8 power of the oxygen pressure. They found for $p_{O_2} = 3.8 \times 10^{-15}$ atm. and 1.4×10^{-13} atm. that $\sigma = 107$ and 205 $ohm^{-1}cm^{-1}$, respectively, at 1000°C. With pertinent values of the vacancy concentration, obtained from equilibration experiments, Hauffe[10] has

calculated the mobility of the electron holes at these pressures and found it to be 1.18 and 1.10 x 10^{-1} $cm^2 sec^{-1} volt^{-1}$. By using the above data for conductivity and mobility and their own values of D^*_{Fe}, Birchenall et al.[9] have calculated the transference number of the cations in wüstite at 1000°C and found it to be approximately 2 x 10^{-4}. Thus wüstite is an almost purely electronic conductor, hence for completely undissociated vacancies and holes, the conductivity should be directly proportional to $[\oplus]$, the concentration of electron holes. Hauffe[10] has also experimentally determined that for wüstite at 950 and 1000°C, $[\oplus]$ - constant · $p_{O_2}^{1/6}$. (He did not measure the electrical conductivity as reported in some books on the solid state.[3]) However the conductivity should be proportional to the 1/6 power, and not the 1/8 power, of the oxygen pressure. In this study conductivity measurements have been made on pure wüstite at 1000°C to determine this pressure dependence, and similar measurements have been made on the doped specimens in an effort to determine any effect of the trivalent impurity.

Heikes and Johnston[56] have described the electrical conductivity in transition metal oxides by an equation identical in form to Equation (35) which describes the temperature and pressure dependence of the oxidation rate. For the same reason that diffusion measurements conducted in specimens held at constant composition yield activation energies comprised only of the enthalpy and entropy of movement of the atomic defects, conductivity measurements on samples of constant composition yield only the enthalpy and entropy of movement of the

electrical defects. Thus hole conduction in wustite at a single composition may be described by a diffusion type equation where

$$\sigma = A[\oplus] \exp\left\{\frac{\Delta H^*_{m_\oplus}}{RT} - \frac{\Delta S^*_{m_\oplus}}{R}\right\} \qquad (39)$$

Here A is a constant which includes the jump frequency of the hole, the lattice parameter of wüstite, the electronic charge and the density of ion pairs. $[\oplus]$ is the hole concentration, and $\Delta H^*_{m_\oplus}$ and $\Delta S^*_{m_\oplus}$ are the enthalpy and entropy of movement of the holes. Substituting Equation (13), for the concentration of holes, into the above equation yields

$$\sigma = A\,(2K)^{1/2}\, P_{O_2}^{1/6} \exp\left\{\frac{-\Delta H^*_m}{RT} + \frac{\Delta S^*_m}{R}\right\} \qquad (40)$$

Now substituting Equation (34) for the equilibrium constant of reaction (31), we get

$$\sigma = A\, P_{O_2}^{1/6} \exp\left[-(\Delta H^*_{m_\oplus} + \frac{\Delta H_f}{3})/RT\right] \exp\left[(\Delta S^*_{m_\oplus} + \frac{\Delta S_f}{3})/R\right] \qquad (41)$$

Thus we see when electrical conductivity measurements are carried out on specimens under conditions of constant oxygen partial pressure, a plot of log σ versus reciprocal temperature will yield a slope which is proportional to the enthalpy of movement of the electron hole plus the enthalpy of formation of one mole of vacancies and two moles of holes. Mitoff[96] has applied the above equations to a conductivity study on nickel oxide, and he has obtained the values $\Delta H_f = 83.1$ kcal

mole and $\Delta H_{m_{\oplus}}$ = 5.4 Kcal/mole.

Thus by employing proper mixtures of CO_2 and CO to ensure conditions of constant composition of wüstite and under other conditions, constant oxygen pressure, the electrical conductivity of pure and doped wüstite has been measured over the temperature range 650° to 1100°C. By comparing the measurements obtained from the chromium-doped wüstites with those from the pure wüstite samples, the effect of impurities on these thermodynamic quantities should be ascertainable. Also from these conductivity experiments it should be possible to observe the range of solid solution of Cr in FeO under the specified experimental conditions. Abrupt changes from the normal pattern in the value of the conductivity should indicate the appearence of iron-chromium spinel as a second phase.

b. Reduction and Oxidation Studies on Pure and Doped Wüstite

If one assumes that the mechanism by which iron ions migrate through wüstite is that of diffusion, then for very thick wüstite samples, the diffusion of iron is expected to be the rate controlling step during any reduction or oxidation process. These processes are particularly adaptable to a study of wüstite because the composition versus temperature phase diagram for CO_2-CO atmospheres is well known from the work of Darken and Gurry.[8] See Figure 8. This portion of the present study is concerned with obtaining diffusion coefficients from the kinetics of reduction and oxidation of wüstite from one fixed composition to another as a function of the variables temperature, oxygen pressure, and composition. Both pure and chromium-doped wüstite

have been studied. From these studies one is able to obtain values of the chemical diffusion coefficients, D, of iron in wüstite which can then be compared to the values of the self-diffusion coefficients of iron in wüstite. From the values of D obtained for the chromium-doped wüstites, one should be able to characterize further the nature of the wüstite scales formed on Fe-Cr alloys.

During the oxidation of wüstite the movement of the iron ions is toward the oxide/gas interface, while during reduction the movement of iron is away from this interface. The concentration across a sample thickness may be shown graphically, as in Figure 10, which represents the cross-section, with faces AB and A B′ as the oxide/gas interfaces. AA′ represents the initial concentration and BB′ the final concentration, both corresponding to a composition of Wüstite in equilibrium with specific CO_2/CO ratios at fixed temperatures. It shall be assumed that at time t = 0 when we admit the atmosphere that the surface concentration drops immediately to the values B and B′, and furthermore, as a simplification, that at any subsequent time, t, the concentration gradient is linear. In actuality, since the slope of the gradient is proportional to the rate of diffusion of iron at any point, this slope must fall off from surface to center-line, and approach zero at the center.

For the interior of the solid wüstite phase, we shall solve the usual differential equation representing Fick's law

$$\frac{\partial C}{\partial t} = - D \frac{\partial^2 C}{\partial X^2} \qquad (42)$$

for the boundary conditions present here, i.e., for a thin plate exposed on both sides. The solution which is identical with that for the diffusion of heat in a similar solid is

$$C = \frac{4}{\pi}\left[e^{-\left(\frac{\pi}{2}\right)^2 k} \sin\frac{\pi X}{2a} + \frac{1}{3} e^{-3^2\left(\frac{\pi}{2}\right)^2 k} \sin\frac{3\pi X}{2a} + \frac{1}{5} e^{-5^2\left(\frac{\pi}{2}\right)^2 k} \sin\frac{5\pi X}{2a} + \ldots\right] \qquad (43)$$

where $C = \dfrac{\text{excess concentration at any time } t}{\text{initial excess concentration}}$ = the concentration gradient curve at any time, $t > 0$

and $k = \dfrac{Dt}{a^2}$

The excess concentration* is that over and above the concentration in equilibrium with the atmosphere admitted at time, $t = 0$.

Since equation (43) gives the theoretical excess distribution at any time t in a slab where diffusion is the rate controlling step, the total excess, Σ, remaining can be determined by integration of the distribution curve at any time t. Thus

$$\Sigma = \frac{1}{a}\int_0^a C\, dX \qquad (44)$$

---

* For a reduction experiment the "excess concentration" is oxygen, whereas for oxidation it is iron ions.

$$\Sigma = \frac{4}{\pi a} \int_0^a \left[e^{-\left(\frac{\pi}{2}\right)^2 k} \sin \frac{\pi X}{2a} + \frac{1}{3} e^{-3^2 \left(\frac{\pi}{2}\right)^2 k} \sin \frac{3\pi X}{2a} + \ldots \right] dX \qquad (44b)$$

$$\Sigma = \frac{8}{\pi^2} \left[e^{-\left(\frac{\pi}{2}\right)^2 k} + \frac{1}{9} e^{-9\left(\frac{\pi}{2}\right)^2 k} + \frac{1}{25} e^{-25\left(\frac{\pi}{2}\right)^2 k} + \ldots \right] \qquad (44c)$$

The percentage of the excess concentration, C, is shown in Figure 11 plotted against the cross-section of the slab. The different curves represent the values of C at different stages of the reduction or oxidation process as represented by the different values of k. As given by Equation (44a), Σ is equal to the area under the concentration gradient curve divided by the initial excess concentration as illustrated by the area $AA'B'B$ in Figure 10. When k is less than 0.7 the first term of the series in Equation (44b) is large as compared to the subsequent terms and the gradients can be represented as sine curves as shown in Figure 11.

But Σ, the excess oxygen or iron at time t is simply $(1 - Q)$ where Q is the fractional amount removed at any time t, or more conveniently $Q \equiv \frac{\Delta m}{\Delta w}$ where

Δm = fractional change in weight at any time t

Δw = total change in weight after the sample is in equilibrium with the atmosphere which was admitted at time t = 0

Because equation (44c) is a rapidly converging series, the second term is very small except for small time periods, we can then write

$$1 - \frac{\Delta m}{\Delta w} = \frac{8}{\pi^2} e^{-\left[\frac{\pi^2 D t}{4 \ell^2}\right]} \qquad (45)$$

or

$$\log_e \left(1 - \frac{\Delta m}{\Delta w}\right) = \log\left(\frac{8}{\pi^2}\right) - \frac{\pi^2 D t}{2.3\ (4\ell^2)} \qquad (46)$$

From the slope of the curve of $-\log\left(1 - \frac{\Delta m}{\Delta w}\right)$ versus time, one can obtain D, the chemical diffusion coefficient of iron in wüstite.

Equations of the type (43) through (46) were apparently first used by Sherwood[57] and Newman[58] in an analysis of the drying of solids. Dunwald and Wagner[59] derived these equations and suggested that they could be used to study the movement of "dissolved" oxygen in cuprous oxide and nickel oxide, and Shenk et al.[60] were able to obtain the diffusion coefficient of dissolved oxygen in stainless steels by their use. More recently, Gerlach and Ellickson[61] showed their applicability to several diffusion studies, and Moser[62] has reported the diffusion of oxygen during oxidation and reduction of rutile.

III. EXPERIMENTAL PROCEDURE

A. The Oxidation of the Alloys

Iron-chromium alloys containing 0.25, 0.88, 1.77, 3.79, and 7.55 wt % chromium and a commercial Type 430 stainless steel containing 18.21 wt % chromium have been oxidized in CO_2-CO mixtures over the temperature range 800° to 1100°C where, in accordance with the phase diagram in Figure 8, wüstite is the only iron oxide formed. The carbon dioxide-carbon monoxide atmospheres used in this study were mixtures of 70% CO_2-30% CO (N_{CO_2} = 0.700), 60% CO_2-40% CO (N_{CO_2} = 0.600), and 50% CO_2-50% CO (N_{CO_2} = 0.500). The total pressure of the gas mixture was always maintained at 1 atm.

The method of determining K_L and K_P was by measuring the weight increase per unit area of the original metal specimen as a function of time. A plot of $(\Delta m/A)$ versus time yields K_L (gm/cm^2-sec) while a plot of $(\Delta m/A)^2$ versus time gives K_p (gm^2/cm^4-sec).

1. Specimen Analysis and Preparation--The iron used as the base metal in this study was kindly furnished by the Battelle Memorial Institute as a specimen of zone-melted, high-purity iron weighing approximately one pound. The analysis provided with this specimen is given in Table II.

The chromium used was Matthey spectrographically standardized chromium which was obtained in pellet form with the provided impurity analysis given in Table III.

The desired amounts of chromium were mixed with iron and the alloys were formed by melting the metals in a water-cooled copper crucible under an argon atmosphere with a consumable tungsten electrode. The standard procedure was to cool and remelt the metal button at least four times in order to obtain the desired homogeneity. The metal buttons were then cold-rolled directly to a thickness of about 0.050 inch. This strip was then cut into specimen coupons 1/2 inch x 3/8 inch. Certain selected samples were analyzed for chromium content and others were examined microscopically to determine if any inhomogeneity existed. All of the samples examined appeared to be homogeneous.

A hole of 0.059 inch diameter was drilled in one end of the metal specimens which were to be used for oxidation experiments. These specimens were then polished on Armour metallographic paper through No. 4/0 and lapped on a wheel covered with a Beuhler AB microcloth which was saturated with Linde Type A fine abrasive. After a mirror-finish had been attained, the dimensions of the specimens were measured with a micrometer. The samples were then washed with ethyl alcohol and weighed on a Mettler Type H5 analytical balance which has an accuracy of ± 0.05 mg. The usual sample, after polishing, had a surface area of about 2 cm^2, was about 0.024" inch thick and weighed about 0.8 gm. The samples were then annealed in cleansed static hydrogen for about 12 hours at 550-600°C in order to relieve any stresses in the metal and to stabilize the grain size. They were then re-weighed and stored in an evacuated dessicator until ready for use.

2. The Oxidation Apparatus--The apparatus used in this study was an Ainsworth vacuum, semi-micro, automatic recording balance. The balance capacity is 100 gm. with an over-all weighing accuracy within the automatic range of ± 0.03 mg. The range of automatic weight operation is 400 mg.

The gain in weight during an oxidation experiment causes a deflection of the beam of the balance which is detected by a variable inductance transducer in a bridge circuit. Any imbalance in this circuit gives an output signal which is then amplified to operate the recorder which records the change in weight on a variable-speed chart. The chart width is 10 inches which corresponds to 10 mg. Whenever the pen reaches 10.25 mg. on the scale, a 10 mg. weight is added to the balance beam and this moves the pen back to 0.25 mg., ready for another sweep across the chart. There are enough combinations of weights to do this switching 39 times, giving a completely automatic range for an increase in weight of 400 mg.

The oxidation chamber consisted of a McDanel mullite tube 3/4 inch I.D. and 24 inches long to which were connected standard-tapered pyrex glass joints. This tube was mounted in a fixed vertical position below the Ainsworth balance. The furnace was a Marshall high-temperature furnace with a maximum operating temperature of 1200°C. The furnace was shunted in parallel across the center portion of the windings in such a manner that a constant temperature zone of ± 2/4° was obtained over a distance of 1 1/2 inches.

The entire assembly was mounted in a rigid steel frame such

that the furnace and mullite tube were fixed. The balance was mounted on an aluminum plate which was fitted at the four corners with precision-fitting ball bushings which allowed for vertical movement along four fixed shafts. The balance was connected to the upper pyrex joint by a machined brass sleeve and a stainless steel tube. See Figure 12. A vacuum-tight sliding joint was maintained between the stainless steel tube and brass sleeve by O-ring seals which were mounted in pairs inside the brass sleeve. When the balance was lifted to its highest position a space of about 8 inches separated the bottom of the brass sleeve from the top of the stainless steel tube. See Figure 13(a). A 24 inch quartz fiber (0.010 inch diameter) which was attached to the balance beam terminated in this gap. The metal specimen was then lowered into the steel tube by a second fiber which was then hooked to the upper fiber. The balance assembly and specimen was then lowered to an intermediate position, Figure 13(b), where the O-ring seals engaged the steel tube and the specimen was in a cold zone above the furnace. While in this position the entire system could be evacuated with a vacuum pump, and then the desired gas mixture admitted into the assembly. While in this position the specimen was counter-balanced in order to maximize the automatic weighing range. The gas flow entered the oxidation chamber from the bottom and exited, to an exhaust system, at the point just below the stainless steel to glass joint. After the desired gas flow and temperature had been established, the balance and specimen could be quickly lowered to the lower position, Figure 13(c), the balance beam arrest disengaged and the recorder chart started.

In this position the stainless steel tube is completely within the brass sleeve and the specimen is positioned at the center of the hot zone. With this movable balance assembly, the specimen could be lowered into the hot zone or raised up to the cold zone within one or two seconds.

At the end of an oxidation run the gas supply to the furnace was shut off and the balance was quickly raised to the intermediate position. This position placed the red-hot specimen on the cold zone where it quickly cooled. The CO_2-CO mixture was then evacuated, air re-admitted and then the balance lifted to the upper position. The oxidized sample was always weighed on the Mettler balance and this gain in weight was always compared to the gain in weight recorded by the Ainsworth balance. For a total of 60 oxidation runs performed in this study the average difference between the two different weighings was $\pm$ 0.00029 gm.

3. The CO_2-CO Gas Control System--Carbon dioxide of Bone-Dry grade and carbon monoxide of C.P. grade were used throughout this study. A typical analysis of these gases is given in Table IV. The carbon dioxide was cleaned by passing it successively through tubes containing activated alumina, hot copper chips at 500°C, and activated alumina. The activated alumina would remove any moisture while the hot copper would remove any oxygen present. The carbon monoxide was passed successively through tubes containing magnesium perchlorate, Ascarite, and magnesium perchlorate. Both gases were metered with

conventional manometric flowmeters using a capillary of about 0.5 m.m. and with the two arms of the manometer containing di-butyl pthalate. A schematic diagram of the gas trains is shown in Figure 14. The flowmeters were calibrated using a "Precision" Wet Test meter. The accuracy of this meter has been confirmed to be within 1 per cent by comparing it to the displacement of a soap bubble in a graduated burette. For a number of different flow rates from zero to 10 l/hr, the value of Δh (cm), the difference in height of the liquid in the two arms of the manometers, was obtained, and a linear relationship was found for both flowmeters. In accordance with the recommendations of Darken and Gurry[8] the total flow of the gases was always maintained at that value which gave a linear velocity of 0.9 cm. per second over the specimen. They found that at flow rates less than this value thermal segregation of the gases occured while at faster flow rates the specimen had a tendency to be cooled by the incoming gases. In order to have a flow of 0.9 cm/sec through the 3/4 in. I.D. mullite tube, a total flow of 9.23 liters per hour was always maintained. In all calculations it was assumed that the gases behave ideally, i.e.,

$$P_{CO_2}/P_{CO} = \text{Volume of } CO_2/\text{Volume of } CO.$$

4. Temperature control--The temperature of the furnace was held to within about ± 3/4°C of a constant value during any one run by using a Leeds and Northrup AZAR-type temperature controller. The input signal to the controller originated from a Pt.-Pt-10% Rh thermo-

couple positioned in a 1/4 inch horizontal thermocouple well located at the midpoint of the vertical furnace. A second Pt-Pt-10% Rh thermocouple was used to measure the specimen temperature and this thermocouple was placed in a vertical position in a well alongside the mullite tube. It was positioned in the center of the hot zone which had been obtained by successive calibrations with different shunts. In order to determine the actual difference in temperature between the specimen and this measuring couple, a third thermocouple was inserted into the mullite tube at the position where the sample would be located and a ΔT vs T curve obtained over the range of 750° to 1150°C. After the calibration was completed, this third thermocouple was removed. With this graph, one could then measure, and set the controller to hold, any desired specimen temperature. The difference between the actual specimen temperature with gases flowing, and the measured temperature varied from 3 1/2°C at 750°C to 1 1/4°C at 1150°C. The temperature at the specimen position was noted to hold constant to within ± 1/2°C.

B. X-Ray Analysis of Pure and Doped Wüstite

The lattice parameters of pure wüstite and wüstite containing 0.67 wt. per cent chromium were measured at room temperature after the oxides had been equilibrated at 1000°C in various CO_2-CO mixtures.

The oxides were formed from metal coupons which were prepared by polishing in the same manner as those prepared for the oxidation experiments. A CO_2-CO gas train and furnace assembly of the exact

same type as used in the oxidation apparatus was constructed for the x-ray and conductivity studies. The specimen was suspended by a quartz fiber at the center of a pre-determined hot-zone (±0.7°C over a distance of 2 inches) in a one-inch mullite tube which had an interchangeable top so that it could be used in both studies. The details of the apparatus are described in Section C-2. After the oxide specimen had been equilibrated in the specific CO_2-CO mixture,* it was quenched in this same atmosphere by drawing it up into the cold zone above the furnace by means of a small winch to which was fastened a small chain above the quartz fiber.

The composition of the wüstite was determined as

$$\text{wt. \% oxygen} = \left\{ 1 - \frac{\text{initial weight of metal}}{\text{final weight of wüstite}} \right\} \cdot 100 \qquad (47)$$

The wüstite samples were then ground to a powder, screened through a 300 mesh sieve and sealed in 0.3 mm. diameter, thin-walled GLASKAPILLAREN for x-ray analysis. Debye-Scherrer powder patterns were obtained by using cobalt radiation with an iron filter and a General Electric camera with a film circumference of 225 mm. All of the photographs were taken at room temperature.

The values of the lattice parameter were calculated from about 10 lines lying between 20 and 70 degrees of θ, and these values of

---

* The time for equilibration was determined from the previous experiments on the rate of oxidation of the metal, and from the rate of equilibration of the specimens used in the reduction and oxidation of wüstite experiments which are discussed in the last section

α were then plotted versus the Nelson-Reilly function. The value of α_o was then obtained by extrapolating to where the Nelson-Reilly function equals zero.

D. Conductivity Measurements

1. Specimen Preparation--A specimen of the high-purity iron and specimens containing 0.88 and 1.70 wt % Cr were prepared by polishing them in the same manner as the specimens for oxidation experiments. They were then carefully measured with a micrometer to determine the width and the thickness. The metal specimens were then wrapped at four evenly-spaced positions with 0.013 inch Pt wire, as shown in Figure 15(a), and the distance, d, between the two inner windings was measured with an optical micrometer. The specimens were then oxidized to wüstite in a 70% CO_2-30% CO mixture at 1000°C. During the oxidation process the movement of iron was outward to the oxide/gas interface and the wrapped Pt wires were completely engulfed by the wüstite as shown in Figure 15(b) and (c). The final wüstite samples were large grained, with the average grain diameter being about 0.3 cm. Because the movement of the iron was perpendicular to the oxide surface, no lateral movement of the Pt wires occurred, hence $d_{FeO} = d_{Fe}$. By neglecting a small "edge-effect," the width of the final wüstite sample is essentially the same as original width of the metal coupon, however, the thickness of the wüstite increased during the oxidation process such that

$$t_{FeO} = t_{Fe} \frac{a_o(FeO)}{a_o(\alpha\text{-}Fe)} \qquad (48)$$

where t_{FeO} and t_{Fe} represent the thickness of wüstite and the original thickness of the iron specimen, and $a_o(FeO)$ is the lattice parameter of wüstite at a given composition as determined from the x-ray studies, and $a_o(\alpha\text{-}Fe)$ is the lattice parameter of α-Fe (= 2.8665 Å).

This method of specimen preparation was decided upon for several reasons. (1) No single crystals of wüstite were available and regardless, in order to compare the doped wüstite with the pure wüstite the experimental conditions should be as near alike as possible. (2) This method eliminated any chance of contamination during preparation, whereas contamination would be possible during the pressing, sintering and handling operations if powdered compacts had been used. (3) Wüstite tends to develop small cracks when re-heated, and by preparing the specimen in the above manner, this problem was avoided.

2. Apparatus--A four point probe method was used for all measurements, and a schematic of the electrical circuit is shown in Figure 16. The conductivity was measured as

$$\sigma\ (ohm^{-1}cm^{-1}) = \frac{d_{FeO}}{R_{spec} \cdot A_{FeO}} \qquad (49a)$$

where

$$R_{spec} = \frac{E_{spec}}{E_{std}} \cdot R_{std} \qquad (49b)$$

and

$$A_{FeO} = w_{Fe} \cdot t_{Fe} \left\{ \frac{a_{FeO}}{a_{\alpha\text{-}Fe}} \right\} \qquad (4\text{-}4c)$$

Here E_{spec}, R_{spec}, E_{std} and R_{std} are the measured voltages and resistances across the specimen and standard resistor, respectively. A_{FeO} is the cross-sectional area of the wüstite specimen. The value of $a_{o_{FeO}}$ varied with composition, hence a different value of a_o was used for each different equilibrium gas mixture. The values of a_o for FeO versus N_{CO_2} were determined by the x-ray studies. Again, from the data of Darken and Gurry, values of p_{CO_2}/p_{CO} were calculated such that the conductivity of wüstite could be measured under conditions of constant composition and constant oxygen pressure.

A furnace assembly and a CO_2-CO gas train of the exact same type as used in the oxidation apparatus was constructed for the conductivity studies. The specimen was suspended at the center of a pre-determined hot zone (± 0.7°C over a distance of 2 inches) in a mullite tube of one inch I.D. to which were fastened two pyrex-glass joints. The gas mixture entered at the bottom and flowed upward over the specimen and was exhausted. The total gas flow was always constant at 16.4 ℓ/hr to insure a linear velocity of 0.9 cm/sec over the sample. The furnace was a Marshall high-temperature type capable of reaching 1200°C. The temperature was controlled to within ± 1°C by a Leeds and Northrup ELECTROMAX type temperature controller which received its input from a chromel-alumel thermocouple mounted in the horizontal thermocouple well at the furnace mid-point. The specimen temperature was measured

by a calibrated Pt-Pt-13% Rh thermocouple which extended down through a quartz tube to within 1/4 inch of the specimen. See Figure 15(a).

D. The Reduction and Oxidation of Pure and Doped Wüstite

1. Specimen Preparation--Samples of zone-melted, high purity iron and samples containing 0.88 wt per cent chromium were prepared as specimens 0.5 in. x 0.3 in. x 0.050 in. These specimens were then prepared in the same manner as those used in the oxidation experiments by polishing them through No. 4/0 metallographic paper, lapping them on a wheel covered with Linde A fine abrasive, and then annealing them in static hydrogen at about 600°C for about 12 hours. The surface area of these specimens was about 2.5 $cm.^2$ and they weighed about one gram. These metal coupons were then oxidized to wüstite at a temperature of 1000°C in a 70% CO_2-30% CO gas mixture. All specimens were oxidized under these same conditions so that the grain size and surface texture would be as near alike as possible for all of the final wüstite samples.

From the data of Darken and Gurry[8] on the equilibrium compositions of wüstite in various CO_2-CO mixtures, values of N_{CO_2} in equilibrium with wüstite of the constant oxygen to iron ratios of 1.050 (23.13 wt. % oxygen), 1.075 (23.55 wt. % oxygen), 1.100 (23.86 wt. % oxygen), and 1.125 (24.37 wt. % oxygen) were determined for the temperatures 900°, 950°, 1000°, 1050° and 1100°C. These values of constant composition are shown plotted on the wüstite phase field in Figure 8. After the specimen was completely converted from iron to

wüstite, it was equilibrated at the desired initial composition by fixing the temperature and adjusting the gas flow to the desired calculated value of p_{CO_2}/p_{CO} for that composition and temperature.

2. Apparatus and Procedure--The Ainsworth automatic balance described in the previous section was used in this study. To begin an oxidation or reduction run, the gas flow which was in equilibrium with the specimen was shut off and a new value of p_{CO_2}/p_{CO} was established by by-passing the furnace. At a time designated as t = 0. the newly established value of p_{CO_2}/p_{CO}, the gas mixture which would be in equilibrium with the desired final composition of wüstite at that specific temperature, was admitted to the furnace, the recorder chart started, and the reaction began almost immediately. The specimen was not lifted from the hot zone because it was found that by cooling and reheating the wüstite small cracks sometimes developed on the samples. The existence of such cracks could, of course, complicate the final analyzed results by causing the surface area exposed to the gases to be greater than the measured value.

During a reduction experiment the operation of the Ainsworth balance was just the reverse of that for an oxidation experiment. Whenever the pen reached a value on the chart of -0.25 mg. a switch was activated, a 10 mg. weight was removed, and the pen moved to 9.75 mg. ready to make another decreasing sweep across the scale.

E. Metallographic Examinations

The samples to be used for metallographic examination were mounted in Koldmount self-curing resin. The oxide specimens were generally supported within a mounting ring by a quartz fiber which passed through the hole at one end of the sample. This assembly was then placed on a microscope slide and filled with the resin which hardened in about 30 minutes at room temperature. The samples were then polished on metallographic paper to expose the desired cross-section and finally lapped lightly on a wheel which was saturated with Linde A fine abrasive. Whenever any of the specimens required etching a 2% nital solution was used.

IV. EXPERIMENTAL RESULTS AND DISCUSSIONS

A. The Oxidation of Iron-Chromium Alloys

The oxidation of iron-chromium alloys containing 0.20, 0.88, 1.70, 5.70, 7.55 wt % chromium and a commercial Type 430 stainless steel containing 18.21 wt % chromium were oxidized in carbon monoxide-carbon dioxide mixtures of mole fractions of CO_2, N_{CO_2}, equal to 0.500, 0.600 and 0.700 over the temperature range 800° to 1100°C. The rate constants for the oxidation experiments under the above various conditions were obtained from a continuous recording of the gain in weight as a function of time.

The experimental results have shown that all of the above alloys oxidize in CO_2-CO mixtures with the same sequence of mechanisms. The first stage of the reaction is one of linear oxidation where the rate controlling step is a phase-boundary reaction at the oxide-gas interface. This occurs when the rate of diffusion of the metal ions through the oxide scale exceeds the rate at which oxygen ions can be supplied at the oxide-gas interface. This initial linear period is sometimes divided into a short first linear and a longer second linear reaction where the second linear is always the faster of the two rates. Pettit[27] has found that the rate of oxidation of pure iron during this first linear region is dependent upon the grain size of the metal substrate, while the value of K_{L_2}, the rate constant for the second linear region, is independent of the structure of the metal substrate. Furthermore, it was found that the first linear rate constants were not very

reproducible since the grain size of the metallic substrate varied from one specimen to another, and as the size of the metal grains increased, the rate of oxidation of the first linear also increased. As mentioned earlier, the rate of growth of wüstite on iron is dependent upon the orientation of the oxide crystals, and the first linear apparently results from the simultaneous growth of oxide crystals of all possible orientations. However, in time, the faster growing crystals are able to engulf the slower growing ones and the final rate of oxidation is that observed for the second linear rate which represents the rate of increase in thickness of the preferred wüstite crystals. This mechanism for the initial growth of a wüstite scale on iron was first suggested by Gulbransen et al,[28] and a number of investigators[27,29,30,31] have shown that wüstite with a (100) plane parallel to the metallic substrate exhibits the most rapid rate of growth.

Because the first linear rate was not observed in all of the oxidation experiments performed in the present study, and because it was not very reproducible even when observed, all linear rates mentioned in this study refer to the "second" linear rate, which was always present and reproducible.

As the oxidation reaction continues a critical oxide thickness is eventually reached where the phase-boundary reaction is no longer the slow step and diffusion of the metal ions through the wüstite layer becomes rate controlling. At this thickness, the initial linear rate transforms to the second stage of the reaction, and parabolic oxidation kinetics ensue.

Shown in Figure 17 are representative curves for the linear oxidation of 0.20 and 0.88 % Cr-Fe alloys and for the Type 430 commercial stainless steels, oxidized in a 60 vol % CO_2-CO mixture at different temperatures. The arrows indicate the time and oxide thickness at which linear oxidation kinetics transform to parabolic oxidation kinetics. The type 430 stainless steel, for example, oxidizes linearly for over 16 hours at 1100°C and until an oxide thickness of 2.8×10^{-2} cm. is reached.

Figure 18 shows the rate of oxidation of the 7.55 % Cr-Fe alloy in a 60 vol % CO_2-CO mixture at 1100°, 1000° and 900°C plotted both as linear ($\Delta m/A$ vs. time) and as parabolic [$(\Delta m/A)^2$ vs. time]. These types of kinetics are typical of the oxidation of iron-chromium alloys in CO_2-CO mixtures, and the weight gain as a function of time was plotted in this same manner for all of the oxidation experiments. The values of the linear and parabolic oxidation rate constants for the alloys oxidized under different conditions of gas mixture and temperature are listed in Table V.

During the following discussion, the experimental results of this oxidation study will be compared primarily with the results of Pettit[27] and Wagner *et al*[26] for the oxidation of pure iron in CO_2-CO mixtures and with the results of Birchenall *et al*[40] for the oxidation of iron-chromium alloys in oxygen.

Under the oxidizing conditions used in the present study, wüstite is the only iron oxide formed. The oxide formed on the alloys which contained chromium in an amount less than the solubility limit of chromium

in wüstite is a single phase oxide. For the alloys with a chromium content in excess of this solubility limit, a two-layered oxide scale is formed where, in accordance with the Fe-Cr-O phase diagram and the relative positions of the free energies of formation of the oxides, the outer layer is identified as chromium-doped wüstite, and the inner layer is an iron-chromium spinel. Cross-sections of metal specimens which were converted completely to oxide are shown in Figure 19. By comparing the oxides of the alloys with Figure 19(a), which is a sample of pure wüstite formed by the oxidation of a coupon of the pure iron, it is seen that the oxide products of the alloys containing 0.20 and 0.88 % Cr are, for the most part, single phase oxides existing as Cr-doped wüstite, while for the scales on the alloys containing greater than 1.70 % chromium, two layers are visible which indicates that the solubility limit of chromium in wüstite has been exceeded.

1. Oxidation of the 0.20 wt % Cr-Fe Alloy--In order to study the effect of a trivalent ion on the oxidation kinetics of iron in CO_2-CO mixtures, pure iron doped with 0.20 wt % Cr was oxidized in gas mixtures of N_{CO_2} = 0.500, 0.600 and 0.700 over the temperature range 800° to 1100°C. From x-ray analysis, this amount of chromium has been found to be soluble in wüstite over the temperature range studied.

a. Linear Kinetics

Linear oxidation kinetics result when the rate of adsorption and/or the rate of dissociation of the CO_2 into CO and oxygen atoms or ions is slower than the rate of diffusion of the metal ions from the

metal/oxide interface through the oxide scale to the oxide/gas interface. Under the conditions where a phase-boundary reaction is the rate determining step, Wagner[63] has derived the equation where

$$\frac{\dot{n}}{A} = k P (1 + K) [N_{CO_2} - N_{CO_2}\ (equilib)] \qquad (50)$$

where $\dot{n}/A$ is the number of equivalents of oxide formed per unit area per unit time, k is the rate constant for the phase-boundary reaction, P is the sum of the partial pressure of the CO and CO_2, K is the equilibrium constant for iron, wüstite and the gas mixture, N_{CO_2} is the mole fraction of the CO_2 in the oxidizing gas mixture and N_{CO_2} (eq) is mole fraction of CO_2 in the CO_2-CO mixture which is in equilibrium with Fe-FeO at the specific temperature of the oxidation experiment. Since $\dot{n}/A$ is proportional to the linear reaction rate constant, K_L, it is seen that when P = 1 atm., K_L should be proportional to the mole fraction of CO_2 in the oxidizing gas mixture. Plots of K_L versus N_{CO_2} are shown in Figures 20 and 21 for the oxidation of the 0.20 % Cr-Fe alloy at various temperatures. These results show that the linear rate of oxidation is directly proportional to the mole fraction of CO_2 in the gas mixture and that the rate determining step of the oxidation process is a phase-boundary reaction which occurs at the wüstite/gas interface.

The temperature dependence of the linear reaction rate for each of the three gas mixtures is shown in Figures 22, 23 and 24. It is seen that the linear reaction rate constant follows an Arrhenius-type temperature dependence where the slope of the log K_L vs. $1/T$ curve

contains the activation energy for the phase-boundary reaction. Each of the three curves is seen to have a distinct break in the vicinity of 950° - 1000°C. The activation energy for the low temperature portion of the curve is found to be about 23 Kcal while that for the high temperature region is about 90 Kcal.

For comparison, the linear oxidation data for pure iron in a 60 vol % CO_2-CO mixture is also shown in Figure 23. There is a similar deviation in the curve, but it occurs at 923°C for the oxidation of pure iron while for the 0.20 % Cr-Fe the break is at 986°C. Also, while the activation energy for the low temperature region of the curve is about the same for both metals, 26.3 Kcal for pure Fe and 22.2 Kcal for 0.20 % Cr-Fe, there is considerable difference in the activation energies of the high temperature portion where values of 56.2 Kcal and 88.0 Kcal were obtained for pure Fe and the 0.20 % Cr-Fe alloy, respectively. A list of all of the activation energies for the linear oxidation is given in Table VI.

By substituting the values of $\dot{n}/A$, K, N_{CO_2}, and $N_{CO_2}(eq)$ into Equation (50), the value of k, (equiv./cm^2-sec) the rate constant for the phase-boundary reaction, can be obtained. The temperature dependence of this rate constant is identical to the curves in Figures 22 to 24 for log K_L vs. 1/T, and this is to be expected inasmuch as they both represent the temperature dependence of the phase-boundary reaction, i.e., the adsorption and/or dissociation of CO_2 into CO and oxygen.

b. Parabolic Kinetics

(1) Temperature Dependence--The temperature dependence of the parabolic rate constants for the oxidation of 0.20 % Cr-Fe in CO_2-0.500, 0.600 and 0.700 are also shown in Figures 22, 23 and 24, respectively. Also shown in Figure 23 is temperature dependence for the oxidation of pure iron under the same conditions. The activation energies for these oxidation reactions are given in Table VIII. From Figure 23 one can see that the parabolic oxidation of the 0.20 % Cr-Fe alloy proceeds, for the most part, at a rate somewhat faster than that for pure iron. There is, however, a deviation of the temperature dependence for the oxidation of the 0.20 % Cr-Fe alloy at 1000°C which is not observed for the oxidation of the pure iron. A similar deviation was observed for the oxidation of the alloy in a 50 vol % CO_2-CO mixture (Figure 22), but it was not present during the oxidation of the alloy in the 70 vol % CO_2-CO mixture shown in Figure 24. The possibilities for the existence of this break will be discussed later.

The parabolic rate constants for the oxidation of iron-chromium alloys containing 0.20, 2.00, 4.35, and 8.97 % Cr in oxygen have been calculated from the work of Birchenall et al.[40] and the logarithm of these values are plotted as a function of reciprocal temperature in Figure 33. These rates afford a good comparison for Fe-Cr alloys of similar chromium content which have been oxidized in CO_2-CO mixtures in the present study. It is seen that the rates of oxidation of these alloys in oxygen are considerably lower than that of pure iron, which oxidizes at nearly the same rate whether in oxygen or CO_2-CO mixtures.

The activation energies for the oxidation reactions at 1000°C and below in N_{CO_2} = 0.500 and 0.600, and for all the temperatures in the gas mixture of N_{CO_2} = 0.700, are 20.9, 19.6 and 25.6 Kcal respectively. Because the composition of the oxide at the oxide/gas interface is nearly constant over the temperature range for a fixed value of N_{CO_2}, and because the gradient of the vacancy concentration across the scale, during parabolic oxidation, is constant, the activation energies given above represent, according to Birchenall,[50] only the energy for movement, ΔH_m^*, of the iron ions through the wüstite lattice. Hauffe[10] has shown that the mobility of the electrons is about 10^3 faster than the rate of diffusion of the iron atoms, hence, their contribution to the activation energy for the rate-determining process should be negligibly small.

Himmel, Mehl and Birchenall[9] have obtained an activation energy of 29.7 Kcal for the self-diffusion of Fe^{55} in wüstite of constant composition (76.00 wt % Fe). The self-diffusion of iron in wüstite containing 76.20 wt % Fe has also been measured by Carter and Richardson[34], and they report an activation energy of 30.2 Kcal. For the oxidation of pure iron where wüstite was the only oxide formed, Engell[35] and Pettit[27] have obtained activation energies of 30.5 and 31.7 Kcal, respectively. These activation energies represent the enthalpy of movement of the iron ions through the wüstite lattice.

However, for the oxidation experiments, even though the concentration difference across the scale remains constant, the composition of the wüstite varies from that in equilibrium with iron on the iron

equilibrium with the gas mixture. Hence the activation energy represents an average value of the enthalpy of movement of iron ions across the wüstite scale of varying composition rather than than at a single composition.

(2) Pressure Dependence--The pressure dependence of the oxidation rate of the 0.20 % Cr-Fe alloy at various temperatures from 800° to 1100°C is shown in Figure 25. In this figure the logarithm of K_p is plotted as a function of 2 log (p_{CO_2}/p_{CO}). This, however, is equivalent to a plot of log K_p versus log p_{O_2} since in Equation (22) it was shown that p_{O_2} is proportional to $(p_{CO_2}/p_{CO})^2$. From Equation (35) we saw that for the oxidation of iron to wüstite, where complete dissociation of the electron holes and vacancies was assumed, K_p is proportional to $p_{O_2}^n$ where n = 1/6. For the oxidation of this chromium-doped alloy in CO_2/CO ratios of 1.00, 1.50, and 2.33 (N_{CO_2} = 0.500, 0.600 and 0.700) the value of n is seen to decrease from a value of 0.46 at 800°C to 0.23 at 1100°C. The theoretical value of n = 1/6 was not observed for any of the oxidation experiments. Except for the oxidation experiments performed at 1000°C, the decrease in the value of n is consistent from 800°C to 1100°C. This means that at the lower temperatures there is apparently a considerable amount of association between the electron holes and the vacancies and as the amount of thermal energy is increased, the association decreases. Both Richardson[64] and Hoar[65] have reported that there exists considerable association between the trivalent iron ions and the vacancies during the oxidation of iron.

For the pressure dependence where n = 1/2, we can write the

equation

$$2\ Fe + O_2 = 2\ FeO + V_{Fe}^{-} + \oplus \qquad (51)$$

then

$$K = \frac{[V_{Fe}^{-}] \cdot [\oplus]}{p_{O_2}} \qquad (51a)$$

and when $[V_{Fe}^{-}] = [\oplus]$,

$$[\oplus] = K^{1/2} \cdot p_{O_2}^{1/2} \qquad (51b)$$

and as shown by Equations (13), (14), and (35), $K_p \propto p_{O_2}^{1/2}$. Similarly, at 1100°C, one can postulate the oxidation reaction

$$Fe + 1/2\ O_2 = FeO + V_{Fe}^{-} + \oplus \qquad (51c)$$

where, by the same argument, $K_p \propto p_{O_2}^{1/4}$. In both of these equations the iron ion vacancy is assumed to be singly ionized rather than doubly ionized as written in Equation (31). Moore[66] has written an equation similar to Equation (51c) for the pressure dependence of the electrical conductivity of nickel oxide where he shows n = 1/4.

In deriving $K_p \propto p_{O_2}^{1/6}$ in Equation (29), the assumption was made in Equation (28) that $V_g >> V_m$. This is not true for the formation of wüstite on iron for, at 1000°C, wüstite in equilibrium with iron contains nearly 5 per cent vacancies and nearly 12 per cent at the FeO/Fe_3O_4 phase boundary. Hence, a one-sixth pressure dependence should

not be observed necessarily for the oxidation of an iron-based alloy, and the values of n shown in Figure 25 probably represent an accurate pressure dependence for the parabolic oxidation rates.

When the oxidation of a metal is carried out under the conditions of constant oxygen partial pressure, over a range of temperature, the activation energy should include the enthalpy of formation of ionic and electronic defects, ΔH_f, in addition to the enthalpy of movement, ΔH_m^*. This results because the composition of the oxide at the oxide/gas interface does not remain constant as the temperature is changed. An example of the change in the composition of wüstite with temperature at a constant oxygen partial pressure of 6.83×10^{-14} atm. is shown in Figure 8. Because wüstite exists at constant oxygen pressure over only a very small range of temperature, oxidation experiments were not performed under these conditions. However, it is still possible to obtain the values of ΔH_f by using Equation (35) where it was shown that

$$K_p = A\, p_{O_2}^{1/6} \exp\left\{-\left(\frac{\Delta H_f}{3} + \Delta H_m^*\right)/RT\right\} \qquad (35)$$

Since K_p has been obtained as a function of oxygen partial pressure (Figure 25), and if we use the average dependence of $p_{O_2}^{1/3}$, we can write

$$K_p/p_{O_2}^{1/3} = A \exp\left\{-\left(\frac{2\Delta H_f}{3} + \Delta H_m^*\right)/RT\right\} \qquad (36)$$

and a plot of the logarithm of $(K_p/p_{O_2}^{1/3})$ versus reciprocal temperature

should yield an activation energy which includes ΔH_f and ΔH_m. Such a plot is shown in Figure 26 where the activation energies ($\frac{2\Delta H_f}{3} + \Delta H_m$), are equal to -23.9, -25.9, and -20.4 Kcal for the oxidation of the 0.20 % Cr-Fe alloy in the 50,60, and 70 vol % CO_2-CO mixtures, respectively. By substituting the values of ΔH_m obtained earlier into the above expression, we get the enthalpy of formation of the ionic and electronic defects in wüstite, ΔH_f, to equal -67.2, -63.2, and -69.0 Kcal, or an average value of -66.5 Kcal. The enthalpy of formation for the conditions stated above, i e., for a change in composition of the wüstite at the wüstite/gas interface with temperature, thus represents the partial molar enthalpy of mixing of oxygen in the wüstite lattice, $\Delta \bar{H}^m_{1/2\ O_2}$, for the reaction

$$2\ Fe^{++} + 1/2\ O_2 = 2\ Fe^{+++} + O^{=} + V_{Fe} \qquad (53)$$

It is also possible to obtain the enthalpy of formation from a determination of the deviation from stoichiometry over a range of temperatures at constant oxygen pressure. The measurements are difficult unless the deviations are large, however Darken and Gurry[8] were able to determine that ΔH_f = -63.7 Kcal for wüstite. Other values of ΔH_f for reaction (53) are -28 Kcal (Birchenall, et al[9]), -17 Kcal (Hauffe[10]), and -26.0 Kcal (Pettit[27]). Moore[68] has calculated the theoretical value of ΔH_f to be -56 Kcal.

2. Oxidation of the 0.88 and 1.70 % Cr-Fe Alloys--The oxidation of iron-chromium alloys containing 0.88 and 1.70 wt % chromium was

performed in a 60 vol% CO_2-CO mixture over the temperature range 900 to 1100°C. Under these conditions X-ray analysis indicated that wüstite was the only oxide formed on the 0.88 % Cr-Fe alloy. However, on the 1.70 wt% Cr-Fe alloy the scale formed exhibited two layers, a thick outer layer of wüstite and a thin inner layer of spinel and wüstite. After the specimen was completely oxidized, as shown in the cross-section of Figure 19(d), it was possible to separate the two layers with a razor blade and sufficient material could be obtained from the inner layer for X-ray analysis. During the oxidation reaction a non-equilibrium condition apparently existed where the spinel was able to form, because after the oxide scale of a 1.70 % Cr-Fe alloy was equilibrated at 1000°C in the gas mixture, for 120 hours, an X-ray powder pattern of the inner scale showed only a very faint trace of the existence of iron-chromium spinel. Conductivity measurements, which will be discussed later, showed that 0.67 wt% Cr is soluble in FeO above about 860°C (formed by the oxidation of 0.88 % Cr-Fe metal), and 1.30 wt% Cr is soluble in FeO above about 925°C (formed by the oxidation of 1.70 % Cr-Fe metal).

a. Linear Kinetics

The temperature dependence of the linear rate of oxidation of the 0.88 % and the 1.70 % Cr-Fe alloy is shown in Figure 27. For comparison, the linear rate of oxidation of pure iron is also shown. It is seen that the addition of chromium causes a decrease in the rate of the phase-boundary reaction. The activation energies obtained for these two regions are given in Table VI. A discussion and analysis

of these results is given in Part 6 of this section.

b. Parabolic Kinetics

The temperature dependence of the parabolic rate of oxidation of the 0.88 % Cr-Fe alloy in a 60 vol% CO_2-CO mixture is shown in Figure 28. With exception of the anomaly at 1000°C and at 1050°C, the rate of oxidation of this alloy is more rapid than that of pure iron. Of three oxidation experiments carried out at 1000°C only one was faster than that of pure iron and near the expected value shown by the curve drawn by the method of least squares. The other two rates at 1000°C were actually slower than the rate of oxidation of the same alloy at 960°C. Likewise, the rate of oxidation of two specimens at 1050°C was slower than the expected value. A possible reason for this deviation is discussed later.

The rate of parabolic oxidation of the iron-chromium alloy containing 1.70 % chromium is shown in Figure 29, and it is seen that at every temperature studied, the rate of oxidation of this alloy is more rapid than that of pure iron. Of significance is the fact that no deviation or break in the rate of oxidation as a function of temperature was observed during the oxidation of this alloy. This fact will be important in the later discussion of the occurrence of the deviation observed at about 1000°C in the oxidation of the more dilute Fe-Cr alloys.

The activation energies calculated from the least squares curves for the oxidation of the 0.88 % Cr and 1.70 % Cr-Fe alloys are 35.2 and 35.4 Kcal, respectively, while that for pure iron under the same

conditions is 33.0 Kcal. Since under these oxidizing conditions the activation energy represents essentially only the enthalpy of movement of the metal ions across the oxide scale, it is possible to infer that the rate controlling step of the parabolic oxidation of these alloys is diffusion of the metal ions through the outer wüstite layer. There is perhaps a small contribution to the activation energy as a result of the formation of a small amount of spinel in the wüstite scale.

3. Oxidation of the 5.70 % Cr-Fe Alloy--Oxidation experiments were carried out on a 5.70 wt% Cr-Fe alloy in a 60 vol% CO_2-CO gas mixture at 850°, 900°, 1000°, 1050° and 1100°C. Both the initial linear and subsequent parabolic regions were observed. The oxide scale formed was two-layered, as shown in Figure 19(e), where the outer layer was identified as wüstite and the inner layer was iron-chromium spinel. Figure 30 shows the oxide scale on the alloy substrate where, again, both layers are visible.

The temperature dependence of the linear rate is shown plotted in Figure 31. The rate is seen to be slightly slower than the linear rate of oxidation of the 0.88 % Cr-Fe alloy which is also shown for comparison. This trend toward a decrease in the linear rate with increased chromium content in the alloy is similar to that shown in Figure 27 for the linear rates of oxidation of the 0.20 and 0.88 % Cr-Fe alloys.

The temperature dependence of the parabolic oxidation rate for this alloy is shown in Figures 29 and 33. Again the rate of oxidation

of this alloy is seen to be faster than that of pure iron in the same CO_2-CO mixtures and considerably faster than the rate of oxidation of all of the iron-chromium alloys which were oxidized in oxygen.[4] The activation energy for oxidation of this alloy at essentially constant composition is 31.5 Kcal which again indicates that diffusion of the metal ions through the wüstite scale to the oxide/gas interface is the rate determining step of the oxidation reaction.

4. Oxidation of the 7.55 and 18.21 % Cr-Fe Alloys--An iron-chromium alloy containing 7.55 wt% Cr and a Type 430 commercial stainless steel containing 18.21 % Cr were oxidized in a 60 vol% CO_2-CO mixture. From the cross-sections shown in Figure 19(f) and (g), it is seen that an outer layer which was identified as wüstite is formed over a thick inner layer of spinel.

Both alloys oxidized according to an initial linear rate and a subsequent parabolic rate, as shown in Figure 18 for the 7.55 % Cr-Fe alloy, and in Figures 17 and 32 for the 18.21 % Cr-Fe alloy. The values of the rate constants obtained at the various temperatures are given in Table V. The temperature dependence of the linear rate constants for these alloys is shown in Figure 31. The linear rate of oxidation of the 7.55 % Cr-Fe alloy was slower than that of the 0.88 % Cr-Fe alloy, which is also shown for comparison, and nearly the same as the 5.70 % Cr-Fe alloy. The rate of oxidation of the 18.21 % Cr-Fe alloy is seen to be considerably slower.

The temperature dependence of the parabolic rate of oxidation

is shown in Figures 29 and 33 for the 7.55 % Cr-Fe alloy and in Figure 33 for the 18.21 % Cr-Fe alloy. Both alloys oxidized at a rate slower than that for pure iron but the 7.55 % Cr-Fe alloy still oxidized at a rate considerably faster than all of the Fe-Cr alloys studied by Birchenall et al[40] in pure oxygen. At high temperatures the 18.21 % Cr-Fe alloy oxidizes in a CO_2-CO mixture at a rate about comparable to those for the 0.20, 2.00 and 4.35 % Cr-Fe alloys in O_2 but somewhat slower at the lower temperatures. However, in the CO_2-CO mixture the rate of oxidation is seen to be much faster than the rate of oxidation of the 8.97 % Cr-Fe alloy in oxygen. Ratios of the rate constants for the oxidation of Fe-Cr alloys in a 60 vol% CO_2-CO mixture to those in pure oxygen are shown in Table VIII for experiments conducted at the same temperatures on alloys of nearly the same chromium content.

The activation energy for the oxidation of the 7.55 % Cr-Fe alloy is 33.2 Kcal. This value is nearly the same as that found for pure iron and for the alloys which contained less chromium. However, the activation energy for the parabolic oxidation of the 18.21 % Cr-Fe alloy is 91.8 Kcal which is near the value of 110.5 Kcal which was calculated from the rate of oxidation of the 8.97 % Cr-Fe alloy in oxygen after Birchenall et al.[40]

5. The Transition from Linear to Parabolic Kinetics--During the oxidation of the iron-chromium alloys in CO_2-CO mixtures, there is a critical oxide thickness at which the diffusion of the metal ions through the scale layer becomes rate determining, and, subsequently, parabolic oxidation kinetics are observed. As mentioned in Section

II-4, this transformation actually occurs over a small range in thickness. In Equation (37c) this thickness was shown to be dependent upon the linear and parabolic rates of oxidation. The oxide thicknesses (as gm/cm^2) at which the observed rate was no longer linear, at which the observed rate became parabolic, and the average of these two values are listed in Table IX for all of the alloys studied. For comparison, the calculated transition thickness given as $K_p/2\ K_L$ in Equation (37c) is also listed. The agreement is seen to be quite good.

From Equation (38c) the transition thickness was shown to be temperature dependent and to be a function of the differences between the activation energies for linear and parabolic oxidation. The temperature dependence of the transition thicknesses for the 0.20% Cr-Fe alloy in the different CO_2-CO mixtures is shown in Figure 34 and corresponding plots for the 0.88, and 1.70, and 5.70, 7.55 and 18.21 % Cr-Fe alloys are presented in Figures 35 and 36. The transition thicknesses for pure iron are also shown, and in every instance but one, the iron-chromium alloys oxidized linearly to a greater oxide thickness than did pure iron. This would be expected since it has been seen that for the low chromium alloys studied, the linear rate is slower and the parabolic rate is for the most part, faster than that for pure iron.

The deviation in the transition thickness in the vicinity of 950° - 1000°C would be expected also since a large change in the activation energies for linear oxidation was observed at about this temperature. The differences between the activation energies for parabolic

and linear oxidation, and approximate values obtained from the curves of $\log (\Delta m/A)_{tr.}$ vs. 1/T are listed in Table X. Agreement between these values is, however, not particularly good, and only a trend can be inferred.

6. Discussion and Analysis

a. Linear Kinetics

It has been shown that the rate determining step during the linear oxidation of iron-chromium alloys is due to a phase boundary reaction at the wüstite/gas interface. This rate of oxidation also has been shown to be a linear function of the mole fraction of CO_2 in CO_2-CO mixtures for values of N_{CO_2} greater than the value in equilibrium with iron and wüstite at a given temperature. This necessarily means, therefore, that the rate controlling reaction must be the adsorption and/or dissociation of CO_2 into CO and oxygen atoms or ions. It should be possible to deduce the probable mechanism because at any one time only one of the following reactions should be rate-controlling.

$$CO_2\ (gas) = CO_2\ (adsorbed) \tag{54}$$

$$CO_2\ (ads.) = CO\ (ads.) + 1/2\ O_2\ (ads.) \tag{55}$$

$$1/2\ O_2\ (ads.) + 2\ominus = O^{=}\ (ads.) \tag{56}$$

$$O^{=}\ (ads.) + 2Fe^{++} = 2Fe^{+++} + O^{=} + V^{=}_{Fe} \tag{57}$$

Smeltzer[25] in a study of the mechanism of the linear oxidation of iron in pure CO_2 observed a break in the Arrhenius plot in the vicinity of 920°C. He obtained an activation energy of 28.8 Kcal for the low temperature region, and since this value is close to that for vacancy diffusion, he concludes that this is equivalent to vacancy formation in the vicinity of an adsorbed oxygen ion, hence he attributes the rate controlling step, below 920°C, to be the incorporation of oxygen into wüstite as given by Equation (57) above. This is incorrect because the enthalpy of vacancy diffusion, ΔH_m^* is not the same as the enthalpy of formation of a vacancy, ΔH_f, in Equation (52), and the two values represent the enthalpies for two entirely different processes. For the activation energy above 920°C, Smeltzer obtained a value of 50.5 Kcal which is considerably larger than the value of 30 Kcal found for vacancy diffusion. Since the dissociation energy of CO_2 in reaction (55) is 67.6 Kcal, he concludes that the rate controlling process for linear oxidation above 920°C is the dissociation of carbon dioxide and incorporation of chemisorbed oxygen into wüstite.

The basic premise of the rate of linear oxidation controlled by the rate of chemisorption of the gases on wüstite of different orientations on α and γ-Fe was originally proposed by Hauffe and Pfeiffer.[24] Pettit[27] has disputed this reaction mechanism, and the one of Smeltzer, and he has proposed that the change in the activation energy of the process is dependent upon the slope of the Fe-FeO phase boundary as a function of temperature. At any given temperature, the composition of the wüstite is that in equilibrium with iron, and he proposes that

above about 900°C where the oxide composition does not vary appreciably with temperature, the activation energy involves only the heat of dissociation of CO_2, while below 900°C, where the wüstite composition changes rapidly with temperature, the activation energy for the process is the sum of the enthalpy of defect formation and the energy of dissociation of CO_2. During the linear oxidation of pure iron (99.999 + % Fe). Pettit obtained an activation energy of about 52 Kcal above 923°C, and about 26 Kcal below this temperature. He attributes the difference between these two values (-26 Kcal) to the energy of formation of a vacancy plus two holes according to reaction (57).

The mechanism suggested by Pettit for the rate controlling reaction during linear oxidation of iron below about 900°C is also not acceptable for several reasons. If the activation energy obtained for this range of temperatures includes an enthalpy of formation term, then oxidation experiments performed as a function of temperature, under conditions where diffusion of iron is rate-controlling across a wüstite layer which is held at constant composition at the wüstite/gas interface, would also yield an activation energy composed of both ΔH_f and ΔH_m^* terms. All experiments on the oxidation of pure iron and iron-alloys under these conditions yield only ΔH_m^*, the enthalpy of movement of the iron ions, and no ΔH_f term. Also, it is believed that the value of -26 Kcal does not represent the actual value of ΔH_f, the enthalpy of formation of reaction (57). The value of ΔH_f has been found, in the present work, to be -66.5 Kcal, in agreement with that of Darken and Gurry.

In the present study, the activation energy for the high temperature region has been observed to vary from about 70 Kcal for the 0.20% Cr-Fe alloy to 45 Kcal for the 1.7% Cr-Fe alloy, while for the low temperature region, the activation energy was constant at about 26 Kcal for the linear oxidation of all alloys. If the activation energy contains an enthalpy of formation term, then this means that ΔH_f must necessarily change for wüstite of different chromium contents. However, from conductivity measurements, to be discussed later, the value of ΔH_f has been found to be independent of the chromium content in wüstite, and to agree very closely with the value obtained from the oxidation of the alloys.

It is proposed, therefore, that the rate controlling step during linear oxidation of iron over the entire temperature range is simply that of adsorption and/or dissociation of the gases on the wüstite surface. Reaction (56) can be eliminated immediately as one of the possible reactions because it has been observed that as the chromium content is increased, the linear rate decreases (See Figure 2?), and if Reaction (56) were rate controlling, the linear rate would be expected to increase as the concentration of excess electron holes decreased (or $\ominus$ increased) by the addition of chromium. Thus, by inference, the rate controlling reaction at low temperatures is believed to be reaction (51) and that at the higher temperatures, above 950° - 950°C, to be reaction (55). The heat of adsorption on MO_2 has been reported as 28 Kcal, 42 Kcal, and 18 Kcal on $NiO^{[2,3]}$, $CoO^{[3]}$ and Cr_2O_3[70], respectively. The value on FeO appears not to have been

published, but should not vary appreciably from the above values. The average experimental value of 26 Kcal for the low temperature region fits nicely within this range. Although, at the moment, little can be said about the effect of the different orientations of wüstite on α and γ-Fe on the heat of adsorption and degree of coverage of the gases on the oxide surface, the possible effects of this variable cannot be eliminated.

b. Parabolic Kinetics

In CO_2-CO mixtures, the rates of oxidation of Fe-Cr alloys containing 0.20, 0.88, 1.70 and 5.70 wt.% Cr have been shown to be faster than that of pure iron under the same conditions. In these gas mixtures wüstite is the only stable iron oxide, and the rate controlling step during the oxidation of these alloys is the diffusion of metal ions through this chromium-doped wüstite layer. From Equation (15) it is seen that the incorporation of chromium leads to an increased cation vacancy concentration, hence the rate of oxidation is increased until a new oxide phase is formed in sufficient quantity such that the rate of diffusion across this new phase becomes rate determining.

Under conditions where the activation energy represents only the enthalpy of movement of the metal ions through the wüstite layer, this value has been found to be about 22 Kcal, somewhat less than the 29.7 and 30.2 Kcal reported for the self-diffusion of Fe^{55} through wüstite,[9,34] and the 33 Kcal obtained for the oxidation of pure iron under the same conditions.[27] This decrease in the value of $\Delta H_m^{\ddagger}$ appears to reflect the effect of the increase in the vacancy concentration caused

by the soluble chromium, and is in agreement with the predictions of Birchenall et al,[9] but not with their measurements, where they observed the opposite trend. A decrease in $\Delta H_m^{\ddagger}$ with an increase in the vacancy concentration has also been found in the present work on the measurements of the chemical diffusion coefficient of vacancies in wüstite.

The deviation in the Arrhenius plot at about 1000°C which was observed for the oxidation of the 0.20% Cr-Fe alloy in the gas mixtures where N_{CO_2} was equal to 0.500 and 0.600, and for the 0.88% Cr-Fe alloy in N_{CO_2} = 0.600 appears to be an anomaly inasmuch as it was not observed in the Arrhenius plots for the oxidation of any of the other alloys under the various experimental conditions. A number of investigators have observed similar changes in the temperature dependence of the rate of oxidation of both relatively pure metals and alloys. Gulbransen and Andrew[71] observed an increase in the activation energy at 950°C for the oxidation of chromium, and they conclude that at this temperature the rate of evaporation of Cr from the metal exceeds the rate of diffusion, and the metal vapor can penetrate through the film and enhance the normal oxidation process. Similar mechanisms were postulated to account for deviations observed during the oxidation of beryllium,[72] and alloys of Fe-Cr[73] and Ni-Cr.[74] It is doubtful that this mechanism can account for the changes observed in the present work because they were observed only on the alloys with the lowest chromium content where the vapor pressure of Cr would be extraordinarily low.

The presence of impurity elements in iron have been shown to exhibit a marked effect upon the oxidation kinetics. Tylecote[75] has

shown that foreign atoms in wüstite cause a decrease in its plasticity and, consequently, tend to reduce the adherence at the iron/wüstite interface. Paidassi[76] and Moreau[77] have also shown that the impurities tend to decrease the adherence of wüstite by accumulating at the metal/oxide interface and increasing the stresses at this point. Peters and Engell[78] have shown that impurities which form oxides with higher free energies of formation than iron also reduce the adherence of wüstite on iron. An occurrence of this type is believed to be the cause of the change in rate shown in Figure 28 where the loss of adherence could impede the transfer of metal ions from the metal into the wüstite lattice.

Foley[79] has observed a deviation in the activation energy in the range 800° - 900°C during the oxidation of Fe-Ni alloys in oxygen-nitrogen-water vapor gas mixtures, and he has interpreted the results in terms of changes in the physical condition of the oxide film. Gulbransen[73] has proposed also that a transformation in the oxide crystal structure was responsible for an observed change in rate during the oxidation of a Type 304 stainless steel in oxygen at 0.1 atm. pressure. Such changes in the oxidation kinetics of the high-chromium alloys as a function of temperature were not observed in the present study.

A problem of practical importance often observed during the oxidation of high-chromium stainless steels in oxygen-rich atmospheres is that of a "break-away" of the oxide and a subsequent acceleration in the rate of oxidation until a new protective scale layer is formed.

oxidation of Fe-Cr alloys in oxygen by Birchenall et al.,[47] who found Cr_2O_3 as an outer layer on all of the scales, and also as an inner layer on most. The intermediate layer was an iron-chromium spinel. The oxide product on Fe-Cr alloys containing greater than about 13% Cr has been found, in nearly every study, to be only Cr_2O_3. Thus under conditions where an excess supply of oxygen is available, the chromium apparently is selectively oxidized to form Cr_2O_3, and since diffusion through this layer is about 10^{+7} slower than through wüstite, the subsequent oxidation kinetics are much slower. Only in the initial few minutes of the oxidation reaction did Birchenall find that the rates of oxidation of the Fe-Cr alloys were faster than that of pure iron. This would seem to indicate, however, that wüstite was present initially.

Based on the above observations, Birchenall thus concluded that the functions of Cr during the oxidation of Fe-Cr alloys in oxygen-rich atmospheres is to reduce the rate of growth of the wüstite phase by decreasing its range of stability, and if enough Cr is present, to eliminate wüstite as an oxide product. Obviously, this is not true for Fe-Cr alloys oxidized in CO_2-CO mixtures where the partial pressures of oxygen are those in equilibrium with the wüstite phase. From lattice parameter measurements, oxide equilibration, and electrical conductivity data in the present study, it has been observed that as much as 1.30 wt.% Cr dissolved in wüstite does not appreciably change the limits of the wüstite phase. Fujii and Meussner[81] have oxidized a series of Fe-Cr alloys in a gas mixture of 90 vol.% argon - 10% water vapor at

700°, 900° and 1100°C. Under these conditions, magnetite is stable and formed as an outer layer, nevertheless, they also found that wüstite existed as a major product on the alloys containing up to 15% Cr.

Thus when Fe-Cr alloys are oxidized under very low partial pressures of oxygen where a phase boundary process is the rate-controlling reaction, it appears that wüstite is formed initially and that the chromium is not selectively oxidized to Cr_2O_3. For chromium contents in the alloy which are greater than the amounts soluble in wüstite, the excess Cr partitions into the spinel phase which exists at the oxide/alloy interface in accordance with the Fe-Cr-O phase diagram and the oxidation potential diagram in Figure 4. This condition is seen to exist for the Fe-Cr alloys containing as much as 7.55 wt.% Cr. During the oxidation of the 18.21% Cr-Fe alloy, a layer believed to be Cr_2O_3 formed at the oxide/alloy interface, however, the equilibrated oxide (Figure 19) shows no evidence of a Cr_2O_3 phase. Apparently during the oxidation process a non-equilibrium condition exists which permits the formation of this inner phase by an accumulation of chromium in this region. It is doubtful that this enrichment could be caused by a depletion of chromium in the alloy because of the rapid rate of oxidation and because the rate of diffusion of Cr and Fe in Fe-Cr alloys is nearly the same.[82] Birchenall[40] has pointed out that the studies of Yearin et al[38] indicate that the iron ions diffuse more rapidly than the chromium in spinel approaching the composition $FeCr_2O_4$. This would leave a concentration of chromium ions in the

oxide layer near the alloy interface, and thus result in the observed layer of Cr_2O_3.

In Figure 37 the rates of parabolic oxidation of Fe-Cr alloys as a function of chromium content in a 60 vol% CO_2-CO mixture, as determined in the present study, are compared to the rates obtained by Birchenall et al[40] for the oxidation of similar alloys in pure oxygen. The ratios of the parabolic rate constants are shown also in Table VIII, and from these two presentations of data, it is seen that the rate of parabolic oxidation of Fe-Cr alloys is considerably faster in a CO_2-CO mixture than in pure oxygen.

c. The Mechanism of Oxidation of the Alloys when a Multilayered Scale is Formed.

When chromium-doped wüstite is the only oxide formed, the mechanism is relatively straight-forward in that the wüstite forms by the outward movement of metal ions and electrons. In most cases, the oxide is sufficiently plastic to maintain an adherent contact with the receding metal interface.

The formation of the two-layered oxide involves a more complicated mechanism which must be able to explain the formation of the porous inner spinel while diffusion across the wüstite is still rate controlling. A 0.005 inch platinum wire which was placed on the original surface of the alloy has been found to be located at the interface between the wüstite and the spinel layers. See Figure 30. This is in agreement with the observations of Fujii and Meussner, and also with Rahmel[83] who studied the scale formation on Fe-V, Fe-Cr, Fe-Si, and

Fe-Mo alloys oxidized in oxygen at 1000°C.

On the basis of the positions of the Pt markers, there must be preferred oxygen diffusion in the spinel phase and only iron ion diffusion through the wüstite layer. The diffusion of oxygen ions over lattice defects in wüstite can be excluded since all experimental evidence shows only diffusion of iron ions in wüstite during oxidation. A high rate of diffusion of oxygen ions through the spinel lattice is also very improbable. Maak and Wagner,[84] for the oxidation of Cu-Be alloys, observed a similar scale structure, and they concluded that the dense outer layer dissociated into gaseous oxygen and metal ions at the inner surface. Likewise, one sees that the outer layer of wüstite, in the present study, is dense and gas-tight, therefore, the gaseous oxygen must arise from a dissociation of the wüstite at the inner surface. The freed iron ions and electrons are able to diffuse, as the rate controlling step, through the wüstite to the oxide/gas surface. The gaseous oxygen is able either to react with cations at the outer surface of the spinel or to "diffuse" through the porous spinel to the alloy interface and react at that point. This dissociation of wüstite also accounts for the pores observed at the spinel/wüstite interface.

In order for wüstite to be observed as a final product in the outer surface oxide scale, and for the rate of oxidation to be determined by the diffusion through the wüstite lattice, the rate of transport of the iron and chromium ions across the spinel layer must necessarily be more rapid than the dissociation of the wüstite and

the diffusion of these cations through the wüstite. It is rather uncertain how this occurs since the bulk diffusion of cations through spinel is normally much slower than through wüstite.

The position of the platinum marker probably does not indicate the position of the original metal interface, however, because the spinel layer should increase in thickness by formation at both the metal and wüstite interfaces. Thus the position of original metal interface would lie at some point within the spinel layer.

This mechanism is in agreement with those suggested in the other studies on the oxidation of Fe-Cr alloys mentioned above, and it appears to be consistent with the results of the present study.

B. X-Ray Analysis of Pure and Doped Wüstite

The results of the lattice parameter measurements for both pure wüstite, prepared from zone-refined iron (99.999+% Fe), and wüstite doped with 0.67 wt.% chromium, prepared by the oxidation of 0.88 wt.% Cr-Fe alloy, are shown in Figure 38. Also shown for comparison are the values of a_o obtained by Jette and Foote[18] and the approximate values of a_o from the works of Willis and Rooksby[51] and Bénard.[52] The measured values of the lattice parameters for the pure wüstite in the present study are in excellent agreement with those of Jette and Foote.

The range of composition over which lattice parameters were measured was extended to the phase limits of the wüstite field at 1000°C as determined by Darken and Gurry.[8] These phase boundaries and those determined by Jette and Foote are indicated in Figure 38 by arrows.

The value of a_o has been found to decrease from 4.3110 Å at the Fe-FeO phase boundary to 4.2817 Å near the FeO-Fe_3O_4 boundary. These values are listed in Table XI.

The values of a_o for the most oxygen rich wüstite deviate from the indicated straight-line trend, and are larger than expected because of the precipitation of/eutectoid magnetite which occurs during cooling, regardless of the rate of quenching. When this magnetite forms, it does so at the expense of the oxygen content in the wüstite, according to the reaction

$$4FeO = Fe_3O_4 + Fe \qquad (58)$$

and the remaining wüstite actually has a higher iron content than that given by the composition. Jette and Foote, in their attempt to define the limits of the wüstite phase field, found that when wüstite was quenched directly from temperature into a mercury bath, the rate was still too slow to prevent the precipitation of magnetite.

The wüstite which was in equilibrium with iron was formed as a thin layer on an iron coupon, and then the reaction was stopped while still in the linear range. The CO_2-CO mixture was adjusted to a reducing potential and the reaction continued until small nuclei of iron were formed on the wüstite surface. The values of a_o for wüstite near the Fe-FeO boundary are smaller than expected, and this, again, is probably caused by an insufficient rate of quench where in this case, iron is precipitated from the wüstite lattice. Hence, these values of a_o probably indicate the composition of wüstite which is equilibrium

with iron at a temperature below 1000°C. From Figure 8 it is seen that the Fe-FeO phase boundary occurs at a larger oxygen content at the lower temperatures. In order to avoid these problems of precipitation of iron and magnetite, measurements of the parameter of wüstite should be carried out at temperature while in equilibrium with the various CO_2-CO mixtures. Measurements of this type have not been reported for any metal-oxygen systems.

A number of compositions of wüstite which were equilibrated at 1000°C in CO_2-CO mixtures in the present study are shown in Figure 39. The crosses indicate the limits of the wüstite phase field at 1000°C as determined by Darken and Gurry. Agreement between these two studies is seen to be very good. Also shown in Figure 39 are the equilibrium compositions of wüstite specimens which contain 0.67 wt.% Cr. It is seen that under the same conditions of temperature and equilibrating atmosphere, the chromium-doped samples contain a greater weight percentage of oxygen than do the pure wüstite specimens. This indicates that the effect of the addition of chromium into the wüstite lattice is to cause an increase in the vacancy concentration and a corresponding increase in the fractional oxygen content. From the data shown in Figure 39 and listed in Table XI, it is seen that the addition of 0.67 wt.% Cr causes an increase of about 0.13 wt.% in oxygen content over that of pure wüstite. This is equivalent to 0.69% more sites existing as vacancies on the cation lattice. The width of the wüstite field is seen not to be appreciably affected by the addition of chromium.

Shown also in Figure 38 are the values of the lattice parameters

as a function of oxygen content for the wüstite doped with 0.67 wt.% chromium. These values of a_o are considerably smaller (about 0.006 Å) than the corresponding values for pure wüstite of the same composition (wt.% oxygen) which also indicates that the chromium addition causes an increase in the number of vacancies, and a corresponding decrease in a_o similar to the effect of increased oxygen content of about 0.25 wt.% oxygen. From this data it would appear that about 1.3% more of the cation sites exist as vacancies.

Based on Equation (15) for the formation of one additional vacancy for the addition of every two chromium ions into the wüstite lattice, one would expect that the wüstite containing 0.67 wt.% Cr would exhibit an increase of about 0.47% in the number of cation sites existing as vacancies over that of pure wüstite having the same oxygen composition. This value is relatively close to that obtained from the equilibration data, however, the effect observed is greater in both cases than that expected.

It can be concluded that the effect of the incorporation of soluble chromium into the wüstite lattice is to cause a corresponding increase in the vacancy concentration. As seen in the last section on the oxidation of iron containing less than 6 percent chromium, this effect is manifested as an increase in the rate of oxidation under conditions where the rate-controlling step is the diffusion of metal ions through the chromium doped wüstite layer.

C. The Electrical Conductivity of Pure and Doped Wüstite

In an effort to determine further the effect of a dissolved ion on the defect structure of wüstite and to relate the electronic hole concentration to the linear kinetics observed when iron and iron-chromium alloys are oxidized in CO_2-CO mixtures, electrical conductivity measurements have been performed on pure wüstite, and wüstite doped with 0.67 and 1.30 wt.% chromium. The doped wüstite was prepared by the oxidation of iron alloys containing 0.88 and 1.70 wt.% chromium.

From the increase in the rate of oxidation of the low-chromium alloys over that of pure iron, and from the decrease in the lattice parameter of the doped wüstite as compared to pure wüstite of the same composition, it has been seen that the effect of soluble chromium in the wüstite lattice is to cause the formation of additional vacancies on the cation lattice. According to Equation (16) any increase in the vacancy concentration should cause a corresponding decrease in the electron hole concentration, and hence, a decrease in the electrical conductivity for experiments carried out on wüstite at any given temperature and oxygen partial pressure. In the present study, the wüstite doped with 0.67 wt.% Cr exhibited very little change in the electrical conductivity from that of pure wüstite, however, the sample doped with 1.30 wt.% Cr showed a small, but definite, decrease.

1. Pressure Dependence--The dependence of the electrical conductivity, σ, of pure wüstite, and wüstite doped with chromium, upon the equilibrium partial pressure of oxygen at [illegible] is shown in Figure 4[illegible]

Also shown are the two values of conductivity which Wagner and Koch obtained on pressed samples of FeO at 1000°C. The dashed line indicates the one-sixth dependence as predicted by Equation (40) for measurements made at constant temperature. It is seen that the conductivity measurements obtained in the present work follow approximately the ideal pressure dependence of the mass action law. This is in agreement with Smyth[7] and Hauffe[10] who have reported the 1/6 pressure dependence for the formation of vacancies and electron holes in wüstite. From the values of Wagner and Koch[54] (σ = 107 and 205 $ohm^{-1}cm^{-1}$ at p_{O_2} = 3.8 x 10^{-15} and 1.4 x 10^{-13} atm., respectively) the pressure dependence of σ is seen to be actually 1/5.5 and not 1/8 as they report. The values of σ at 1000°C for wüstite in equilibrium with various partial pressures of oxygen are listed in Table XII.

There is no apparent effect of chromium on the pressure dependence. This is expected from the reaction

$$Fe^{++} + 2Cr^{+++} + 1/2\ O_2 = 2Cr^{+++}_{(Fe)} + FeO + V_{Fe} + 2\oplus \qquad (59)$$

where the effect of soluble chromium is to cause the formation of additional-ionic and electronic defects, but according to the same 1/6 pressure dependence.

2. Temperature Dependence--From Equation (39) it was seen that when conductivity measurements are obtained as a function of temperature for wüstite of a constant composition, the activation energy represents the enthalpy of movement of the electron holes, $\Delta H^*_{m\oplus}$, through

the wüstite lattice. Such measurements have been performed on specimens of pure FeO, FeO + 0.67 wt.% Cr, and on FeO + 1.30 wt.% Cr where the nominal oxygen/metal ratio is 1.060. The results of these measurements are listed in Table XIII and are shown in Figures 41 and 42 where log σ has been plotted versus reciprocal temperature. The values of $\Delta H^{*}_{m\oplus}$ obtained from the slopes of these curves are 1.842 ± 0.009 Kcal for the pure wüstite, 1.939 ± 0.003 Kcal for the FeO + 0.67 wt.% Cr, and 2.201 ± 0.003 Kcal for the FeO + 1.30 wt.% Cr. The small increase in the values of $\Delta H^{*}_{m\oplus}$ is probably caused by the fact that the hole is more tightly bound to the $Cr^{++\oplus}$ than to the $Fe^{++\oplus}$.

Tannhauser[85] in a recent study of the resistance of wüstite and magnetite obtained an activation energy of 1.543 Kcal for the resistance of wüstite of constant composition as a function of temperature. Kuper[86] also has reported a value of $\Delta H^{*}_{m\oplus} \approx 2$ Kcal.

From these same measurements of conductivity at constant composition as a function of temperature, it has been possible also to determine certain solubility limits of chromium in wüstite. The values of conductivity shown in Figure 42 represent both the value measured immediately after cooling from the next higher temperature and the value of conductivity after 24 hours. At the higher temperatures, there was no change in conductivity with time, however, as the temperature was decreased, a point was reached where iron-chromium spinel began to precipitate as a second phase in the wüstite, and this caused the increase in the values of conductivity. At temperatures farther below this solubility limit, the change in conductivity is seen to be

quite marked. To confirm that this effect was caused by the formation of precipitated spinel, the sample of FeO + 1.30 wt.% Cr was converted completely to spinel by oxidizing it in pure CO_2. At 901°C, the conductivity increased from 105.5 $ohm^{-1}cm^{-1}$, when the chromium was soluble in wüstite, to 244.6 $ohm^{-1}cm^{-1}$ after the sample was completely converted to spinel. Thus, on the basis of the conductivity measurements shown in Figure 42, it can be concluded that 0.67 wt.% Cr is soluble in wüstite above about 860°C, and 1.30 wt.% Cr is soluble in wüstite above about 925°C.

Earlier it was seen that the enthalpy of formation of the ionic and electronic defects in wüstite could be obtained from oxidation experiments under oxidizing conditions where the oxygen pressure is held constant, or where the rate constant was known as a function of the oxygen partial pressure. Similar results can be obtained from conductivity studies where according to Equation (41),

$$\sigma = B\, p_{O_2}^{1/6} \exp\left\{-\left(\frac{\Delta H_f}{3} + \Delta H^*_{m\oplus}\right)/RT\right\} \qquad (41)$$

Thus one can obtain the quantity $\left[\frac{\Delta H_f}{3} + \Delta H^*_{m\oplus}\right]$ as the activation energy from a plot of ℓog σ versus 1/T at a constant oxygen pressure, or from a plot of ℓog $(\sigma/p_{O_2}^{1/6})$ versus 1/T at a constant CO_2/CO ratio. Conductivity measurements obtained by the first method are listed in Table XIV and shown plotted in Figure 43 for a constant p_{O_2} = 6.83 x 10^{-4} atm. where $(\frac{\Delta H_f}{3} + \Delta H^*_{m\oplus})$ = -20.7 ± 0.9 Kcal for the pure wustite and -20.4 ± 0.2 Kcal for wüstite doped with 1.30 wt % Cr. Figure 44 shows ℓog

($\sigma/p_{O_2}^{1/6}$) plotted versus 1/T for pure wüstite held in a constant CO_2-CO mixture where N_{CO_2} = 0.467. The values of σ measured by this method are listed in Table XV. The activation energy obtained from this curve is equal to -20.4 ± 0.2 Kcal, nearly the same as that from Figure 43, thus confirming that the two methods are equivalent. By this second method, the activation energy for the formation of defects and the movement of the holes is found to be -20.6 ± 0.1 Kcal and -20.5 ± 0.4 Kcal for FeO + 0.67 wt.% Cr and FeO + 1.30 wt.% Cr, respectively.

By subtracting the enthalpies of movement of the electron holes obtained from Figures 41 and 42 from the activation energies, $(\frac{\Delta H_f}{3} + H^*_{m\oplus})$, obtained from Figures 43 and 44, we get ΔH_f, enthalpy of formation of one vacancy and two electron holes for the reaction

$$Fe + 1/2\ O_2 = FeO + V''_{Fe} + 2\oplus \qquad (60)$$

The value of ΔH_f thus represents the partial molar enthalpy of mixing of one mole of oxygen into the wüstite lattice $\equiv \Delta\bar{H}^m_{\frac{1}{2}O_2}$. The average of the values obtained by the two methods are -66.6, -67.6, and -67.9 Kcal for pure wüstite, FeO + 0.67 wt.% Cr, and FeO + 1.30 wt.% Cr, respectively. Thus, while the enthalpy of movement of the electron holes increases slightly with the addition of soluble chromium into the wüstite lattice, the enthalpy of formation of the defects appears to be relatively unchanged. As a summary, these values of $\Delta H^*_{m\oplus}$ and ΔH_f are listed in Table XVI.

These values of ΔH_f obtained from the electrical conductivity studies agree quite closely to the average value of ΔH_f = -66.3 Kcal

obtained in the earlier section on the oxidation of the 0.20 wt.% Cr-Fe alloys, and to the value of $\Delta\bar{H}^m_{FeO_2}$ = -63.7 kcal of Darken and Gurry[8] for wüstite.

3. Comparison with Linear Oxidation--While the addition of 0.67 wt.% Cr appeared to have little effect on the measured value of electrical conductivity, the addition of 1.30 wt.% Cr caused a definite decrease in the measured value. From Equation (6) it was seen that at any given temperature, $[\oplus] \cdot [\ominus] = K$, thus the observed decrease in the concentration of holes should lead to a corresponding increase in the number of electrons. As emphasized in Section II-A1, it would be expected that the increased electron concentration in the chromium-doped wüstite would cause an acceleration in the phase boundary reaction if reaction (56) were rate controlling. The fact that this increase in electron concentration apparently does exist, and that the linear rate of oxidation of the alloys decreases, rather than increases, with added chromium content, adds further confirmation that the rate controlling reactions are ones of adsorption and dissociation of CO_2, reactions (54) and (55), rather than reactions (56) and (57) where a transfer of charges and the incorporation of oxygen ions into the wüstite lattice occurs.

D. Diffusion Coefficients from the Reduction and Oxidation of Wustite

1. Pure Wüstite--After the iron specimen had been completely converted to wüstite, the CO_2-CO mixture was adjusted so that the wüstite could be equilibrated at the desired initial composition in the

temperature of the specific reduction or oxidation run to be carried out. For all reduction experiments, the initial composition of the wüstite was 24.37% oxygen (oxygen/iron ratio = 1.125). From this initial O/Fe value, the reduction experiments were conducted, as a function of temperature in increments of 50°C from 900° to 1150°C, to final equilibrium O/Fe ratios of 1.100 (23.86 wt.% oxygen), 1.075 (23.55 wt.% oxygen), and to 1.050 (23.13 wt.% oxygen). Figure 8 shows the relative positions of these values of constant composition in relation to the boundaries of the wüstite field. When these predetermined initial and final compositions are used, the difference in concentration is constant regardless of the temperature at which the experiments are performed.

The weight of the wüstite sample equilibrated at O/Fe = 1.125 was 1.20283 gm ± 0.00005 gm. and after reduction experiments to O/Fe ratios of 1.100, 1.075 and 1.050 the decreases in weight were 0.00618 gm , 0.01324 gm. and 0.01967 gm., respectively. These changes in weight were reproducible to within 2.4%, 2.0%, and 0.05%, respectively, over the temperature range studied for both the reduction experiments and for the oxidation experiments back to the initial composition.

The oxidation experiments were carried out simply as the re-equilibration of the reduction experiments, i.e., from initial O/Fe values of 1.050, 1.075 and 1.100 to a final equilibrium value of O/Fe = 1.125.

It should be mentioned at this that while the ratio of CO_2 and CO used in these experiments to obtain the desired composition of wüstite

are those calculated from the work of Darken and Gurry, the actual wüstite compositions obtained for these ideal O/Fe ratios, as determined in this study are O/Fe = 1.1254 (24.38 Wt.% O), 1.101 (23.98 wt.% O), 1.074 (23.53 wt.% O) and 1.052 (23.15 wt.% O). This close comparison should suffice to confirm the accuracy of the work of Darken and Gurry and the results obtained with the equipment used in this study.

Examples of the type of rate curves obtained for the reduction of wüstite from an O/Fe ratio of 1.125 to 1.050 as a function of temperature are shown in Figure 45. The rate curves are shown plotted as a negative change in weight per unit area of the original metal specimen versus time. During the initial stages of the reduction and oxidation processes, i.e., from the time t = 0, until the process was about 30 percent completed, the kinetics obeyed the parabolic law. This is illustrated by plotting the values of $(\Delta m/A)^2$ versus time as shown in Figures 46 to 48. The values of K_p for the oxidation and reduction of wüstite are listed in Table XVII. Since the initial and final concentrations are fixed (AA′ and BB′ in Figure 10), the kinetics represent the steady-state diffusion between these two different concentrations. By plotting the logarithm of K_p versus reciprocal temperature, one can obtain the activation energy for diffusion between these concentration limits as shown in Figure 49. The activation energies obtained from the slopes of these curves are given in Table XVIII.

In arriving at the solution of Fick's law for the concentration

gradient in a thin slab exposed on both sides, Equation (43), one must make several assumptions which are (1) the validity of Fick's law of diffusion, (2) the diffusion coefficient is constant during the reduction or oxidation experiment, (3) the wüstite sample is of a uniform composition at the start of an experiment, (4) the diffusing element does not precipitate or take part in any phase change, (5) the cations are the only mobile species and diffusion is normal to the surface plane, and (6) the "excess concentration" falls essentially to zero at the surface at the start of the reduction or oxidation process. This last assumption is equivalent to saying that the diffusion of the cations is the rate controlling step rather than any phase boundary process, such as the adsorption of CO and/or desorption of CO_2 during a reduction experiment.

Figure 50 shows Equation (46) plotted as $-\log (1 - Q)$ versus Dt/a^2 where the quantity $(1 - Q)$ represents the fractional saturation or fractional completion of the diffusion process. The quantity Dt/a^2 contains the independent variables (diffusivity x time/length squared) and is dimensionless. Normally D is given in the literature in $cm.^2/sec.$ The theoretical values of Q and Dt/a^2 presented in Figure 50 were taken from a table given by Newman.[58] If the above assumptions are valid, experimental data obtained under conditions where diffusion is the rate controlling process will indicate a similar relation between $(1 - \Delta m/\Delta w)$ and time, t.

Curves for the experimentally obtained values of $-\log (1 - \Delta m/\Delta w)$ as a function of time are shown as Figures 51, 52 and 53 for the

reduction of pure wüstite from O/Fe = 1.125 to 1.050, 1.075 and 1.100. Figure 54 shows the experimental curves of $-\log (1 - \Delta m/\Delta w)$ versus t for the oxidation of wüstite from an initial composition of O/Fe = 1.050 to a final equilibrium value of 1.125. It is seen that these curves are very similar in appearance to the theoretical curve in Figure 50, and it may be concluded that the above assumptions and, hence, Equation (46) are valid for the reduction and oxidation of a wüstite slab. By measuring the slopes of these curves and by knowing the half-thickness, a, of the wüstite sample, one can obtain the value of D, the chemical diffusion coefficient of iron in wüstite, across these different concentration gradients as a function of temperature. The values of D obtained under these different conditions are listed in Table XVII.

A second method of obtaining the activation energies for diffusion across these different concentration limits is afforded by plotting the logarithm of D as a function of reciprocal temperature as shown in Figure 55. These activation energies for diffusion also are listed in Table XVIII.

2. Chromium-Doped Wüstite--The oxidation and reduction experiments of pure wüstite were performed in order that diffusion coefficients could be obtained, and to which diffusion coefficients obtained under the same conditions, but on doped wüstite, could be compared. One of the assumptions used in Equation (46) was that the diffusing element does not precipitate or take part in any phase

change. Thus if a specimen of iron doped with chromium is oxidized completely to wüstite, and if the solid solubility limit of chromium in wüstite is not exceeded, comparable diffusion coefficients can be obtained from reduction and oxidation kinetics carried out under the same experimental conditions. The diffusion coefficients obtained from wüstite doped with 0.67 wt.% chromium (formed from a specimen of 0.88 wt.% Cr-Fe) are listed in Table XVII and are shown plotted as log D versus reciprocal temperature in Figure 56. It is seen that in every instance the diffusion coefficients of the chromium-doped wüstite are lower than those obtained for the pure wüstite sample. It might at first be suspected that the slower rate of diffusion could be due to the formation of a small amount of iron-chromium spinel as a second phase. A number of investigators[9,50] have shown that the rate of self-diffusion of iron through the various spinels is about a factor of 10^3 slower than through wüstite. However, X-ray diffraction patterns of these chromium-doped wüstites show no evidence of a spinel phase, and the conductivity measurements on these same oxides have shown that a solid solution of chromium in wüstite exists above about 860°C. See Figure 42.

3. Discussion of the Results--According to all experimental observations, iron ion vacancies exist in the wüstite lattice, and the material transport which is necessary during the reduction or oxidation of wüstite occurs in the form of diffusion of iron ions and electrons via these vacancies and electron holes. The gradient of the vacancy

concentration can be considered, therefore, as the essential driving force for the material transport through the wüstite lattice. Since the mobility of the holes is approximately a factor of 10^3 greater than that of the vacancies,[10] it is proposed that the vacancy transport is essentially the rate determining step for the total reaction, and the measured values of D are the diffusion coefficients of the vacancies across the various concentration gradients. It is seen in Figure 55 that as one reduces to a wüstite composition which is more oxygen-rich (increased vacancy concentration) the value of D decreases, which is in direct contrast to the values of D^*_{Fe} of Birchenall et al,[9] which were found to increase in wüstite of increasing vacancy concentration. However, Engell[35] has calculated the values of D^*_v in wüstite from the experimental values of D^*_{Fe} of Birchenall et al, and he has found that at 800°C the value of D^*_v decreases with increasing vacancy concentration; at 897° and 983°C there was no concentration dependence.

Since the movement of a vacancy from one cation lattice site to an adjacent cation ion lattice site is dependent upon this adjacent site being occupied by an iron ion, it is easy to visualize that if the number of vacant sites were increased, the migration of any one vacancy would be impeded. Hence as the concentration of vacancies is increased, the diffusion coefficient of the vacancies decreases, as has been observed experimentally.

This will account also for the decrease in D observed for the chromium-doped wüstite samples. When a small amount of chromium is dissolved into the wüstite lattice, one can write the defect equation

$$3Fe + Cr_2O_3 = 2Cr^{+}_{(Fe)} + 3FeO + V^{\cdot\cdot}_{Fe} \qquad (61)$$

where $Cr^{+}_{(Fe)}$ is a trivalent chromium ion on an iron site, and $V^{\cdot\cdot}_{Fe}$ is an additional vacant cation site. From an X-ray study on these same chromium-doped wüstites, it has been determined that there is an increase of about 1.3% in the number of cation lattice sites which exist as vacancies. This is equivalent to an increase of about 25% over the vacancy concentration in pure wüstite with an oxygen/iron ratio of 1.050. Thus, under the same experimental conditions, one would expect the value of D to be correspondingly less for the diffusion of the vacancies in the doped wüstite as compared to the pure wüstite.

The values of D obtained in the present study from the reduction and oxidation kinetics of wüstite are about a factor of 10 to 20 times faster than the values of D^{*}_{Fe} in wüstite at the same temperatures. If, as suggested, the rate controlling step of the reaction is the diffusion of vacancies, the above fact can be rationalized by considering that for a vacancy to move, there must be an iron on a neighboring cation site, and vice versa. Since the number of cations as nearest neighbors to a vacancy is greater than the reverse condition, the vacancy is afforded the greater probability for migration. Brebrick,[87] as well as Wagner,[36] have shown that the ratio of the chemical diffusion coefficient to the self-diffusion coefficient is proportional to $1/N_v$ where N_v = the mole fraction of vacancies. For wüstite this ratio is very nearly to $x/(1 - x)$ where the value of x is given in the formula

Fe_xO for wüstite. At 1000°C this ratio is 20.85 at the Fe-FeO phase boundary and 7.14 at the FeO-Fe_3O_4 boundary.

The ratios of D, obtained in the present work, to D^*_{Fe}, from the work of Birchenall et al, are listed in Table XIX for 900° and 1000°C. The oxygen to iron ratio at which the comparison is made represents the final equilibrated composition of wüstite after a reduction experiment from the initial O/Fe ratio of 1.125, in the case of the measured value of D, and it represents the single composition of wüstite at which the value of D^*_{Fe} was obtained. The numbers in parentheses are the values of $x/(1 - x)$ for Fe_xO having the given oxygen-to-iron ratios. While there is deviation from the ideal value, it is obvious that the rate of diffusion of the vacancies across a concentration gradient occurs considerably faster than the rate of self-diffusion of iron, and the ratio of these rates can be correlated with the existing vacancy concentrations in the lattice.

The activation energy for the diffusion of a vacancy should be the same as that for the diffusion of an iron ion, and the activation energies obtained from the curves in Figures 55 and 56 and in Figure 49 are comparable to those reported from the measurements of self-diffusion of iron in wüstite and to those obtained for the oxidation of iron and iron-chromium alloys in CO_2-CO mixtures under conditions where the activation energy represents only the enthalpy of movement of the atomic defects.

V. DISCUSSION OF THE ERRORS

A. The Oxidation Studies

Because the gain in weight during the oxidation experiments in the present study was obtained as a continuous and automatic recording by the Ainsworth balance, the unpredictable human element of error was entirely eliminated. After every experiment for which the difference in the total weight gained between the weighings on the Mettler and Ainsworth balances exceeded 0.4 mg., the Ainsworth balance was re-adjusted against a standard 10 mg. weight which was provided with the balance. The average difference between the two weighings for the oxidation experiments was ± 0.29 mg. No error in time was detected even for experiments which lasted in excess of 300 hours.

Every precaution possible has been taken to minimize systematic errors. The CO_2 and CO flowmeters have been calibrated to within 1 % and the gases have been cleaned. Calibrated thermocouples were used in every instance, and the temperature of the specimen was held at ± 3/4°C of a constant value.

It is not possible to determine the magnitude of the effect of systematic errors on the rate constants, however, these errors cannot affect the values of the enthalpies of movement and formation of the defects; i.e., the activation energies. The random errors in the activation energies shown in the various tables represent the 80% confidence limits of the data.[88] This means that 80% of the time the limiting values of the activation energies so computed can be expected

to include the true value. Before the values of these limits were calculated, two assumptions were made (1) the error in the temperature is negligible and all of the random error is concentrated in the values of the rate constants, and (2) the random error in the values of the rate constants is independent of temperature.

Because the reduction and oxidation experiments of the wüstite samples were performed also with the Ainsworth apparatus, the above discussion can be applicable to these studies. The reproducibility of the weight changes and the agreement with the work of Darken and Gurry was emphasized in Section IV-D. The limits placed on the values of the activation energies of diffusion in Table XVIII also represent the 80% confidence limits.

B. X-Ray Studies

The composition of the wüstite samples was determined as wt.% oxygen according to Equation (47). All of the initial and final weighings were performed on a Mettler Type H15 analytical balance which has an accuracy of ± 0.05 mg. Hence the error in the composition of the wüstite samples used in the present study should be no greater than ± 0.02 wt.% oxygen.

Because the systematic errors in α, the value of the lattice parameter calculated from each line on the Debye-Scherrer powder pattern, approachs zero as θ approaches 90°, these errors may be eliminated by the use of the proper extrapolation function. In the present work, the value of α_o for a given composition of wüstite was obtained

by plotting a versus the Nelson-Reilly function, $\left(\frac{\cos\theta}{\sin\theta} + \frac{\cos\theta}{\theta}\right)$, and extrapolating to $\theta = 90°$. The random errors in a also decrease as θ increases because of the slow variation of $\sin\theta$ with θ at large angles. Since it is not feasible to calculate the average of the standard deviations of a_o from the individual plots of a versus the Nelson-Reilly function, the random error has been determined from the deviations of a_o from the straight-line portion of the curve in Figure 38. By making assumptions similar to the ones stated above, that the error in composition is negligible and that all of the random error is concentrated in the values of a_o, and that the random error in a_o is independent of composition, the standard deviation in the values of the lattice parameters listed in Table XI is ± 0.0007 Å. The random error within the 80% confidence limits is ± 0.0004 Å.

C. Conductivity Studies

Except for the chromium-doped samples where the precipitation of iron-chromium spinel was observed, all of the values of conductivity represent an average of no less than three readings obtained after the specimen was in equilibrium with the specific CO_2-CO gas mixture at temperature. Each measurement also represents the average of two readings obtained with forward and reverse current flow through the specimen. The difference between these two values of σ was less than 1.5%. The reproducibility of the values of σ under given conditions was within 3% in the present work. The probable errors in the enthalpies of movement and formation of the defects in Table XVI represent 80% confidence limits.

VI. SUMMARY AND CONCLUSIONS

In carbon dioxide and carbon monoxide mixtures, under conditions where wüstite is the only stable iron oxide, the rate of oxidation of Fe-Cr alloys containing 0.20, 0.88, 1.70, 5.70, 7.55, and 18.21 wt.% Cr is initially linear to a minimum oxide thickness of 5.4×10^{-3} cm. and to a maximum oxide thickness of 7.7×10^{-2} cm. The rate controlling step of the linear oxidation has been shown to be a phase boundary reaction at the wüstite/gas interface. Below about 950°C, the rate-determining process is believed to be the adsorption of CO_2, and above about 950°C, the reaction is believed to be the dissociation of adsorbed CO_2 into CO and oxygen. At a critical oxide thickness, which is dependent upon temperature and chromium content in the wüstite scale, the linear kinetics transform to parabolic kinetics where diffusion of the metal ions through the scale becomes slower than the rate of adsorption or dissociation of CO_2 on the surface. The parabolic oxidation kinetics of the Fe-Cr alloys containing 0.20, 0.88, 1.70 and 5.70 wt.% Cr have been shown to occur at a maximum rate of 1.5 times faster than that of pure iron in CO_2-CO mixtures. This increase in the rate of oxidation occurs because the effect of soluble chromium in the wüstite scale is to cause an increase in the equilibrium concentration of vacancies on the cation lattice which enhances diffusion of the metal ions via the vacancy mechanism. The increase in the vacancy concentration with the addition of chromium in the wüstite lattice has been confirmed from equilibrium composition determinations and from the

measured decrease in the lattice parameters of doped wüstite over that of pure wüstite.

The rate of oxidation of Fe-Cr alloys containing 7.55 and 18.21 wt.% Cr in CO_2-CO mixtures, while slower than that of pure iron, is considerably faster than the rate of oxidation of the comparable alloys in oxygen over the same temperature range. This occurs because the major portion of the scale consists of wüstite and an iron-chromium spinel, and the chromium is not selectively oxidized to chromic oxide (Cr_2O_3).

Under the same conditions of temperature and oxygen pressure, chromium-doped wüstite has a slightly lower value of electrical conductivity than that of pure wüstite. From these measurements, it has also been determined that 0.67 wt.% Cr is soluble in wüstite above about 860°C and 1.30 wt.% Cr is soluble in wüstite above about 925°C. The enthalpy of movement of an electron hole has been found to increase slightly with chromium content in wüstite with a oxygen/metal ratio = 1.060, where ΔH_m^* = 1.842, 1.939, and 2.201 Kcal, for pure wüstite, FeO + 0.67 wt.% Cr, and FeO + 1.30 wt.% Cr, respectively, while the enthalpy of formation of a vacancy and two electron holes has been observed to be -67.4 Kcal and independent of the chromium concentration in the wüstite. This value of ΔH_f is in very good agreement with the value of ΔH_f = -66.5 Kcal obtained from the oxidation studies on the 0.20% Cr-Fe alloy.

From reduction and oxidation experiments on slabs of pure and chromium-doped wüstite, it has been possible to obtain values of the

chemical diffusion coefficients of vacancies, which are the values of D for the propagation of a concentration gradient through a sample. These values of D are considerably faster than the values of the self-diffusion coefficients of iron in wüstite, and they are found to decrease with increasing vacancy concentration. This has been observed also in identical reduction and oxidation experiments on pure wüstite and wüstite containing 0.67 wt.% of soluble chromium.

ACKNOWLEDGMENTS

I wish to express my sincere thanks to Professor J. Bruce Wagner, Jr., my thesis advisor, for his advice and guidance during the course of this work.

I am indebted also to the following persons:

Dr. Frederick Pettit for his helpful comments during the initial stages of this research;

Professor C. N. J. Wagner (Yale University) and Professor J. B. Cohen (Northwestern University) for the use of their X-Ray laboratory facilities;

My student colleagues for their interesting discussions; and,

The United States Navy Postgraduate School for their financial assistance, and the Atomic Energy Commission under whose auspices the present work was sponsored.

Lastly, I give my most sincere thanks to my wife, Barbara, for the many hours which she spent tabulating and calculating data, and for her kind encouragement and generous moral support which she so ably provided.

BIBLIOGRAPHY

1. J. Frenkel, Ztch. Physik., 35, 652 (1926).

2. W. Schottky and C. Wagner, Ztch. Physik. Chem., B11, 163 (1931).

3. R. A. Swalin, Thermodynamics of Solids, Wiley, New York, 1962.

4. M. W. Davies and F. D. Richardson, Trans. Faraday Soc., 55, 604 (1959).

5. E. H. Greener and W. M. Hirthe, J. Electrochem. Soc., 109, 600 (1962).

6. E. H. Greener, D. Whitmore and M. Fine, J. Chem. Phys., 34, 1017 (1961).

7. D. M. Smyth, J. Phys. Chem. Solids, 19, 167 (1961).

8. L. S. Darken and R. W. Gurry, J. Am. Chem. Soc., 67, 1398 (1945); 68, 798 (1946).

9. L. Himmel, R. F. Mehl and C. E. Birchenall, Trans. A.I.M.E., 197, 827 (1953).

10. K. Hauffe and H. Pfeiffer, Ztch. Metallkunde, 44, 27 (1953).

11. F. Pettit and J. B. Wagner, Jr., to be published.

12. G. Gensch and K. Hauffe, Ztch. Physik, Chem., 196, 427 (1950).

13. C. Wagner and K. Zimens, Acta Chem. Scand., 1, 547 (1947).

14. E. J. W. Verwey, P. W. Hoayman and F. C. Romeyn, Chem. Weekblad, 44, 705 (1948).

15. K. Hauffe and J. Block, Ztch. Physik. Chem., 198, 232 (1951).

16. D. Fuller, Acta Met., 8, 743 (1960).

17. L. Pauling, The Nature of the Chemical Bond, Cornell University Press, Ithaca, N. Y., 1960.

18. E. R. Jette and F. Foote, J. Chem. Phys., 1, 29 (1933); Trans A.I.M.E., 105, 276 (1933).

19. A. Muan, Am. Journ. of Science, 256, 171 (1958).

20. J. Paĭdássi, Acta Met., 6, 184 (1958).

21. H. M. Davies, M. T. Simnad and C. E. Birchenall, Trans. A.I.M.E., 191, 889 (1951).

22. K. Fischbeck, L. Neundeubel and F. Saltzer, Ztch. Electrochem. und ang. physik. chem., 40, 517 (1934).

23. J. Bénard and J. Talbot, Comp. Rendus Acad. Sci., 226, 912 (1948).

24. K. Hauffe and H. Pfeiffer, Ztch. Electrochemie, 56, 390 (1952).

25. W. W. Smeltzer, Acta Met., 8, 377 (1960); Trans. A.I.M.E., 218, 674 (1960).

26. F. Pettit, R. Yinger and J. B. Wagner, Jr., Acta Met., 8, 617 (1960).

27. F. Pettit, Dissertation, Yale University, 1962.

28. E. A. Gulbransen and R. Ruka, J. Electrochem. Soc., 99, 360 (1952).

29. E. A. Gulbransen, W. R. McMillan and K. F. Andrews, Trans. A.I.M.E., 200, 1027 (1954).

30. R. F. Mehl and E. L. McCandless, Trans. A.I.M.E., 125, 531 (1937).

31. J. B. Wagner, Jr., K. R. Lawless and A. T. Gwathmey, Trans. A.I.M.E., 221, 257 (1961).

32. J. Bardolle, Revue de Met., 51, 833 (1954).

33. J. Bardolle and J. Bénard, Revue de Met., 49, 613 (1952).

34. R. E. Carter and F. D. Richardson, Trans. A.I.M.E., 200, 1244 (1954).

35. H. J. Engell, Acta Met., 6, 439 (1958).

36. C. Wagner, Atom Movements, p. 153, American Society for Metals, Cleveland, Ohio, 1951.

37. W. C. Hagel and A. U. Seybolt, J. Electrochem. Soc., 108, 1146 (1961).

38. H. J. Yearin, E. C. Randell and R. A. Longo, Corrosion, 12, 515 t (1956).

39. A. U. Seybolt, G. E. Report No. 59-RL-2265-M, August, 1959.

40. D. Lai, R. J. Borg, M. J. Brabers, J. D. MacKenzie and C. E. Birchenall, Corrosion, 17, 357 t (1961).

41. M. J. Brabers and C. E. Birchenall, Corrosion, 14, 179 t (1958).

42. H. M. McCulloch, M. A. Fontana and F. H. Beck, Trans. A.S.M. 43, 404 (1950).

43. D. Caplan and M. Cohen, Trans. A.I.M.E., 194, 1057 (1952).

44. J. Moreau, Comptes Rend., 236, 85 (1953).

45. H. Kobayashi and C. Wagner, J.Chem. Phys., 26, 1609 (1957).

46. C. Wagner, Ztch. physik Chemie, B21, 25 (1933).

47. J. S. Dunn, Proc. Royal Soc. (London), A111, 203 (1926).

48. N. F. Mott, Trans. Faraday Soc., 36, 472 (1940).

49. S. Glasstone, K. Laidler and H. Eyring, The Theory of Rate Processes, McGray-Hill, New York, 1941.

50. C. E. Birchenall, Metallurgical Reviews, 3, 235 (1958).

51. B. T. M. Willis and H. P. Rooksby, Acta Cryst., 6, 827 (1953).

52. J. Bénard, Ann. Chim., 12, 5 (1939).

53. K. Hauffe and J. Block, Ztch. physik Chemie, 198, 232 (1951).

54. C. Wagner and E. Koch, Ztch. physik Chemie, B32, 439 (1936).

55. R. R. Heikes and W. D. Johnston, J. Chem. Phys., 26 582 (1957).

56. S. P. Mitoff, J. Chem. Phys., 35, 882 (1961).

57. T. K. Sherwood, J. Ind. and Eng. Chem., 21, 12 (1929); Trans. A.I.Ch.E., 27, 190 (1931).

58. A. B. Newman, Trans. A.I.Ch.E., 27, 203 and 310 (1934).

59. H. Dunwald and C. Wagner, Ztch. physik Chemie., B24, 53 (1934).

60. T. E. Brower, B. M. Larsen and W. E. Shenk, Trans. A.I.M.E., 113, 61 (1934).

61. B. Serin and R. T. Ellickson, J. Chem. Phys., 9, 742 (1941).

62. J. Moser, Dissertation, Northwestern University (1961).

63. C. Wagner, Class notes, Course 3.23, Kinetics in Metallurgy, Massachusetts Institute of Technology, Spring, 1955.

64. F. D. Richardson, Disc. Faraday Soc., 4, 244 (1948).

65. T. P. Hoar, Disc. Faraday Soc., 4, 320 (1948).

66. J. S. Choi and W. J. Moore, J. Phy. Chem., 66, 1308 (1962).

67. W. J. Moore, J. Electrochem. Soc., 100, 302 (1953).

68. R. M. Dell and F. S. Stone, Trans. Faraday Soc., 50, 501 (1954).

69. F. S. Stone, Advances in Catalysis, 13, 1 (1962).

70. D. A. Dowden and W. E. Garner, J. Chem. Soc., p. 893 (1939).

71. E. A. Gulbransen and K. F. Andrew, J. Electrochem. Soc., 104, 334 (1957).

72. E. A. Gulbransen and K. F. Andrew, J. Electrochem. Soc., 97, 383 (1950).

73. E. A. Gulbransen and K. F. Andrew, J. Electrochem. Soc., 106, 294 (1959); 109, 560 (1962).

74. E. A. Gulbransen and K. F. Andrew, J. Electrochem Soc., 106, 941 (1959).

75. R. F. Tylecote, J. Iron and Steel Inst., 195, 135 and 380 (1960).

76. J. Paidassi, Bol. Soc. Chilena Quin., 7, 20 (1955).

77. J. Moreau, Rev. Met., 53, 703 (1956).

78. F. K. Peters and H. J. Engell, Arch. Eisenhutten., 30, 275 (1959).

79. R. T. Foley, J. Electrochem. Soc., 109, 278 (1962).

80. J. D. MacKenzie and C. E. Birchenall, Corrosion, 13, 783 t (1957).

81. C. T. Fujii and R. A. Meussner, N. R. L. Report 5506, Naval Research Laboratories, September 21, 1960.

82. V. T. Heumann and H. Böhmer, Arch. Eisenhuttenw., 31, 749 (1960).

83. A. Rahmel, Ztch. Electrochemie, 66, 363 (1962).

84. F. Maak and C. Wagner, Werkstoffe und Korrosion, 12, 273 (1961).

85. D. S. Tannhauser, J. Phy. Chem. Solids, 23, 25 (1962).

86. A. B. Kuper, unpublished research quoted in (50).

87. R. F. Brebrick, J. Applied Phy., 30, 811 (1959).

88. A. H. Bowker and G. L. Lieberman, Engineering Statistics, Prentice-Hall Inc., 1960.

TABLES OF DATA

TABLE I

Parabolic rate constants for the oxidation of iron and chromium in pure oxygen at various temperatures.

Temperature (°C)	K_p (Cr)* (gm^2/cm^4-sec)	K_p (Fe)** (gm^2/cm^4-sec)	$K_p(Cr)/K_p(Fe)$
700	8.22×10^{-15}	6.00×10^{-9}	1.37×10^{-6}
800	6.95×10^{-14}	5.70×10^{-8}	1.22×10^{-6}
900	3.20×10^{-13}	2.54×10^{-7}	1.19×10^{-6}
1000	4.93×10^{-13}	1.00×10^{-6}	4.93×10^{-7}
1100	5.28×10^{-11}	2.0×10^{-6}	2.64×10^{-5}

* Reference 70

** Reference 21

TABLE II

Analyses of the zone-melted, high-purity electrolytic iron used in the present study**

The amounts are given as parts per million
(1 ppm equals 0.0001 atomic per cent)

Aluminum	15	Manganese	< 0.1
Antimony	< 5 ND*	Molybdenum	< 5 ND
Arsenic	< 5 ND	Nickel	20
Beryllium	< 0.2	Nitrogen	< 1
Boron	< 5	Oxygen	17
Cadmium	< 5 ND	Phosphorus	9
Calcium	<10 ND	Silicon	10
Carbon	<10	Sulfur	12
Chromium	5	Tin	< 5 ND
Cobalt	5	Titanium	< 1 ND
Copper	7	Tungsten	< 5 ND
Hydrogen	0.3	Vanadium	< 1 ND
Lead	< 1 ND	Zinc	<10 ND
Magnesium	< 5	Zirconium	< 1 ND

* ND means not detected. Detection limits are given.

** The high purity iron and this analysis was kindly furnished by the Battelle Memorial Institute.

TABLE III

Analyses of Matthey spectrographically standardized chromium.*

The amounts are given as parts per million
(1 ppm equals 0.0001 atomic per cent)

Element	Estimated Quantity Present
Silicon	3
Copper	<1
Magnesium	<1

The following elements were specifically sought but not detected.

Ag, Al, As, Au, B, Ba, Be, Bi, Ca, Cd, Co, Cs, Fe, Ga, Ge, Hf, Hg, In, Ir, K, Li, Mn, Mo, Na, Nb, Ni, Os, P, Pb, Pd, Pt, Rh, Re, Ru, Sb, Se, Sn, Sr, Ta, Te, Ti, Tl, V, W, Zn, Zr.

TABLE IV

Typical analyses of the gases

A. Carbon dioxide (CO_2), "Bone Dry" Grade

99.95% CO_2

.05% nitrogen and oxygen

B. Carbon monoxide (CO), C. P. Grade

99.5 volume % CO

200 p.p.m. carbon dioxide

20 p.p.m. oxygen

75 p.p.m. nitrogen

* As provided by Johnson, Matthey and Co., Ltd.

TABLE V

Experimental values of the linear and parabolic rate constants for the oxidation of various iron-chromium alloys in CO_2-CO gas mixtures over the temperature range 800°-1100°C.

Experiment No.	Alloy (wt.% Cr)	Temperature (°C)	N_{CO_2}	K_{L_2} (gm/cm^2-sec)	K_p (gm^2/cm^4-sec)
36	0.20	1100	0.500	1.84×10^{-5}	6.58×10^{-7}
37	0.20	1050	0.500	6.19×10^{-6}	3.18×10^{-7}
38	0.20	1000	0.500	1.08×10^{-6}	9.23×10^{-8}
39	0.20	960	0.500	6.66×10^{-7}	8.80×10^{-8}
40	0.20	880	0.500	3.26×10^{-7}	4.39×10^{-8}
41	0.20	850	0.500	2.22×10^{-7}	3.15×10^{-8}
52	0.20	800	0.500	1.32×10^{-7}	2.18×10^{-8}
28	0.20	1100	0.600	2.48×10^{-5}	8.51×10^{-7}
27	0.20	1050	0.600	1.13×10^{-5}	4.11×10^{-7}
26	0.20	1000	0.600	1.53×10^{-6}	1.37×10^{-7}
22	0.20	960	0.600	8.77×10^{-7}	1.32×10^{-7}
23	0.20	925	0.600	5.75×10^{-7}	6.00×10^{-8}
25	0.20	925	0.600	6.13×10^{-7}	5.76×10^{-8}
30	0.20	880	0.600	5.18×10^{-8}	6.42×10^{-8}
24	0.20	850	0.600	3.82×10^{-7}	4.97×10^{-8}
29	0.20	800	0.600	2.09×10^{-7}	3.20×10^{-8}
35	0.20	1100	0.700	3.12×10^{-5}	6.37×10^{-7}
34	0.20	1050	0.700	1.54×10^{-5}	3.16×10^{-7}
33	0.20	1000	0.700	2.25×10^{-6}	2.91×10^{-7}

TABLE V - Continued (2)

Experiment No.	Alloy (wt.% Cr)	Temperature (°C)	N_{CO_2}	K_{L_2} (gm/cm^2-sec)	K_p (gm^2/cm^4-sec)
32	0.20	960	0.700	1.71×10^{-6}	1.43×10^{-7}
60	0.20	925	0.700	1.32×10^{-6}	1.40×10^{-7}
31	0.20	880	0.700	7.33×10^{-7}	9.24×10^{-8}
42	0.20	850	0.700	4.90×10^{-7}	6.47×10^{-8}
51	0.20	800	0.700	3.62×10^{-7}	4.74×10^{-8}
5	0.88	1100	0.600	6.42×10^{-6}	6.53×10^{-7}
4	0.88	1050	0.600	2.99×10^{-6}	1.88×10^{-7}
10	0.88	1050	0.600	3.43×10^{-6}	2.09×10^{-7}
14	0.88	1000	0.600	2.10×10^{-6}	2.13×10^{-7}
1	0.88	1000	0.600	2.07×10^{-6}	7.45×10^{-8}
3	0.88	1000	0.600	2.26×10^{-6}	8.12×10^{-8}
13	0.88	960	0.600	1.07×10^{-6}	1.51×10^{-7}
6	0.88	925	0.600	7.04×10^{-7}	8.94×10^{-8}
7	0.88	880	0.600	6.06×10^{-7}	4.91×10^{-8}
8	0.88	850	0.600	3.83×10^{-7}	3.46×10^{-8}
15	0.88	800	0.600	2.69×10^{-7}	2.10×10^{-8}
18	1.70	1100	0.600	3.41×10^{-6}	6.16×10^{-7}
17	1.70	1050	0.600	2.35×10^{-6}	3.67×10^{-7}
2	1.70	1000	0.600	1.14×10^{-6}	2.34×10^{-7}
21	1.70	960	0.600	5.43×10^{-7}	1.08×10^{-7}
16	1.70	925	0.600	4.14×10^{-7}	8.45×10^{-8}
20	1.70	850	0.600	1.84×10^{-7}	3.29×10^{-8}

TABLE V - Continued (3)

Experiment No.	Alloy (wt.% Cr)	Temperature (°C)	N_{CO_2}	K_{L_2} (gm/cm^2-sec)	K_p (gm^2/cm^4-sec)
59	1.70	800	0.600	1.12×10^{-7}	1.68×10^{-8}
47	5.70	1100	0.600	4.79×10^{-6}	6.05×10^{-7}
55	5.70	1050	0.600	2.17×10^{-6}	3.14×10^{-7}
46	5.70	1000	0.600	1.40×10^{-6}	2.31×10^{-7}
53	5.70	900	0.600	6.45×10^{-7}	7.89×10^{-8}
57	5.70	850	0.600	3.27×10^{-7}	4.22×10^{-8}
48	7.55	1100	0.600	3.76×10^{-6}	2.20×10^{-7}
54	7.55	1050	0.600	2.68×10^{-6}	1.25×10^{-7}
43	7.55	1000	0.600	1.13×10^{-6}	7.11×10^{-8}
50	7.55	900	0.600	3.70×10^{-7}	2.67×10^{-8}
58	7.55	850	0.600	2.64×10^{-7}	1.34×10^{-8}
49	18.21	1100	0.600	5.11×10^{-7}	3.38×10^{-8}
56	18.21	1050	0.600	2.39×10^{-7}	1.50×10^{-8}
44	18.21	1000	0.600	1.12×10^{-7}	1.57×10^{-9}
45	18.21	900	0.600	-	1.32×10^{-9}

TABLE VI

Experimental results obtained from the Arrhenius curves for the linear oxidation of Fe-Cr alloys in carbon dioxide-carbon monoxide mixtures.

Alloy	N_{CO_2}	Pre-exponential term (Kcal-°K/mole)	Activation Energy (Kcal/mole)
0.20% Cr-Fe	0.500		
(800°-960°C)		4.17×10^{-2}	27.1 ± 0.6
(960°-1100°C)		1.23×10^{9}	98 ± 14
0.20% Cr-Fe	0.600		
(800°-960°C)		7.20×10^{-3}	22.2 ± 1.5
(960°-1100°C)		5.34×10^{8}	88.0 ± 1.8
0.20% Cr-Fe	0.700		
(800°-1000°C)		8.03×10^{-2}	26.5 ± 1.8
(1000°-1100°C)		9.01×10^{9}	91 ± 25
0.88% Cr-Fe	0.600		
(800°-925°C)		6.49×10^{-3}	21.8 ± 2.2
(960°-1100°C)		0.282	42.4 ± 2.1
1.70% Cr-Fe	0.600		
(800°-925°C)		3.37×10^{-2}	27.0 ± 0.5
(960°-1100°C)		0.168	

TABLE VII

Experimental results obtained from the Arrhenius curves for the parabolic oxidation of Fe-Cr alloys in carbon dioxide-carbon monoxide mixtures.

Alloy	N_{CO_2}	Pre-exponential term (Kcal-°K/mole)	Activation Energy (Kcal/mole)
0.20% Cr-Fe (800°-1000°C)	0.500	3.92×10^{-4}	20.9 ± 1.3
0.20% Cr-Fe (800°-1000°C)	0.600	3.16×10^{-4}	19.6 ± 2.6
0.20% Cr-Fe (800°-1100°C)	0.700	6.41×10^{-3}	25.6 ± 2.7
0.88% Cr-Fe (800°-1100°C)	0.600	2.47×10^{-1}	35.2 ± 2.4
1.70% Cr-Fe (800°-1100°C)	0.600	2.47×10^{-1}	35.4 ± 2.5
5.70% Cr-Fe (850°-1100°C)	0.600	5.54×10^{-2}	31.5 ± 1.8
7.55% Cr-Fe (850°-1100°C)	0.600	3.87×10^{-2}	33.2 ± 1.6
18.21% Cr-Fe (850°-1100°C)	0.600	6.98×10^{6}	91.8 ± 5.1

TABLE VIII

Rates of oxidation of Fe-Cr alloys in a 60 vol.% CO_2-CO gas mixture and in pure oxygen at 900° and 1000°C.

60 vol.% CO_2-CO		Pure Oxygen*		$K_p)_{N_{CO_2}} = 0.600$
Alloy (wt.% Cr)	K_p (gm^2/cm^4-sec)	Alloy (wt.% Cr)	K_p (gm^2/cm^4-sec)	$K_p)_{O_2}$
		900°C		
0.20	7.00×10^{-8}	0.20	6.10×10^{-10}	87
0.88	7.00×10^{-8}	2.00	6.43×10^{-10}	109
1.70	6.42×10^{-8}	2.00	6.43×10^{-10}	100
5.70	7.76×10^{-8}	4.35	2.27×10^{-8}	3.4
7.55	2.56×10^{-8}	8.97	1.89×10^{-12}	13,500
		1000°C		
0.20	1.91×10^{-7}	0.20	2.71×10^{-9}	71
0.88	2.29×10^{-7}	2.00	4.85×10^{-9}	47
1.70	2.21×10^{-7}	2.00	4.85×10^{-9}	46
5.70	2.24×10^{-7}	4.35	1.34×10^{-8}	17
7.55	7.82×10^{-8}	8.97	7.83×10^{-11}	1000

* Reference 40

TABLE IX

Transition thicknesses ($\Delta m/A$), obtained for the oxidation of various iron-chromium alloys in CO_2-CO gas mixtures over the temperature range 800°-1100°C.

Experiment (No.)	Temperature (°C)	No longer linear $\frac{gm}{cm^2} \times 10^4$	Became Parabolic $\frac{gm}{cm^2} \times 10^4$	Average Thickness $\frac{gm}{cm^2} \times 10^4$	$\frac{K_p}{2K_L}$
0.20% Cr-Fe, N_{CO_2} = 0.500*					
36	1100	140	856	498	179
37	1050	120	675	397	257
38	1000	270	658	464	427
39	960	177	724	450	661
40	880	721	570	646	673
41	850	560	812	686	709
52	800	762	804	783	826
0.20% Cr-Fe, N_{CO_2} = 0.600*					
28	1100	120	839	479	222
27	1050	190	715	452	370
26	1000	306	635	470	448
22	960	785	717	751	753
23	925	190	300	245	522
30	880	500	806	653	620
24	850	565	801	683	651
29	800	550	753	651	766

TABLE IX - Continued (2)

Experiment (No.)	Temperature (°C)	No longer linear $\frac{gm}{cm^2} \times 10^4$	Became Parabolic $\frac{gm}{cm^2} \times 10^4$	Average Thickness $\frac{gm}{cm^2} \times 10^4$	$\frac{K_p}{2K_L}$
0.20% Cr-Fe, N_{CO_2} = 0.700*					
35	1100	70	690	380	102
34	1050	330	456	393	345
33	1000	550	834	692	647
32	960	450	894	672	418
31	880	506	816	611	630
42	850	510	725	617	660
51	800	500	689	595	655
0.88% Cr-Fe, N_{CO_2} = 0.600*					
5	1100	480	527	504	509
4	1050	330	320	325	323
14	1000	190	241	215	507
13	960	175	112	144	133
6	925	628	686	657	635
7	880	340	525	433	405
8	850	260	566	413	452
15	800	656	620	638	619
1.70% Cr-Fe, N_{CO_2} = 0.600*					
19	1150	730	654	692	687
17	1050	325	1023	674	781
2	1000	480	439	460	455
21	960	986	849	917	994
16	925	1110	850	980	1025
18	1100	910	751	903	831

TABLE IX - Continued (3)

Experiment (No.)	Temperature (°C)	No longer linear $\frac{gm}{cm^2} \times 10^4$	Became Parabolic $\frac{gm}{cm^2} \times 10^4$	Average Thickness $\frac{gm}{cm^2} \times 10^4$	$\frac{K_p}{2K_L}$
20	850	985	806	896	894
59	800	838	894	866	750
5.70% Cr-Fe, N_{CO_2} = 0.600					
47	1100	420	751	586	632
55	1050	700	770	735	724
46	1000	912	744	828	825
53	900	286	798	542	612
57	850	523	586	554	645
7.55% Cr-Fe, N_{CO_2} = 0.600					
48	1100	180	349	265	293
54	1050	140	294	217	233
43	1000	170	344	257	315
50	900	310	364	337	360
58	850	169	263	216	254
18.21% Cr-Fe, N_{CO_2} = 0.600					
49	1100	318	318	318	331
56	1050	295	288	292	314
44	1000	71	64	68	71

* To get the approximate scale thickness (cm), multiply $(\Delta m/A)_{tr.} \times 10^{-4}$ (gm/cm^2), by 0.77.

TABLE X

Experimental values obtained from the oxidation of iron-chromium alloys in CO_2-CO mixtures used to test the validity of Equation (38c).

Alloy (wt.% Cr)	N_{CO_2}	$-(E_p - E_L)$ (Kcal/mole) (800°-960°C)	$-(E_p - E_L)$ (Kcal/mole) (960°-1100°C)	ΔE^{**} (Kcal/mole) (800°-960°C)	ΔE^{**} (Kcal/mole) (960°-1100°C)
0.20	0.500	6.2	71.	6.1	17.
0.20	0.600	2.6	68.	- 0.92	21.
0.20	0.700	0.9	65.	- 1.8	27.
0.88	0.600	- 13.4	7.2	- 21.	18.
1.70	0.600	- 8.4	9.8	- 2.6	6.2
5.70	0.600	-	6.0	- 9.0	11.

** From Figures 34, 35 and 36.

TABLE XI

Values of the lattice parameters (a_o) of pure wüstite and wüstite containing 0.67 wt.% chromium of various compositions which were equilibrated in CO_2-CO mixtures at 1000°C and quenched to room temperature.

Specimen (No.)	N_{CO_2}	Pure Wüstite		Wüstite + 0.67 wt.% Cr	
		Composition (wt.% oxygen)	a_o (Å)	Composition (wt.% oxygen)	a_o (Å)
13	*	23.09	4.3110	*	4.3069
12	.290	23.10	4.3101		
14	.292	23.12	-		
1X-10	.300			23.27	4.3013
27	.330	23.20	-		
1	.345	23.25	4.3086		
1X-2	.350			23.39	4.2958
7	.368	23.33	4.3066		
9	.380	23.35	4.3053		
1X-1	.400			23.54	4.2943
28	.400	23.44	-		
18	.440	23.53	4.3005		
24	.450	23.56	-		
25	.450	23.58	-		
1X-6	.500			23.77	-
2	.500	23.72	4.2952		
1X-8	.500			23.80	-
26	.500	23.69	4.2951		
11	.525	23.80	4.2938		
19	.550	23.92	4.2903		
15	.600	23.96	-		
16	.600	24.07	4.2864		

TABLE XI

Values of the lattice parameters (a_o) of pure wüstite and wüstite containing 0.67 wt.% chromium of various compositions which were equilibrated in CO_2-CO mixtures at 1000°C and quenched to room temperature.

Specimen (No.)	N_{CO_2}	Pure Wüstite		Wüstite + 0.67 wt.% Cr	
		Composition (wt.% oxygen)	a_o (Å)	Composition (wt.% oxygen)	a_o (Å)
13	*	23.09	4.3110	*	4.3069
12	.290	23.10	4.3101		
14	.292	23.12	-		
1X-10	.300			23.27	4.3013
27	.330	23.20	-		
1	.345	23.25	4.3086		
1X-2	.350			23.39	4.2958
7	.368	23.33	4.3066		
9	.380	23.35	4.3053		
1X-1	.400			23.54	4.2943
28	.400	23.44	-		
18	.440	23.53	4.3005		
24	.450	23.56	-		
25	.450	23.58	-		
1X-6	.500			23.77	-
2	.500	23.72	4.2952		
1X-8	.500			23.80	-
26	.500	23.69	4.2951		
11	.525	23.80	4.2938		
19	.550	23.92	4.2903		
15	.600	23.96	-		
16	.600	24.07	4.2864		

TABLE XI - Continued (2)

Specimen (No.)	N_{CO_2}	Pure Wüstite		Wüstite + 0.67 wt.% Cr	
		Composition (wt.% oxygen)	a_o (Å)	Composition (wt.% oxygen)	a_o (Å)
1X-5	.600			24.09	4.2897
1X-9	.600			24.11	-
20	.650	24.17	-		
17	.667	24.20	4.2848		
1X-4	.700			24.40	4.2833
22	.710	24.29	-		
21	.710	24.32	-		
3	.743	24.36	4.2826		
1X-7	.750			24.54	-
10	.765	24.45	4.2817		
5	.787	24.54	4.2888		
23	.795	24.54	-		
1X-3	.800			26.04†	-
8	.820	24.64†	4.2896		
6	.831	24.95†	4.2855		

* The oxide was equilibrated with the metal.

† The composition is within the magnetite phase field.

TABLE XII

Values of electrical conductivity of pure and doped wüstite at 1000°C at various partial pressures of oxygen in CO_2-CO mixtures.

N_{CO_2}	CO_2/CO	p_{O_2} (atm.)	σ ($ohm^{-1}cm^{-1}$)
A. Pure Wüstite			
0.300	0.429	1.46×10^{-15}	105.7
0.347	0.528	2.21×10^{-15}	124.3
0.400	0.667	3.53×10^{-15}	138.7
0.467	0.863	5.91×10^{-15}	156.3
0.531	1.13	1.02×10^{-14}	175.9
0.600	1.50	1.79×10^{-14}	197.7
0.700	2.33	4.31×10^{-14}	229.9
0.750	3.00	6.83×10^{-14}	231.1
B. Wüstite + 0.67 wt.% Cr			
0.347	0.528	-	123.5
0.467	0.863	-	160.9
0.531	1.13	-	184.5
0.600	1.50	-	198.4
0.700	2.33	-	229.0
C. Wüstite + 1.30 wt.% Cr			
0.347	0.528	-	118.6
0.499	0.997	7.90×10^{-15}	161.7
0.565	1.30	1.34×10^{-14}	174.7
0.700	2.33	-	212.6
0.750	3.00	-	221.5

TABLE XIII

Values of electrical conductivity of pure and doped wüstite at a constant composition of oxygen/metal = 1.060 at various temperatures.

Temperature (°C)	N_{CO_2}	Conductivity ($ohm^{-1}cm^{-1}$)		
		Pure FeO	FeO + 0.67 wt.% Cr	FeO + 1.30 wt.% Cr
1100	0.323	131.0	135.0	121.0
1050	0.335	128.7	130.0	116.2
1000	0.347	123.3	125.5	112.5
950	0.361	120.6	122.9	109.2
900	0.375	116.3	119.3	105.5
850	0.389	110.8	115.4	101.8
800	0.405	107.4		97.9
750	0.423	103.2		94.9
700	0.443	99.6		
650	0.467	94.8		

TABLE XIV

Values of electrical conductivity of pure and doped wüstite as a function of temperature at a constant oxygen partial pressure of 6.83×10^{-14} atm.

Temperature (°C)	N_{CO_2}	Conductivity ($ohm^{-1}cm^{-1}$)	
		Pure Wüstite	Wüstite + 1.30 wt.% Cr
1100	0.300	127.0	123.4
1075	0.396	150.4	145.4
1050	0.510	178.6	169.3
1025	0.636	204.4	196.7
1000	0.750	229.9	221.5

TABLE XV

Values of electrical conductivity of pure and doped wüstite as a function of temperature in a fixed CO_2-CO ratio where $N_{CO_2} = 0.467$.

Temperature (°C)	Pure FeO	Conductivity ($ohm^{-1}cm^{-1}$)	
		FeO + 0.67 wt.% Cr	FeO + 1.30 wt.% Cr
1100	170.8	173.3	163.4
1050	163.8	167.4	155.2
1000	156.3	160.9	147.8
950	152.8	154.7	144.4
900	147.2	148.7	138.7
850	142.0		
650	94.8		

TABLE XVI

Values of the enthalpy of movement of electron holes ($\Delta H^*_{m\oplus}$) and the enthalpy of formation of ionic and electronic defects (ΔH_f) in pure and doped wüstite as determined from electrical conductivity measurements.

	$\Delta H^*_{m\oplus}$ (Kcal/mole)	$\frac{\Delta H_f}{3} + \Delta H^*_{m\oplus}$ (Kcal/mole)	ΔH_f (Kcal/mole)
Pure wüstite	1.842 ± 0.009	-20.8 ± 0.9*	-67.9 ± 2.7
		-20.4 ± 0.2**	-66.7 ± 0.6
FeO + 0.67 wt.% Cr	1.939 ± 0.003	-20.6 ± 0.1**	-67.6 ± 0.3
FeO + 1.30 wt.% Cr	2.201± 0.003	-20.4 ± 0.2*	-67.8 ± 0.6
		-20.5 ± 0.4**	-68.1 ± 1.2

* at constant $p_{O_2} = 6.83 \times 10^{-14}$ atm.

** at constant $N_{CO_2} = 0.467$

TABLE XVII

Values of the parabolic rate constant (K_p) and the chemical diffusion coefficient (D) for the reduction and oxidation of pure and doped wüstite for various experimental conditions.

Experiment (No.)	Temperature (°C)	K_p (gm^2/cm^4-sec)	D (cm^2/sec)
A. Reduction of pure FeO, O/Fe = 1.125 to 1.050			
72	1100	3.11×10^{-8}	3.25×10^{-6}
74	1050	2.43×10^{-8}	1.85×10^{-6}
76	1000	1.27×10^{-8}	1.02×10^{-6}
78	950	8.21×10^{-9}	4.98×10^{-7}
80	900	3.85×10^{-9}	2.49×10^{-7}
B. Reduction of pure FeO, O/Fe = 1.125 to 1.075			
92	1100	9.22×10^{-9}	1.74×10^{-6}
90	1050	6.97×10^{-9}	8.95×10^{-7}
88	1000	4.19×10^{-9}	5.45×10^{-7}
86	950	2.77×10^{-9}	3.87×10^{-7}
82	900	1.55×10^{-9}	2.16×10^{-7}
C. Reduction of pure FeO, O/Fe = 1.125 to 1.100			
94	1100	9.81×10^{-10}	5.64×10^{-7}
96	1050	6.13×10^{-10}	3.76×10^{-7}
98	1000	3.85×10^{-10}	2.50×10^{-7}
100	950	2.50×10^{-10}	1.80×10^{-7}
101	900	1.37×10^{-10}	1.23×10^{-7}
D. Oxidation of pure FeO, O/Fe = 1.050 to 1.125			
73	1100	6.30×10^{-8}	2.74×10^{-6}
75	1050	3.87×10^{-8}	1.52×10^{-6}
77	1000	1.56×10^{-8}	7.40×10^{-7}
79	950	5.50×10^{-9}	3.88×10^{-7}
81	900	2.94×10^{-9}	2.06×10^{-7}

TABLE XVII - Continued (2)

Experiment (No.)	Temperature (°C)	K_p (gm^2/cm^4-sec)	D (cm^2/sec)
E. Reduction of FeO + 0.67 wt.% Cr, O/metal = 1.125 to 1.050			
106	1100	3.22×10^{-8}	2.56×10^{-6}
104	1050	1.81×10^{-8}	1.13×10^{-6}
102	1000	1.10×10^{-8}	7.23×10^{-7}
108	950	5.88×10^{-9}	3.66×10^{-7}
110	900	3.39×10^{-9}	1.72×10^{-7}
F. Oxidation of FeO + 0.67 wt,% Cr. O/metal = 1.050 to 1.125			
107	1100	4.35×10^{-8}	2.35×10^{-6}
105	1050	2.51×10^{-8}	1.39×10^{-6}
103	1000	1.15×10^{-8}	6.09×10^{-7}
109	950	5.24×10^{-9}	1.16×10^{-7}
111	900	2.93×10^{-9}	5.08×10^{-8}

TABLE XVIII

Experimental Results Obtained from the Arrhenius Curves for the Reduction and Oxidation of Pure and Doped Wüstite.

Experiment	Activation Energy from log K_p vs 1/T (Kcal/mole)	Activation Energy from log D vs 1/T (Kcal/mole)
A. Reduction of pure FeO		
O/Fe = 1.125 to 1.050	33.9 ± 2.4	41.3 ± 3.1
O/Fe = 1.125 to 1.075	30.3 ± 2.9	32.0 ± 1.4
O/Fe = 1.125 to 1.100	31.1 ± 0.4	24.3 ± 0.7
B. Oxidation of pure FeO		
O/Fe = 1.050 to 1.125	51.8 ± 3.6	41.9 ± 0.9
C. Reduction of FeO + 0.67 wt.% Cr		
O/metal = 1.125 to 1.050	36.2 ± 0.6	41.8 ± 1.5
D. Oxidation of FeO = 0.67 wt.% Cr		
O/metal = 1.050 to 1.125	44.6 ± 1.5	-

TABLE XIX

Ratios of the chemical diffusion coefficients obtained from the reduction of pure wüstite to the self-diffusion coefficients[9] of iron in pure wüstite for various experimental conditions.

Temperature (°C)	oxygen/iron ratios 1.050	1.075	1.100
1000	29.0 (20.4)	11.2 (13.3)	4.2 (10.0)
900	12.5 (20.4)	8.3 (13.3)	8.1 (10.0)

( ) indicate the theoretical value.

FIGURES

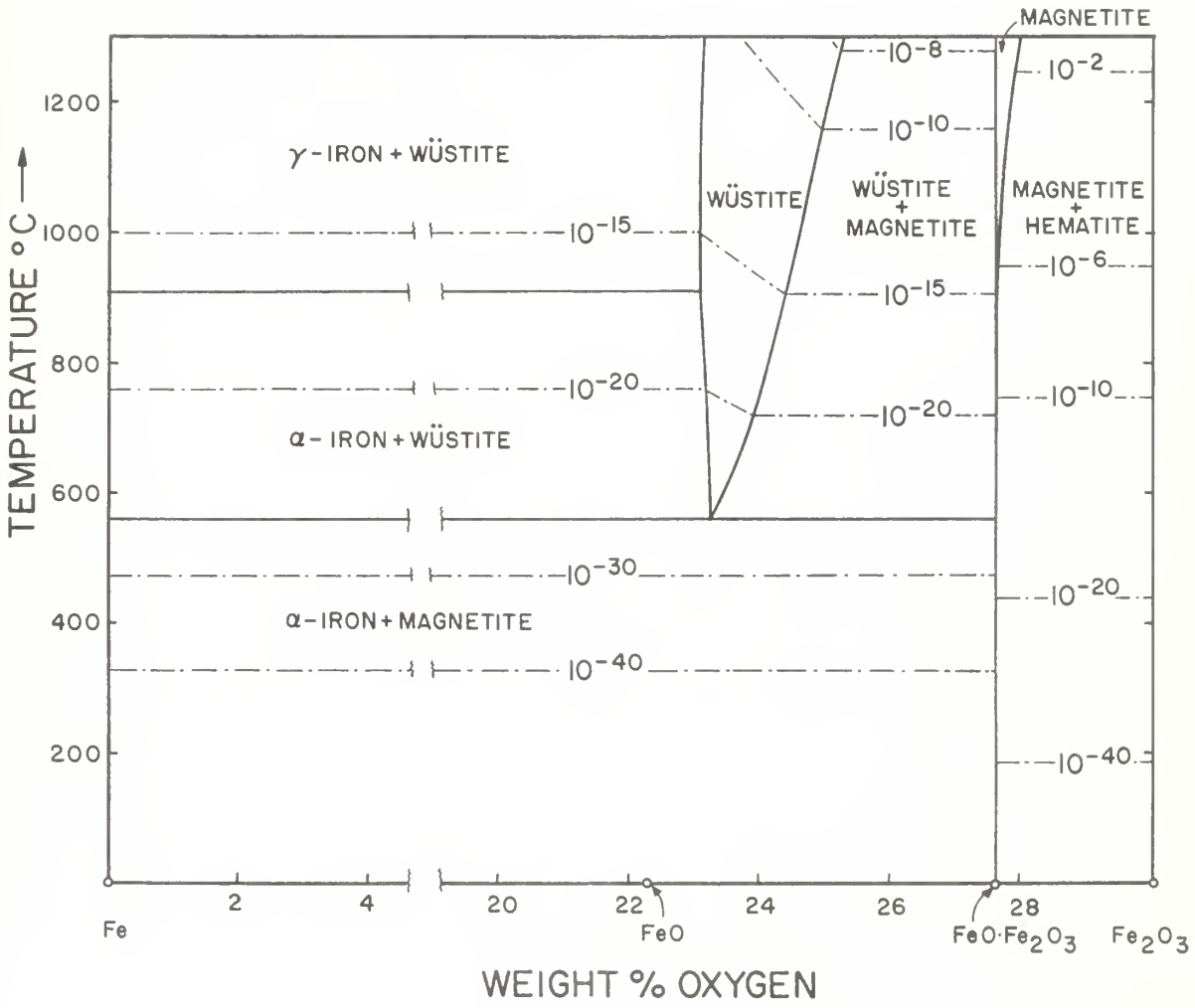

Figure 2. Diagram to show phase equilibrium relationship in the system iron-oxygen. The heavy solid lines are boundary curves separating phase areas labeled in the diagram, and the light dash-dot are O_2 isobars (in atm.).

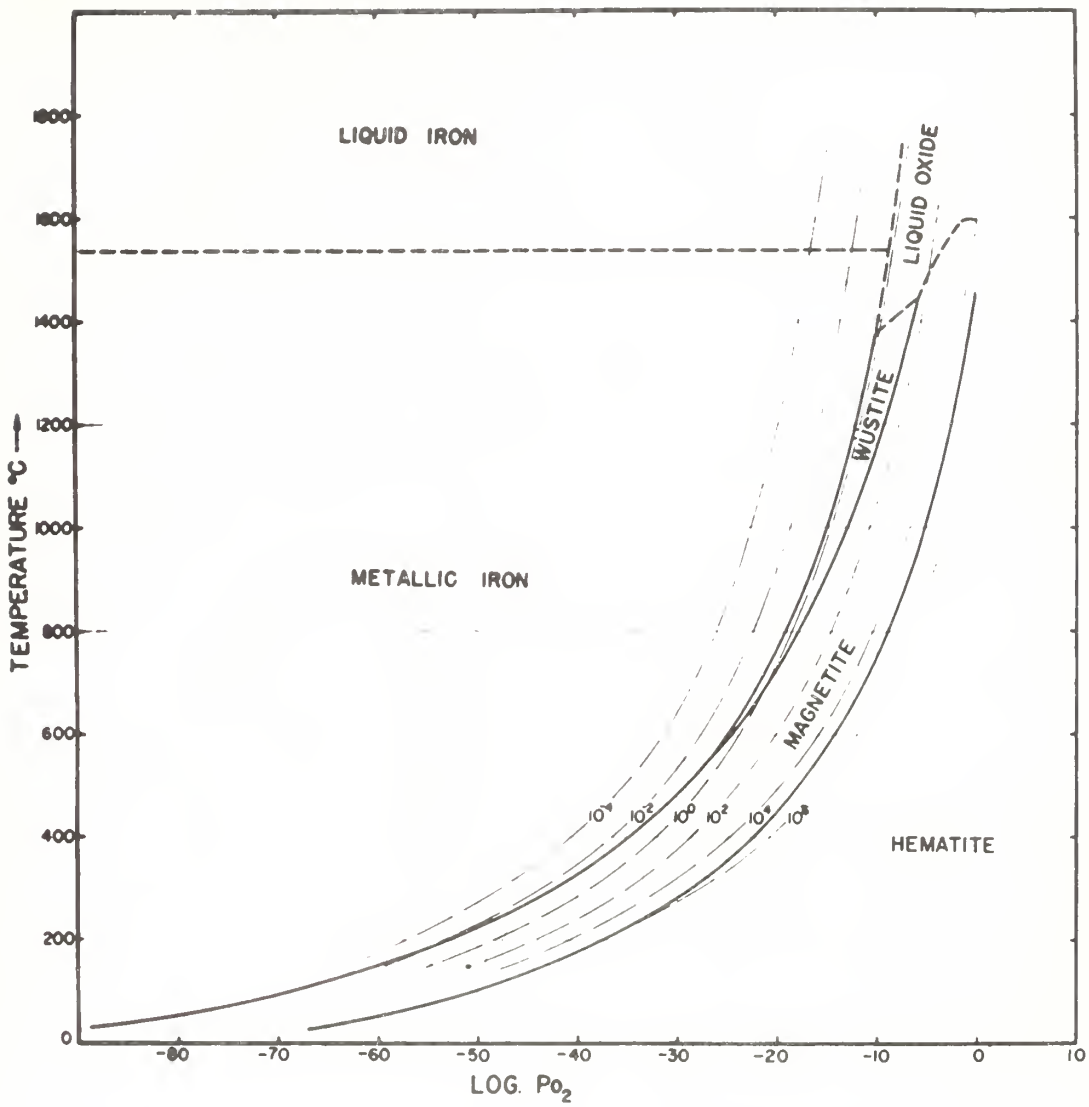

Figure 3. Diagram to show stability relationships among the phases hematite (Fe_2O_3), magnetite (Fe_3O_4), wüstite (FeO), metallic iron (Fe), liquid oxide and liquid iron as a function of temperature (in °C) and O_2 pressure (in atm.). The heavy solid lines are boundary curves separating the various phase areas labeled in the diagram. The light dash-double dot lines are lines of equal p_{CO_2}/p_{CO} ratios of the gas phase at 1 atm. total pressure.

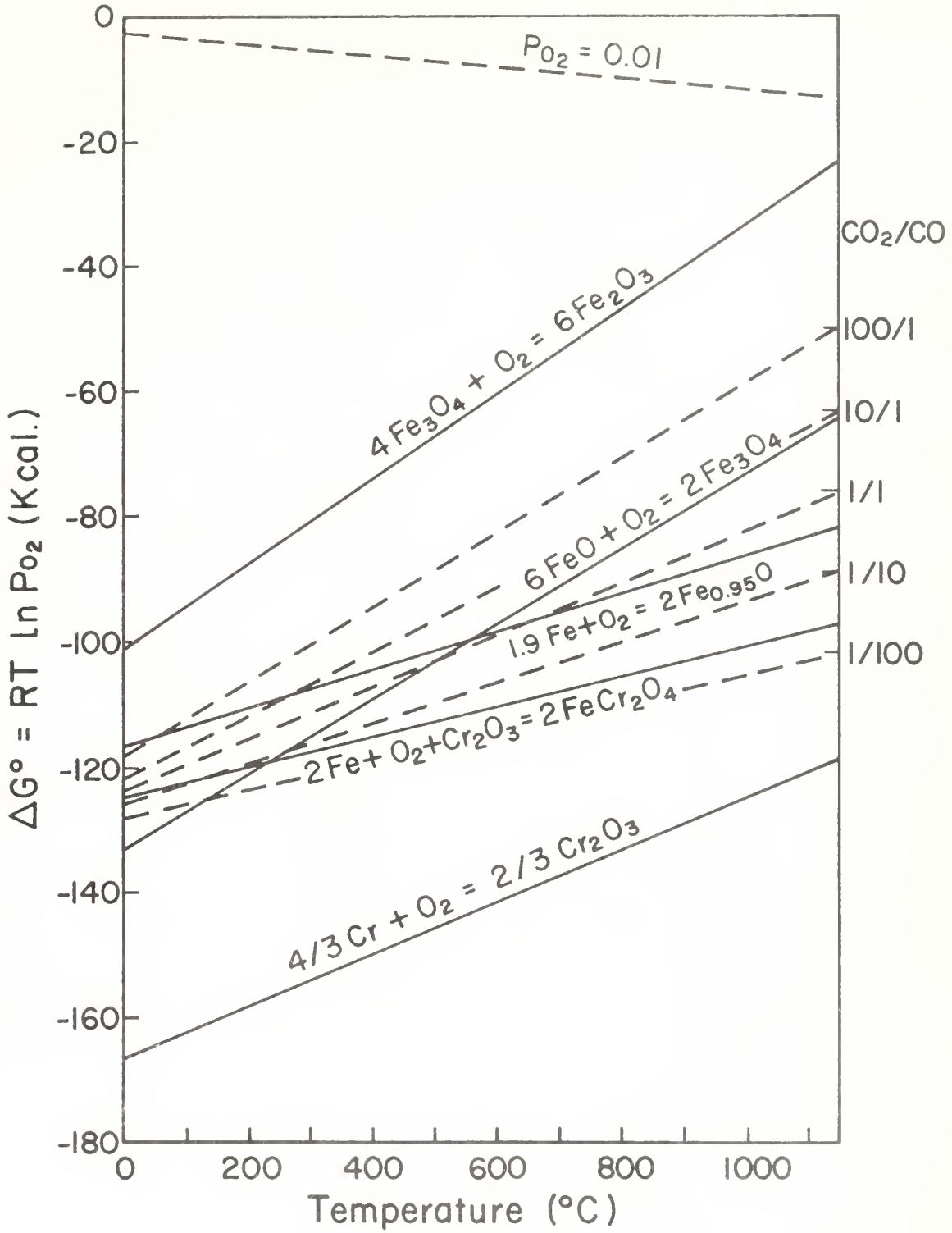

Figure 4. Oxygen potential diagram for various metal/oxide and oxide/oxide systems. The dash lines represent the standard free energies for the various CO_2/CO ratios and for p_{O_2} = 0.01 atm.

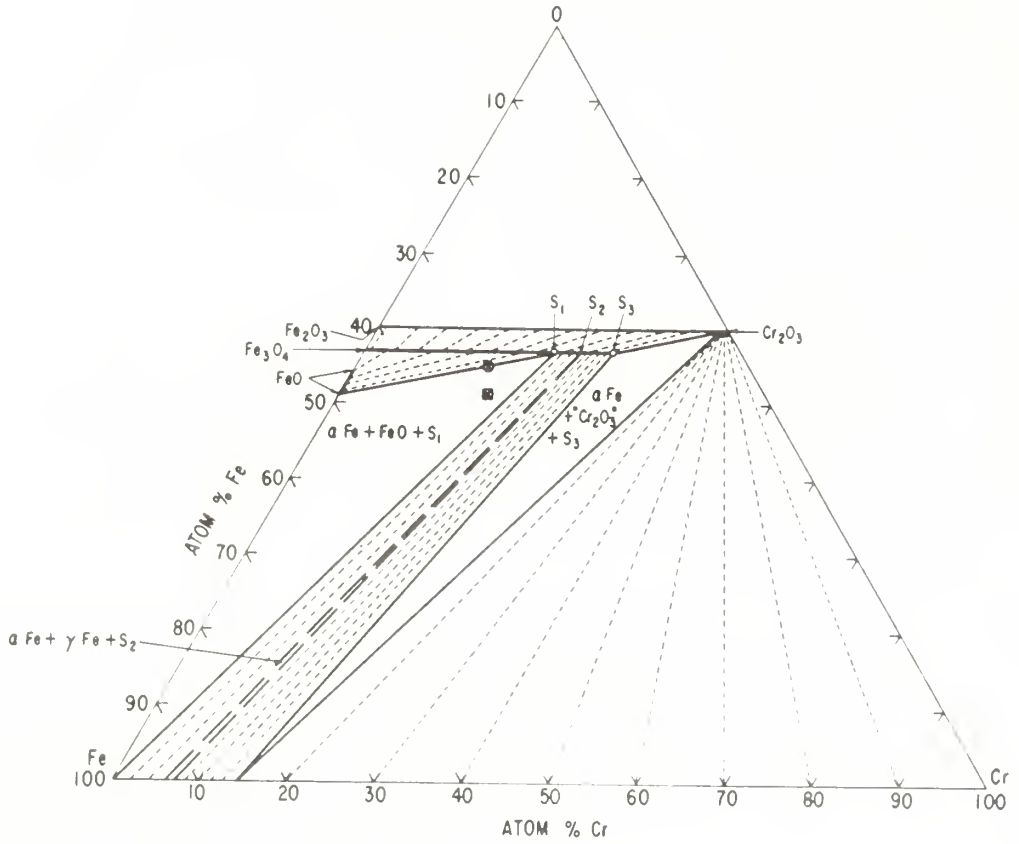

Figure 5. Isothermal Fe-Cr-O phase diagram for 1300°C (39).

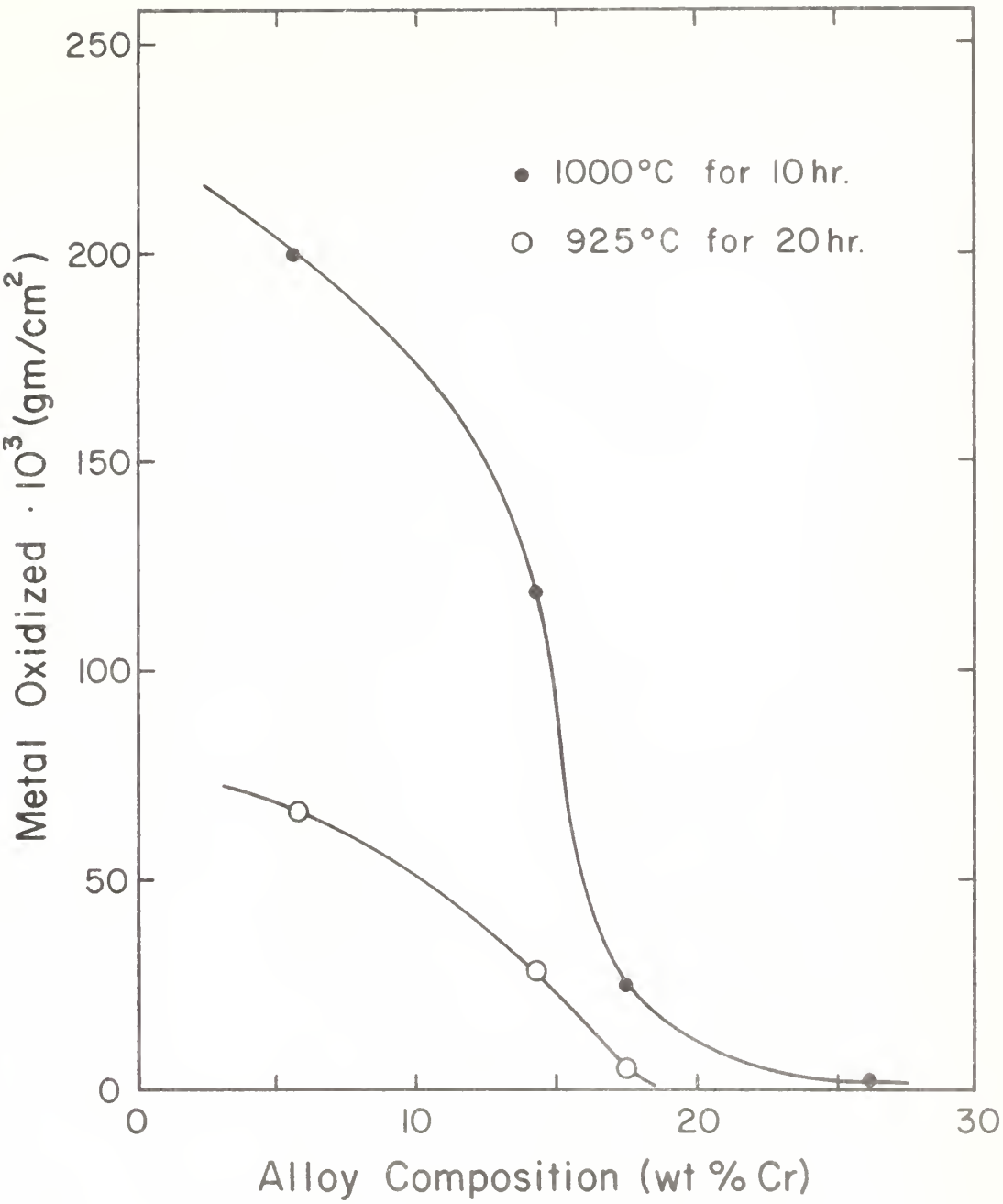

Figure 6. Oxidation of iron-chromium steels in oxygen (38).

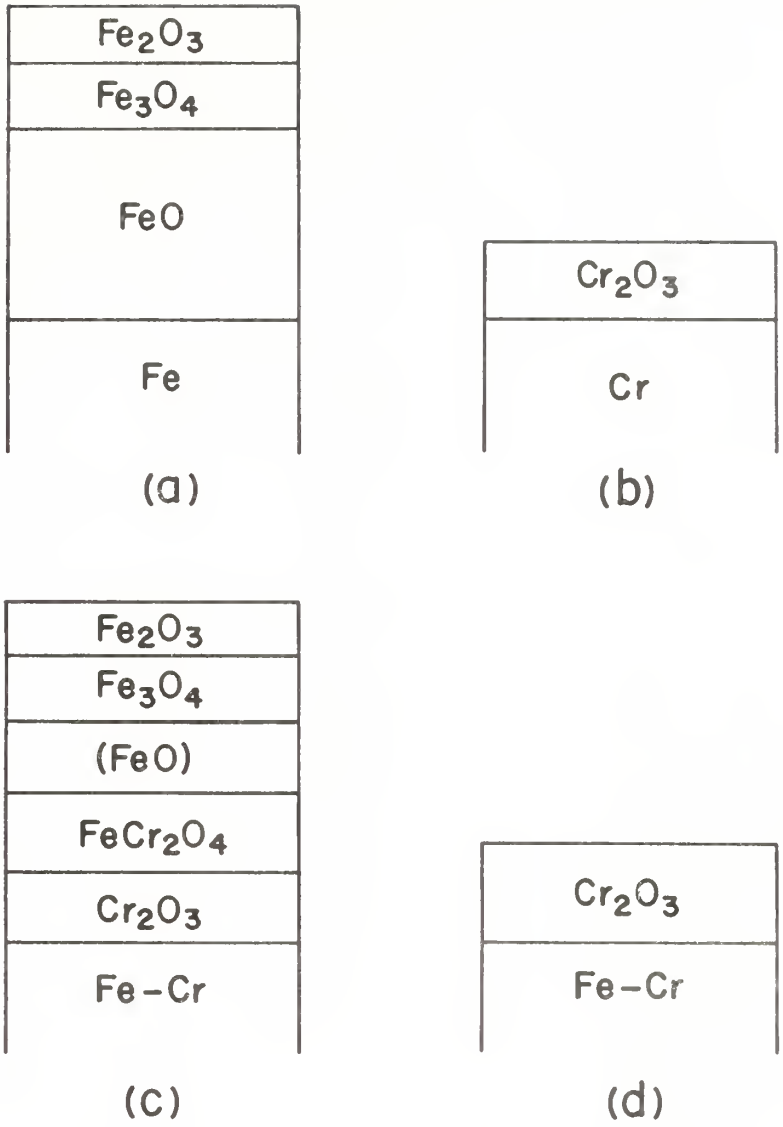

Figure 7. Schematic models of oxide layers formed in air or oxygen on (a) pure Fe, (b) pure Cr, (c) Fe-Cr alloy (< 13% Cr), and (d) Fe-Cr alloy (> 13% Cr).

Figure 8. Diagram to illustrate the stability relationships among magnetite, wüstite and metallic iron as a function of temperature and ratios of CO_2/CO of the gas phase in equilibrium with the condensed phases. The dash-dot line represents the composition of wüstite as a function of temperature which is in equilibrium with wüstite at a constant partial pressure of oxygen. The dash lines are lines of constant wüstite compositions, where at

A. O/Fe = 1.050

B. O/Fe = 1.060

C. O/Fe = 1.075

D. O/Fe = 1.100

E. O/Fe = 1.125

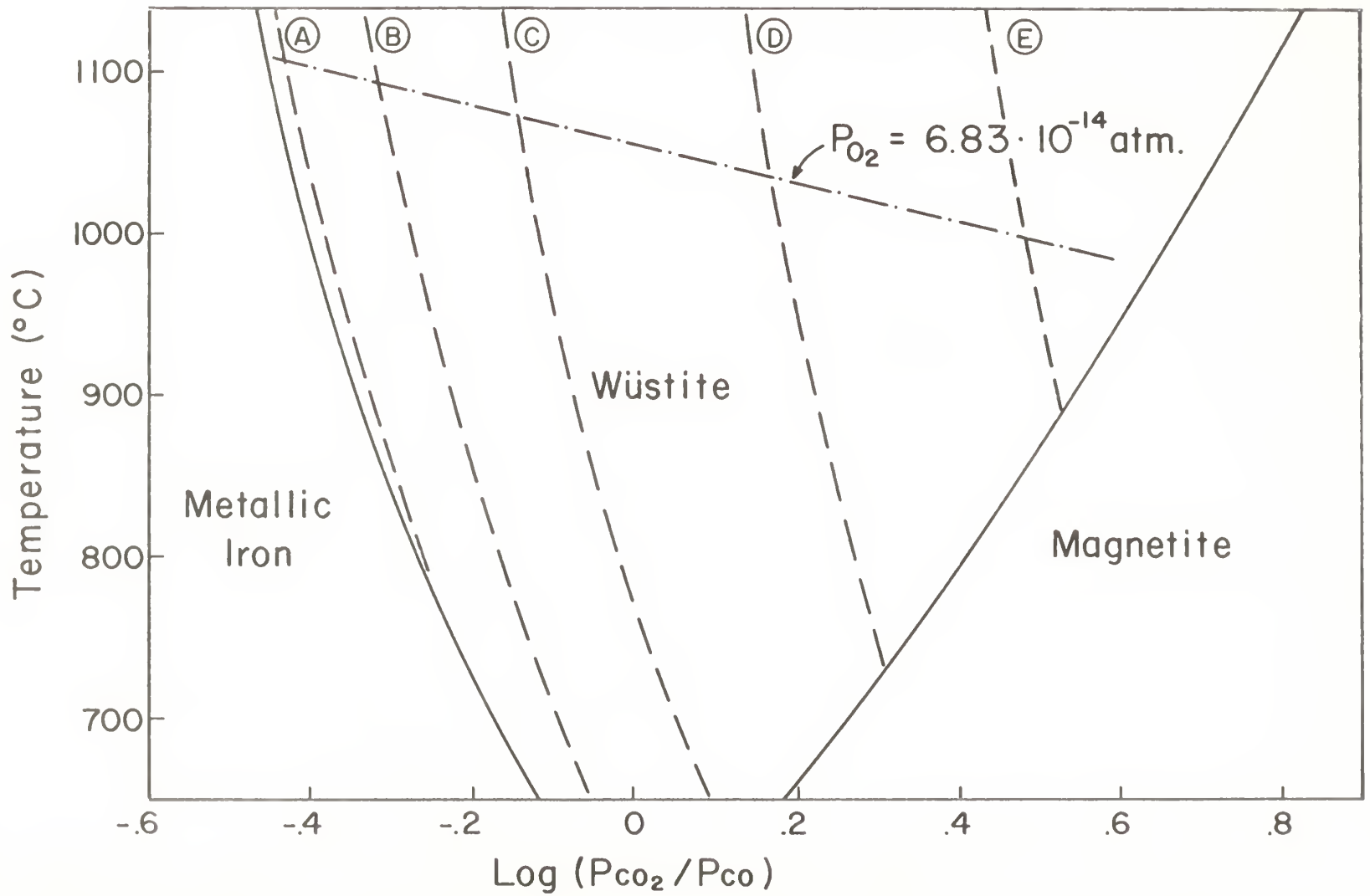
A
B
C
D
E
1100
1000
900
800
700
Temperature (°C)
$P_{O_2} = 6.83 \cdot 10^{-14}$ atm.
Wüstite
Metallic Iron
Magnetite
-.6
-.4
-.2
0
.2
.4
.6
.8
Log (P_{CO_2} / P_{CO})

Figure 8. Diagram to illustrate the stability relationships among magnetite, wüstite and metallic iron as a function of temperature and ratios of CO_2/CO of the gas phase in equilibrium with the condensed phases. The dash-dot line represents the composition of wüstite as a function of temperature which is in equilibrium with wüstite at a constant partial pressure of oxygen. The dash lines are lines of constant wüstite compositions, where at

A. O/Fe = 1.050

B. O/Fe = 1.060

C. O/Fe = 1.075

D. O/Fe = 1.100

E. O/Fe = 1.125

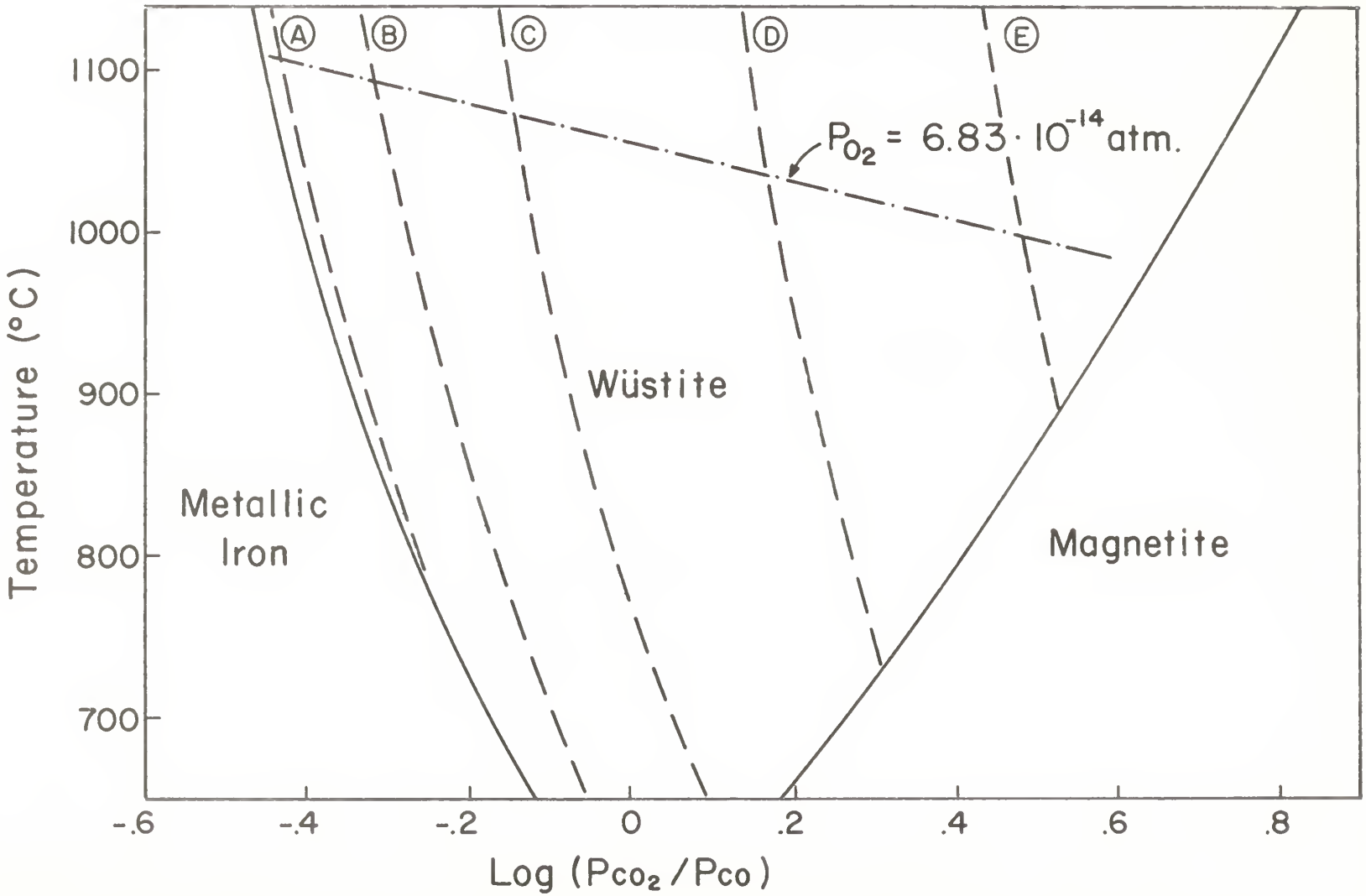
A
B
C
D
E
1100
1000
900
800
700
Temperature (°C)
$P_{O_2} = 6.83 \cdot 10^{-14}$ atm.
Wüstite
Metallic
Iron
Magnetite
-.6
-.4
-.2
0
.2
.4
.6
.8
Log (P_{CO_2} / P_{CO})

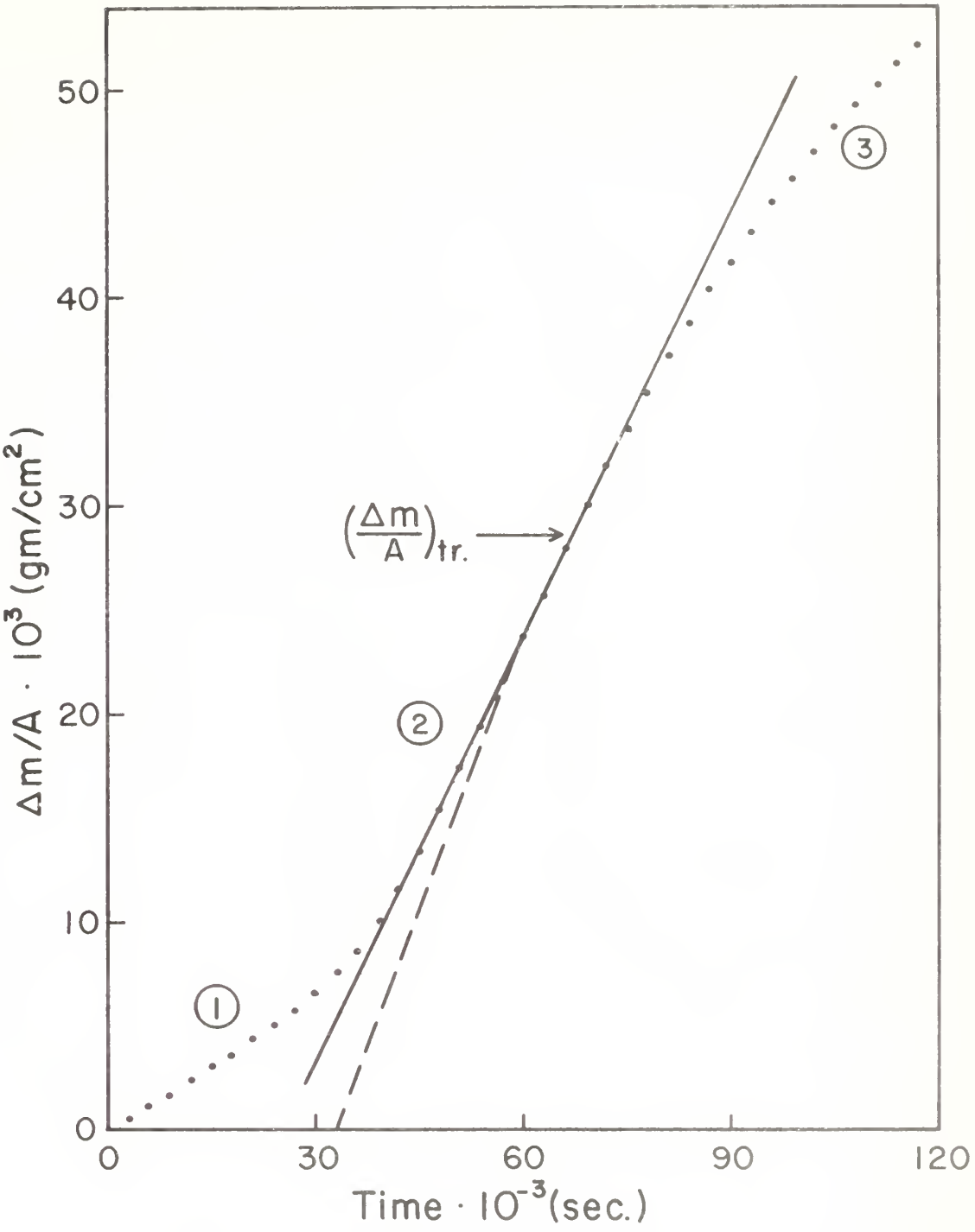

Figure 9. Oxidation rate curve of a 7.55% Cr-Fe alloy in a 50 vol.% CO_2-CO mixture at 1000°C which exhibits (1) first linear region, (2) second linear region, and (3) parabolic region. The point, $(\Delta m/A)tr.$ denotes the transition thickness where the kinetics convert from linear to parabolic.

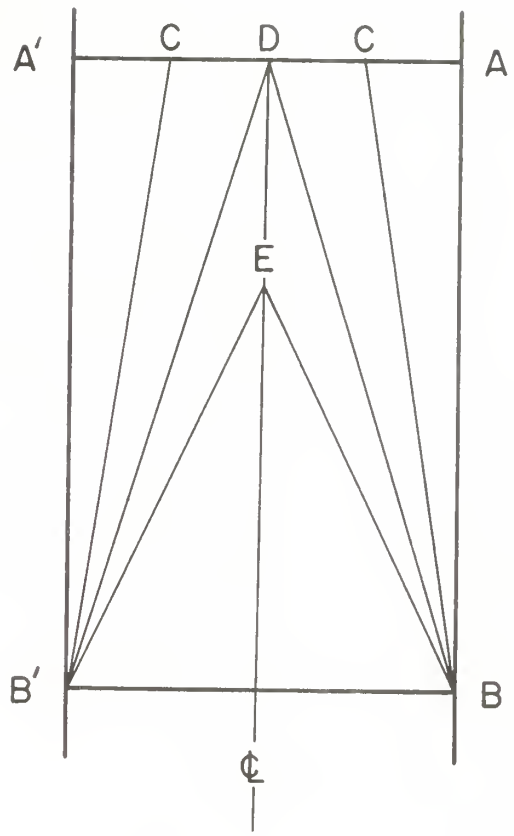

Figure 10. Schematic representation of concentration gradients across a wüstite slab.

AA' = initial concentration at $t = 0$
BB' = final concentration at $t = \infty$
$BC, B'C$ = concentration gradient at time, t_1
BDB' = concentration gradient at t_2
BEB' = concentration gradient at t_3
where $t_3 > t_2 > t_1 > t_0$

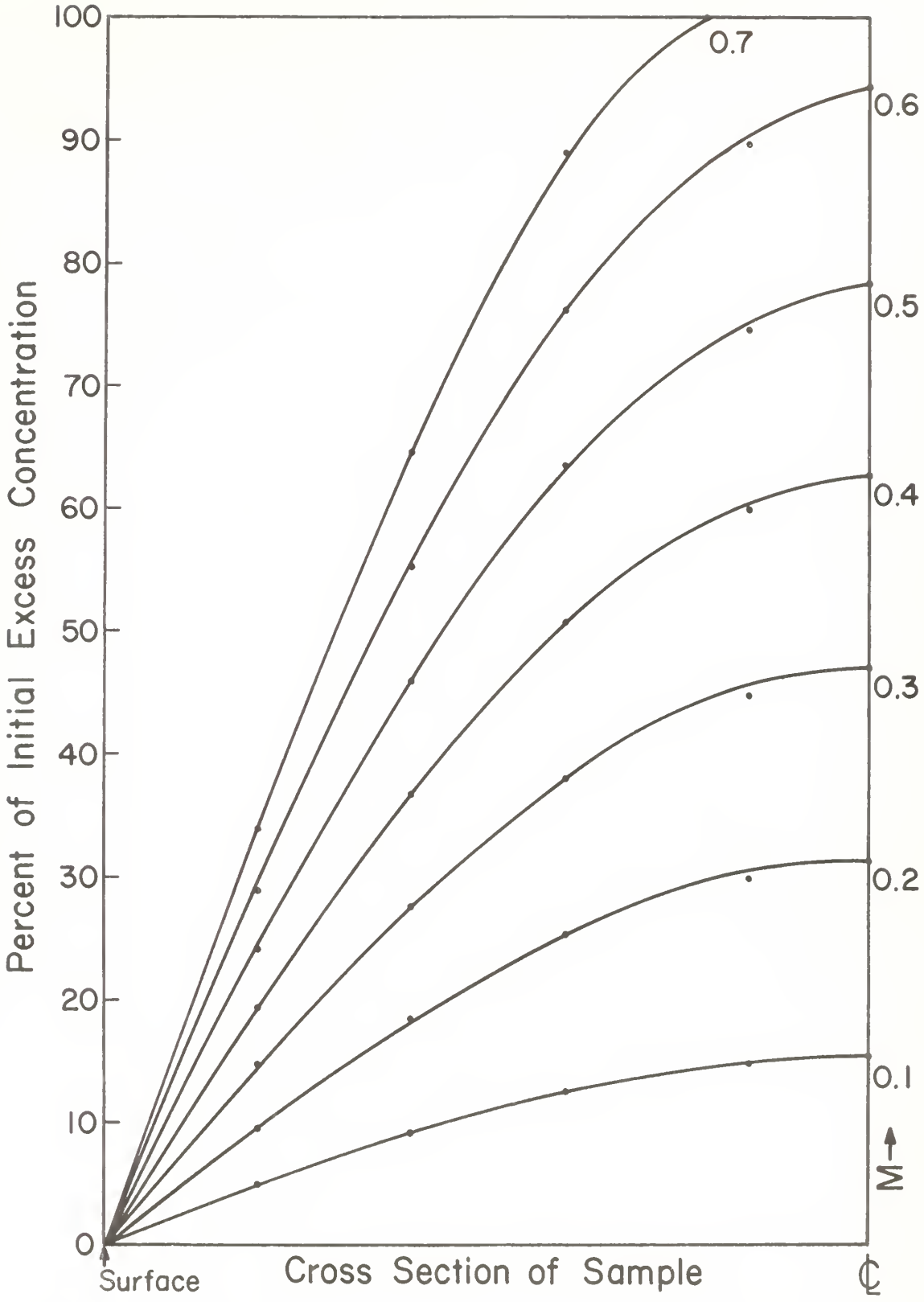

Figure 11. Theoretical concentration gradients existing across a wüstite slab during different stages of the reduction or oxidation process.

Figure 12. Schematic diagram of the oxidation apparatus. The nomenclature of parts numbered on the diagram are as follows:

(1) Bell jar

(2) Weighing chamber flange

(3) Vacuum tight double O-ring seal

(4) Quartz fiber hooks

(5) Indicates lowest position of inner brass sleeve with double O-ring seal.

(6) Ainsworth Vacuum Automatic Recording Balance

(7) Balance load pan

(8) Vacuum Tight Balance base plate

(9) Vacuum tight O-ring seals

(10) 70-30 Brass sleeve

(11) 304 Stainless steel tube with 34/45 standard taper

(12) 34/45 Standard taper joint (Pyrex to 304 stainless steel)

(13) Gas outlet

(14) Quartz fiber

(15) Gas inlet

(16) McDanel to pyrex seal

(17) Specimen in upper, cold zone position

(18) Location where specimen is in lower hot zone position

(19) Marshall High Temperature Furnace

(20) McDanel tube

(21) McDanel to pyrex seal

(22) 34/45 Standard taper pyrex joint

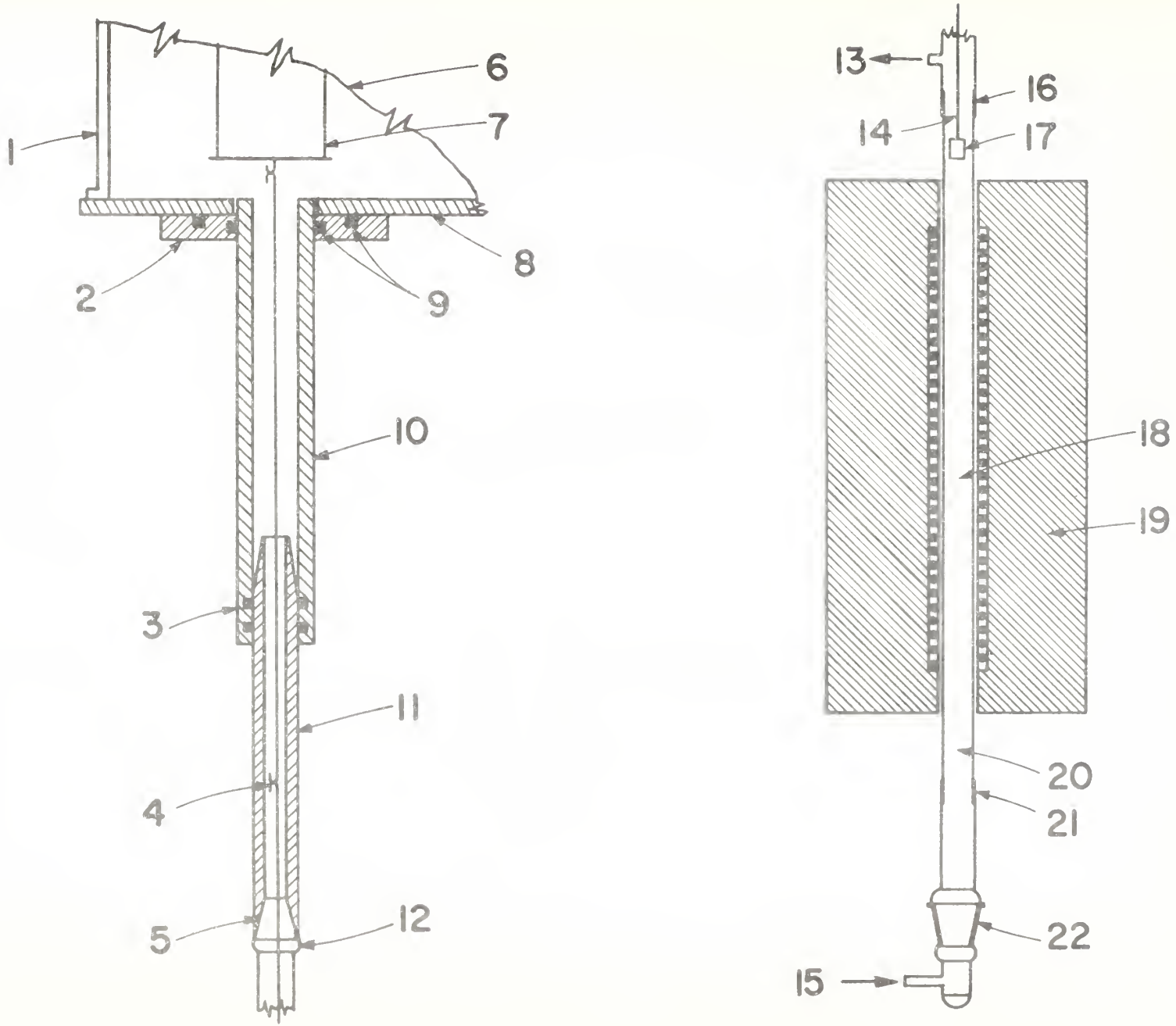
1
2
3
4
5
6
7
8
9
10
11
12
13
14
15
16
17
18
19
20
21
22

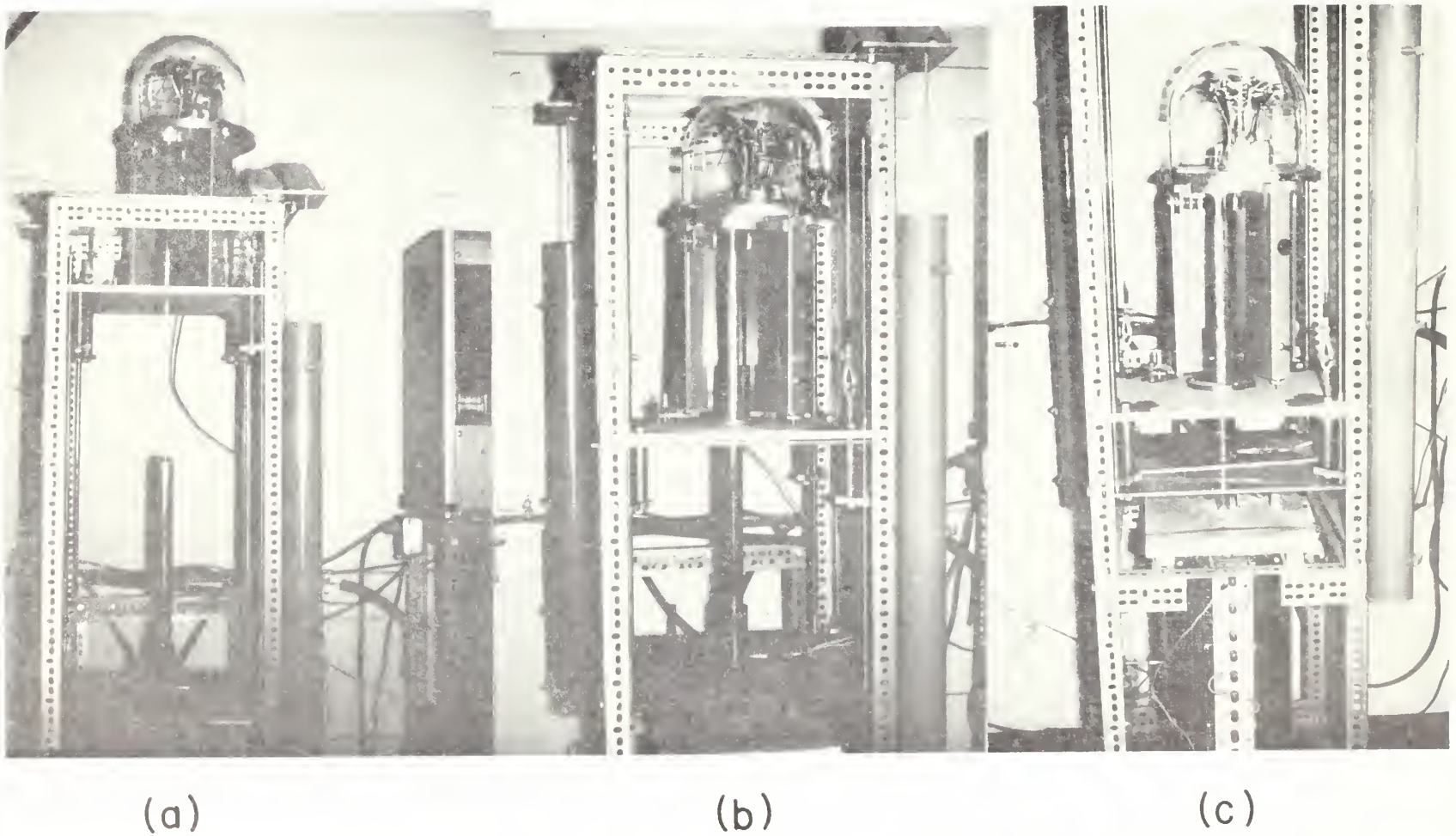

Figure 13. Photographs to show the three positions of the Ainsworth balance in the oxidation apparatus. (a) Balance in the uppermost position, (b) Intermediate position, (c) Lower position.

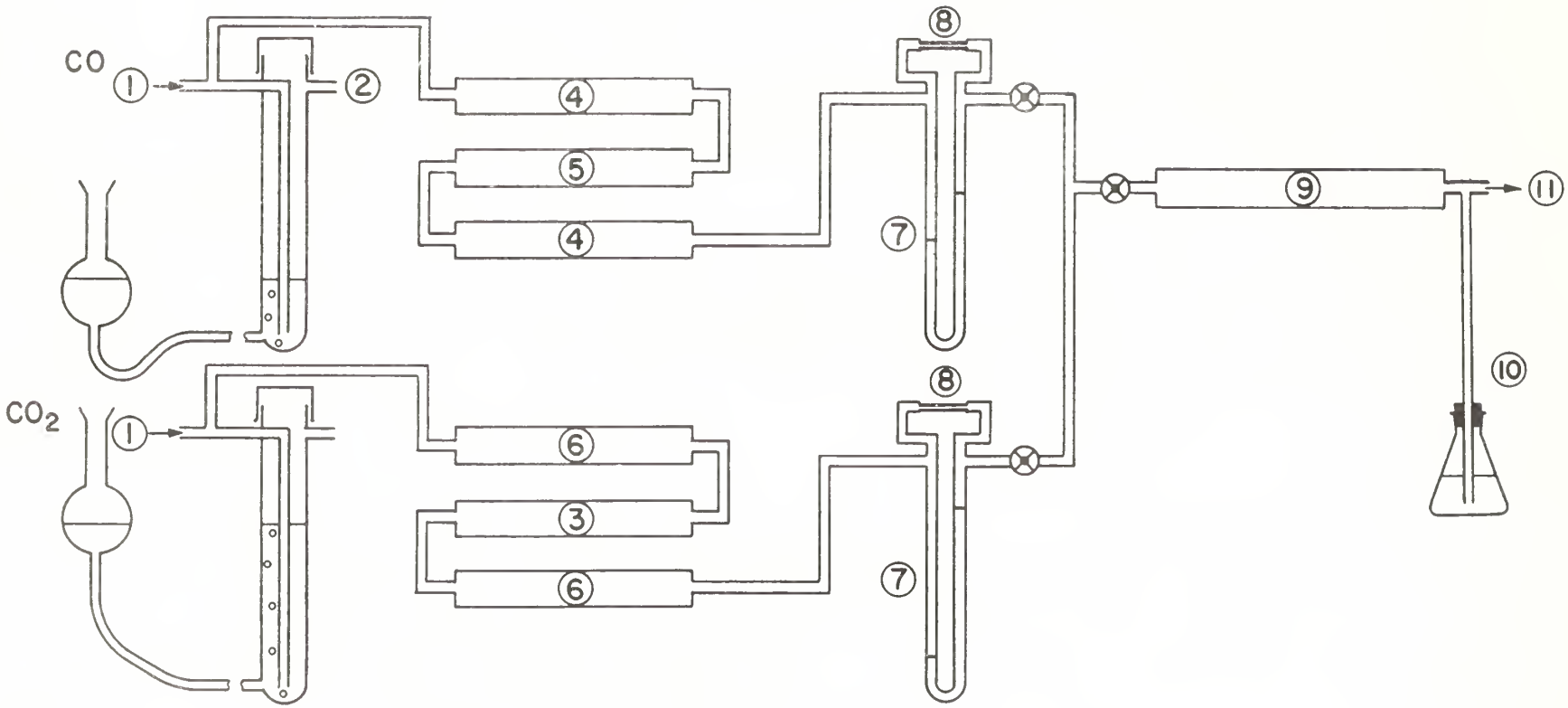

Figure 14. Schematic diagram of the all-pyrex glass apparatus used to clean the gases and measure the flow rates. 1) Gas entrance, 2) CO exit to atmosphere, 3) Copper chips at 500°C, 4) Magnesium perchlorate, 5) Ascarite, 6) Activated alumina, 7) Calibrated manometers, 8) Capillaries, 9) Mixing chamber containing glass beads, 10) Mercury manometer, 11) CO_2-CO entrance to bottom of furnace.

Figure 15. Photographs to show the specimens used for electrical conductivity studies. a) Metal iron sample wrapped with 0.013 inch Pt wire. b) Cross-section of wüstite specimen with Pt wires. c) Wüstite specimen.

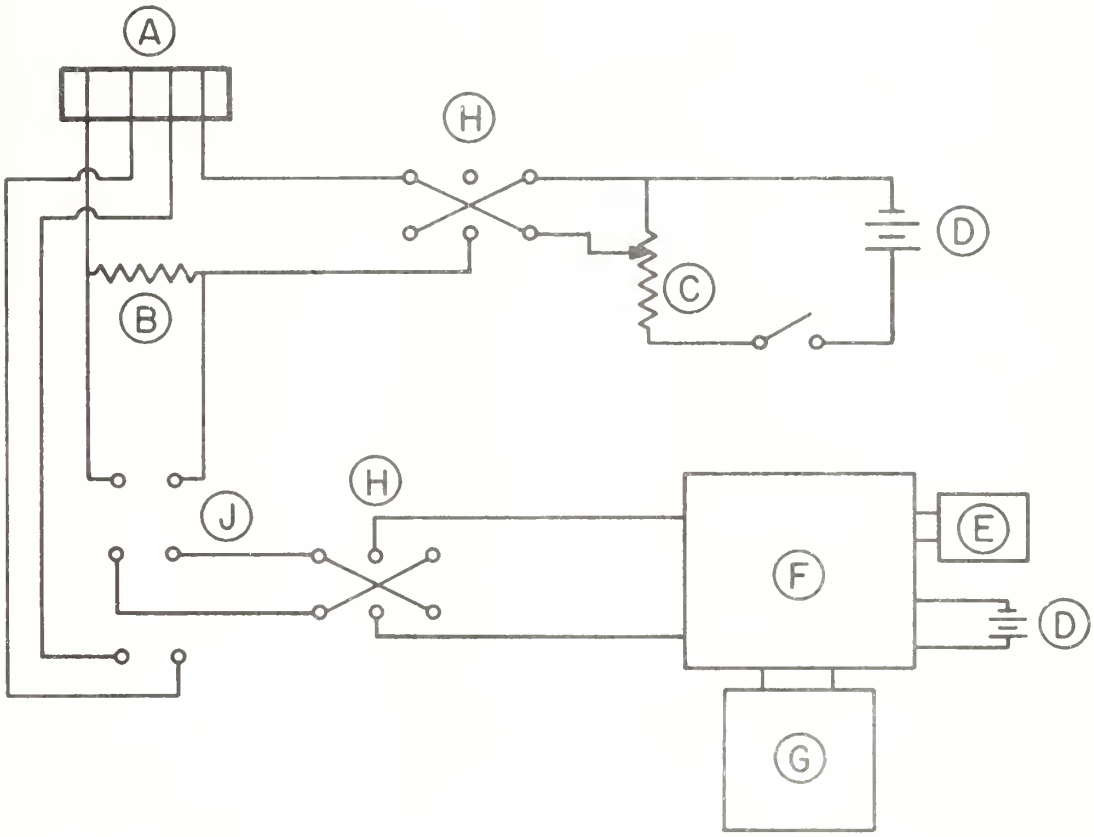

Figure 16. Schematic diagram of the electrical circuit used for conductivity measurements: a) wüstite sample, b) 0.01 ohm standard resistor, c) 1000 ohm variable resistor, d) 3 volt batteries, 3) standard cell, f) Leeds & Northrup Model K2 Potentiometer, g) L & N Model 9834 Null Detector, h) reversing switches, j) D.P.D.T. switch.

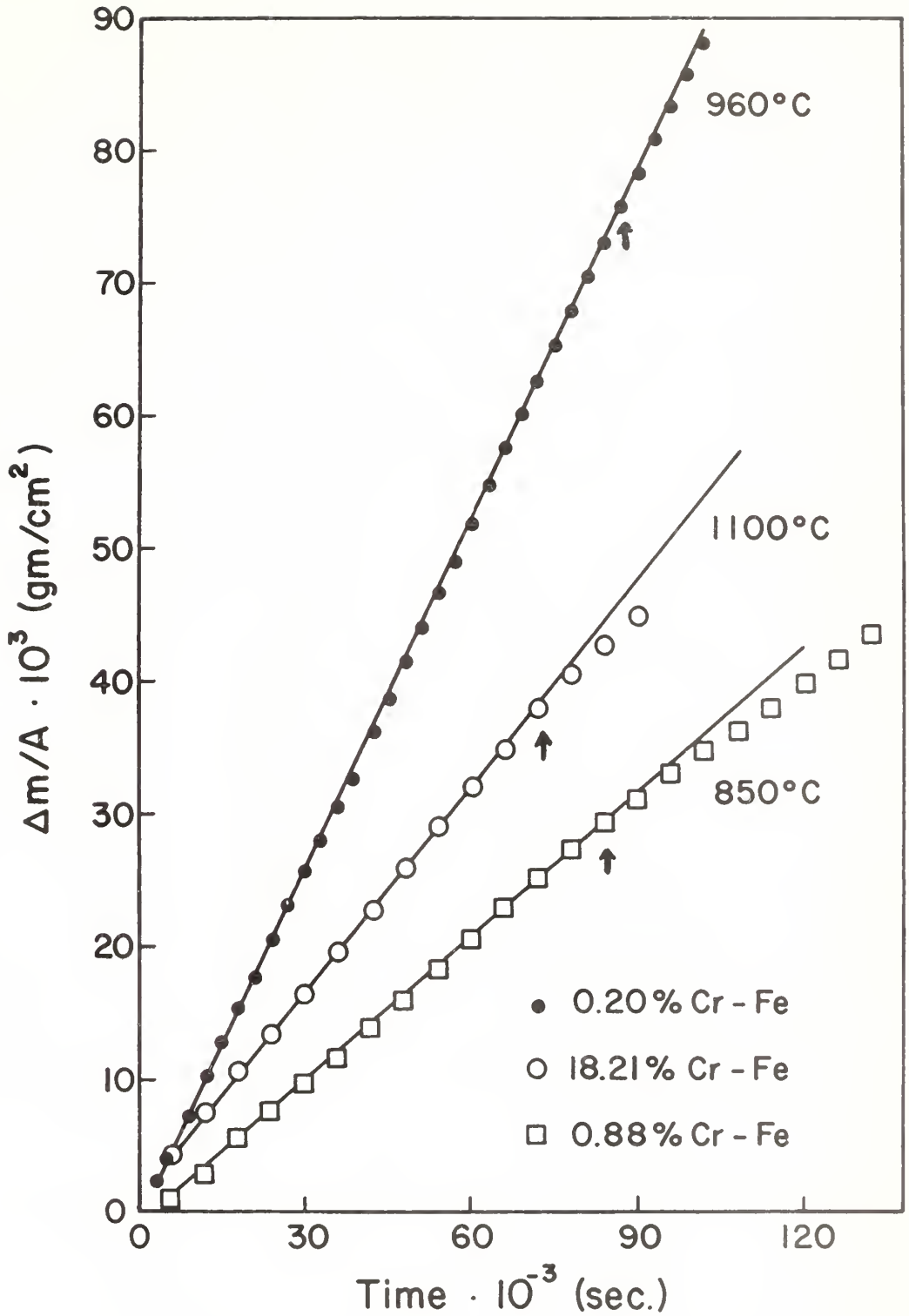

Figure 17. Representative curves for the linear oxidation of Fe-Cr alloys oxidized in a 60 vol.% CO_2-CO mixture.

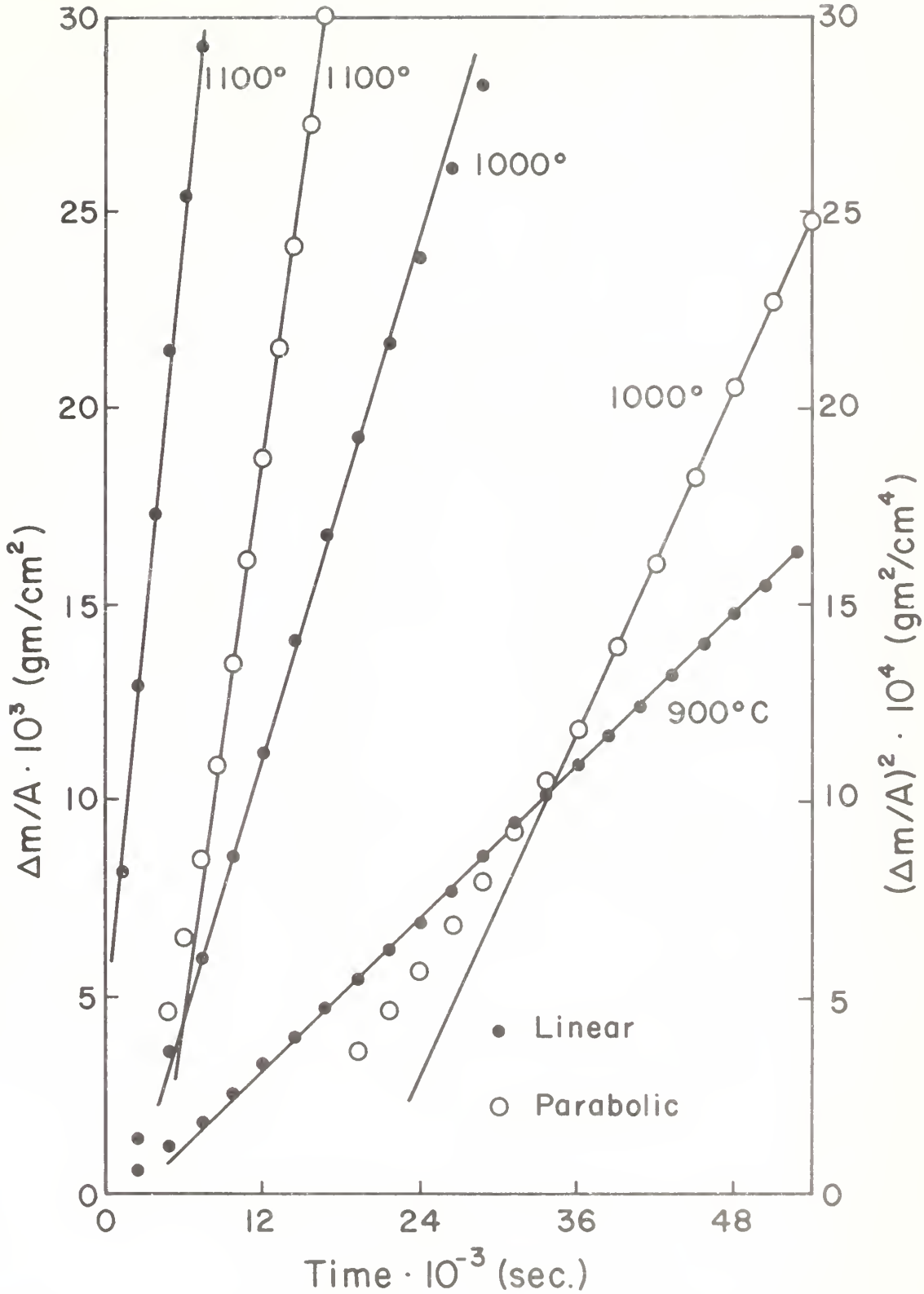

Figure 18. Typical rate curves for the oxidation of 7.55 wt.% Cr-Fe alloy in a 60 vol.% CO_2-CO gas mixture.

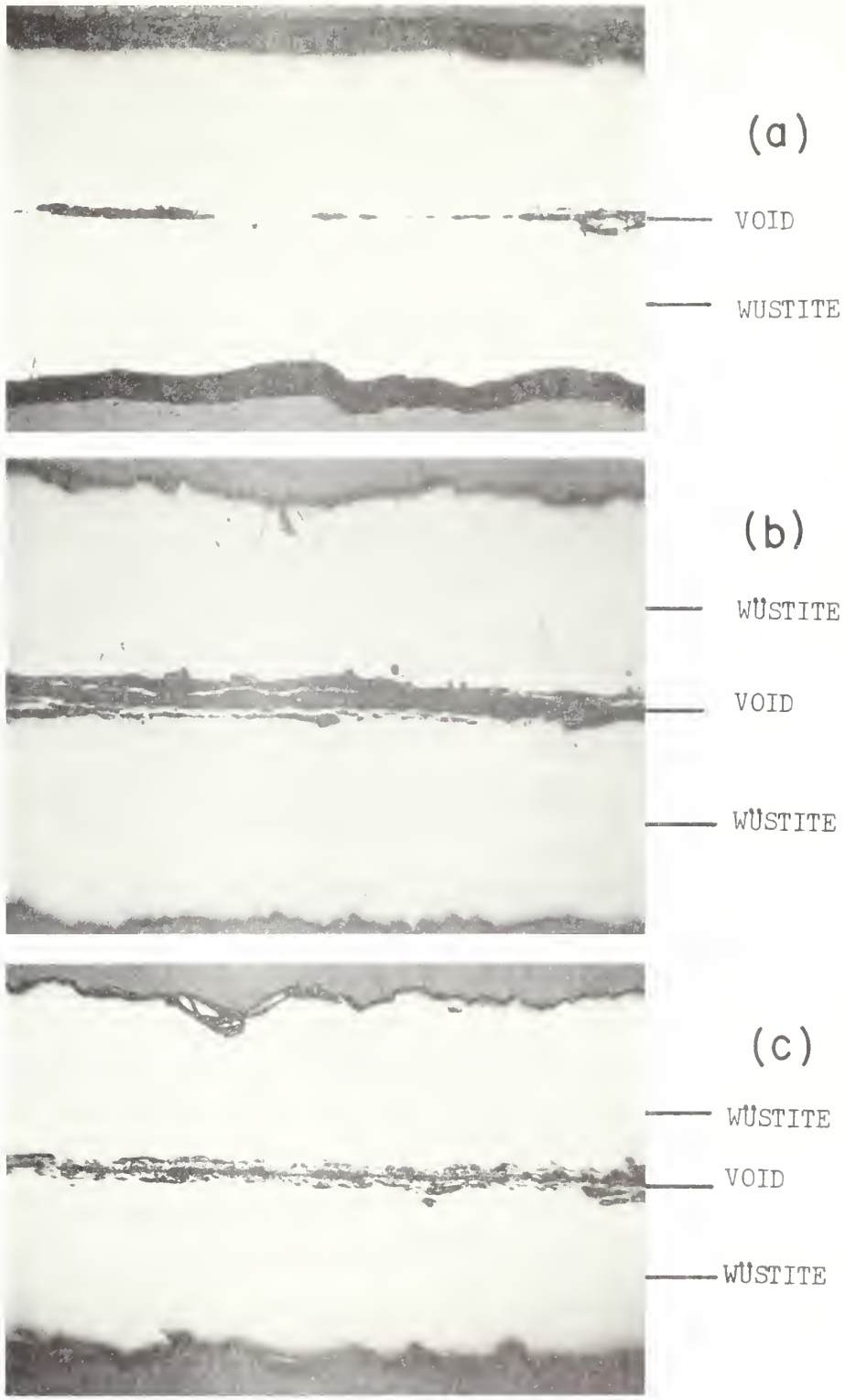

Figure 19. Cross-sections of oxide specimens formed at 1000°C in a 60 vol.% CO_2-CO gas mixture from: a) pure Fe, b) 0.20 wt.% Cr-Fe, c) 0.88 wt.% Cr-Fe, d) 1.70 wt.% Cr-Fe, e) 5.70 wt.% Cr-Fe, f) 7.55 wt.% Cr-Fe, g) 18.21 wt.% Cr-Fe.

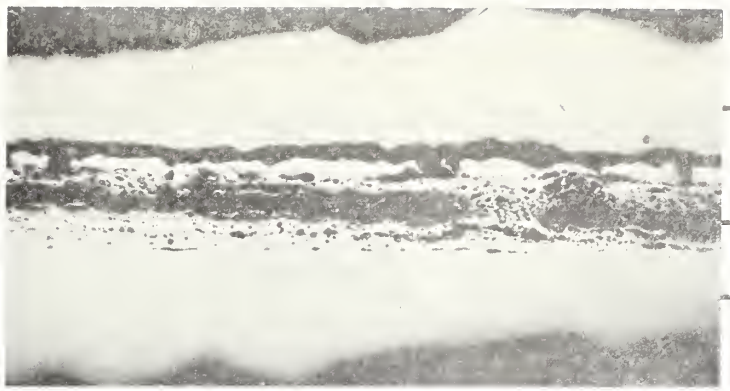

(d)

WÜSTITE

VOID

WÜSTITE

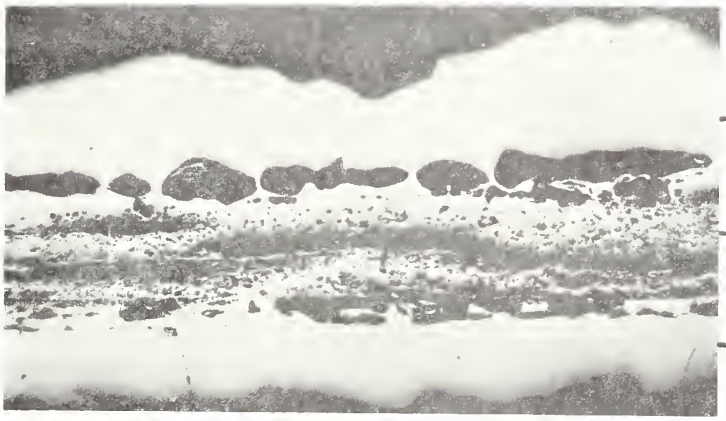

(e)

WÜSTITE

IRON-CHROMIUM SPINEL+WÜSTITE

WÜSTITE

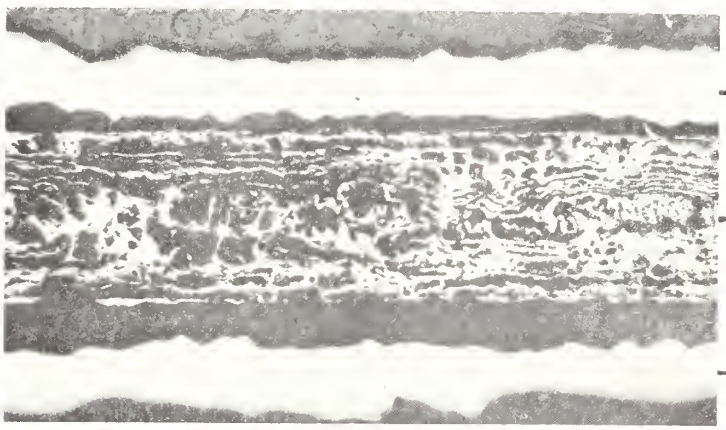

(f)

WÜSTITE

IRON-CHROMIUM SPINEL

WÜSTITE

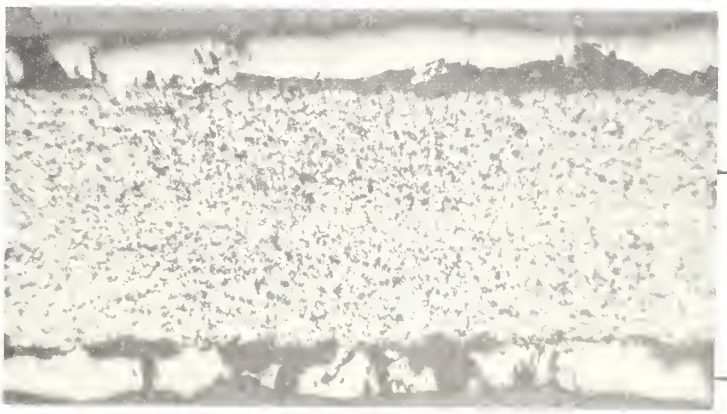

(g)

IRON-CHROMIUM SPINEL

WÜSTITE

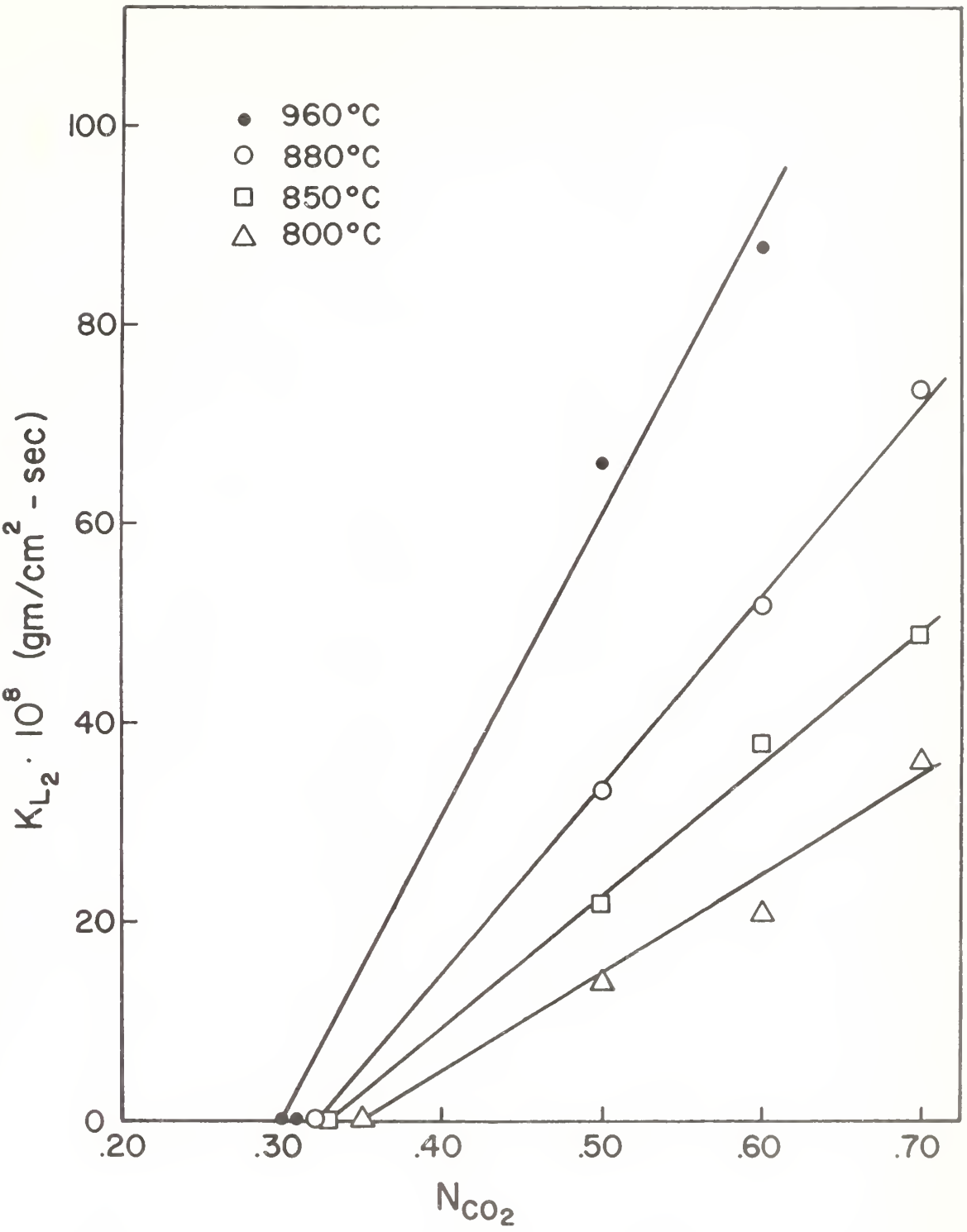

Figure 20. Dependence of the linear rate constants of oxidation of 0.20 wt.% Cr-Fe alloy on the mole fraction of CO_2 in the gas mixture at 800°, 850°, 880° and 960°C.

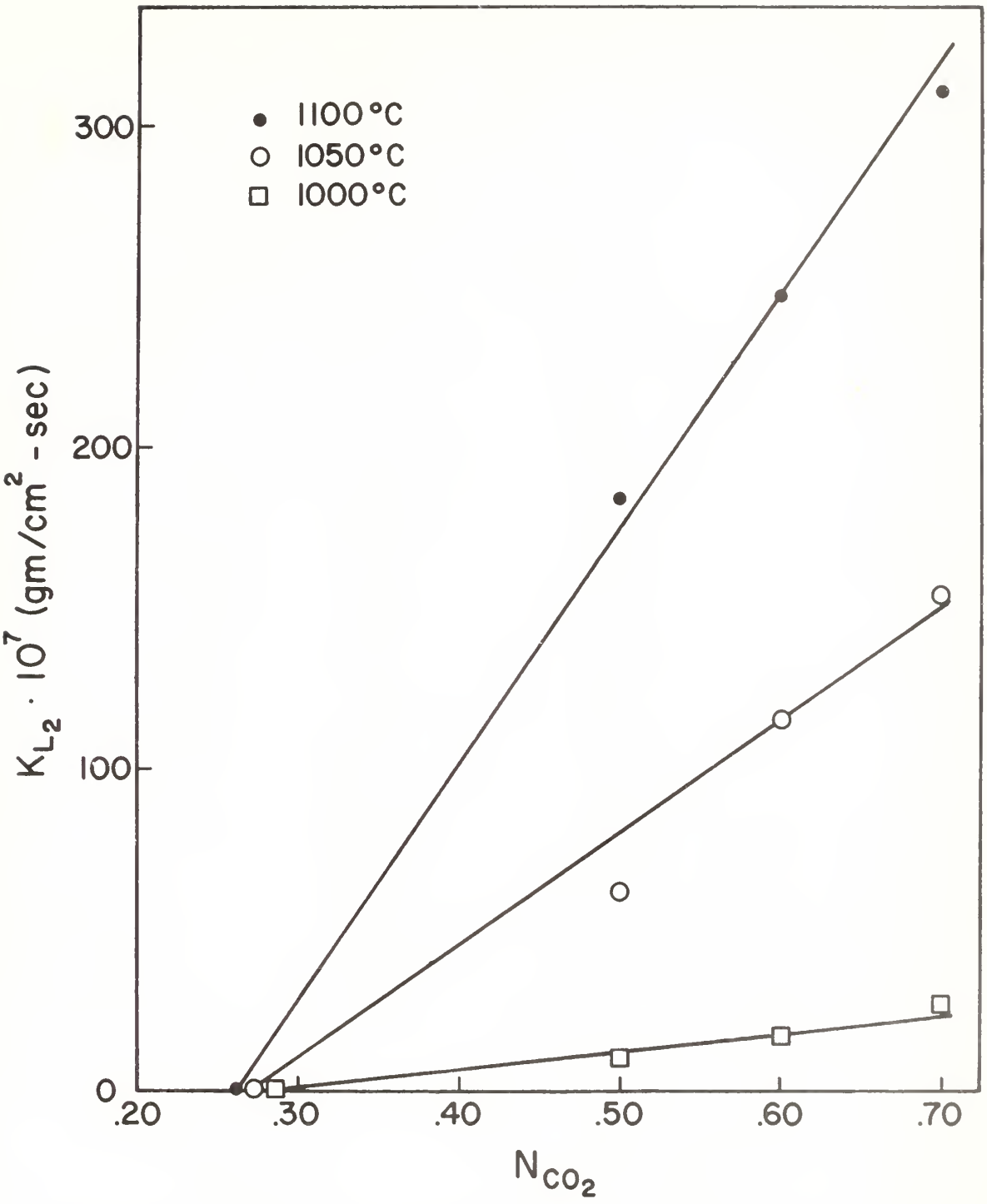

Figure 21. Dependence of the linear rate constants of oxidation of 0.20 wt.% Cr-Fe alloy on the mole fraction of CO_2 in the gas mixture at 1000°, 1050° and 1100°C.

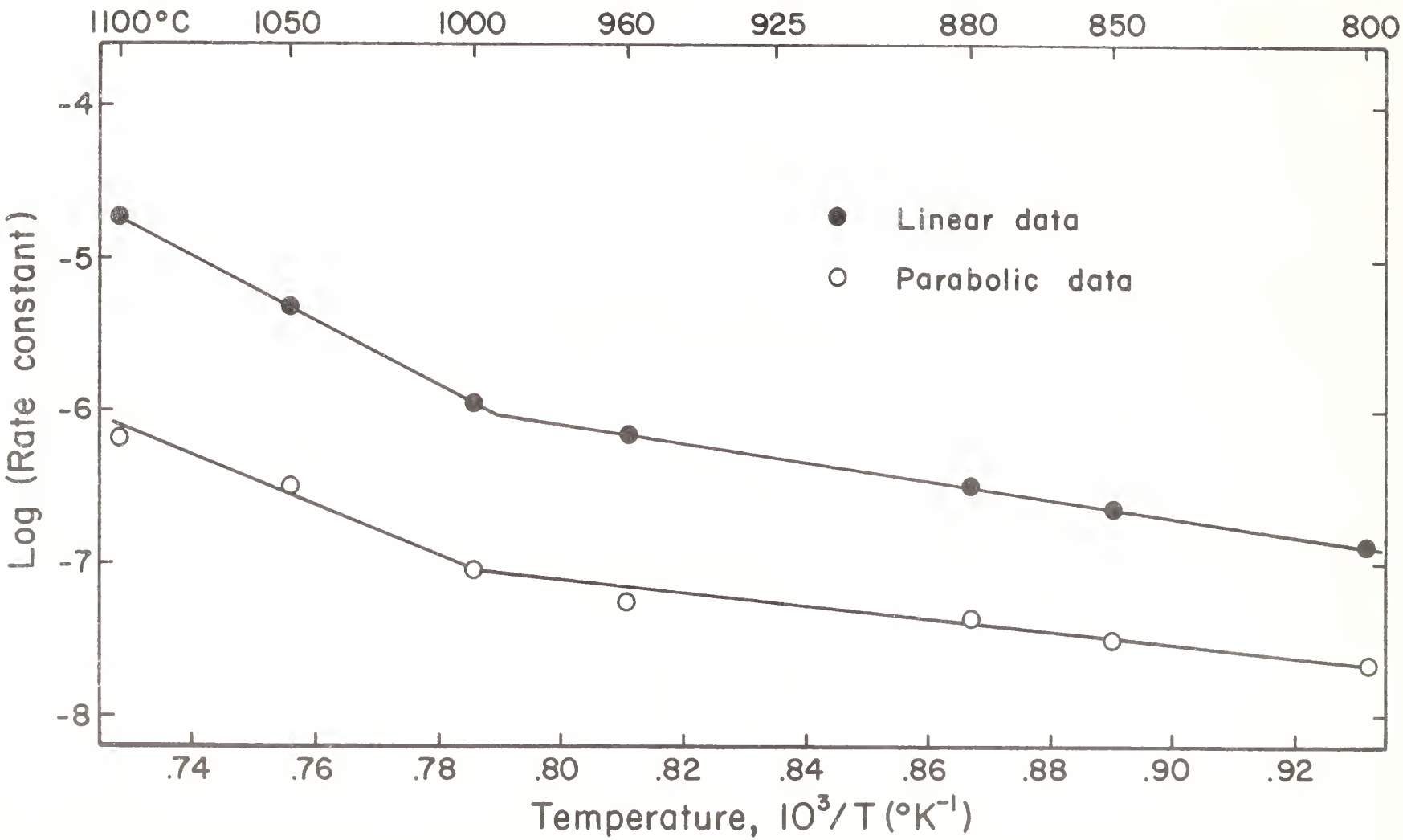

Figure 22. Temperature dependence of the linear and parabolic rate constants of oxidation of the 0.20 wt.% Cr-Fe alloy in a 50 vol.% CO_2-CO mixture.

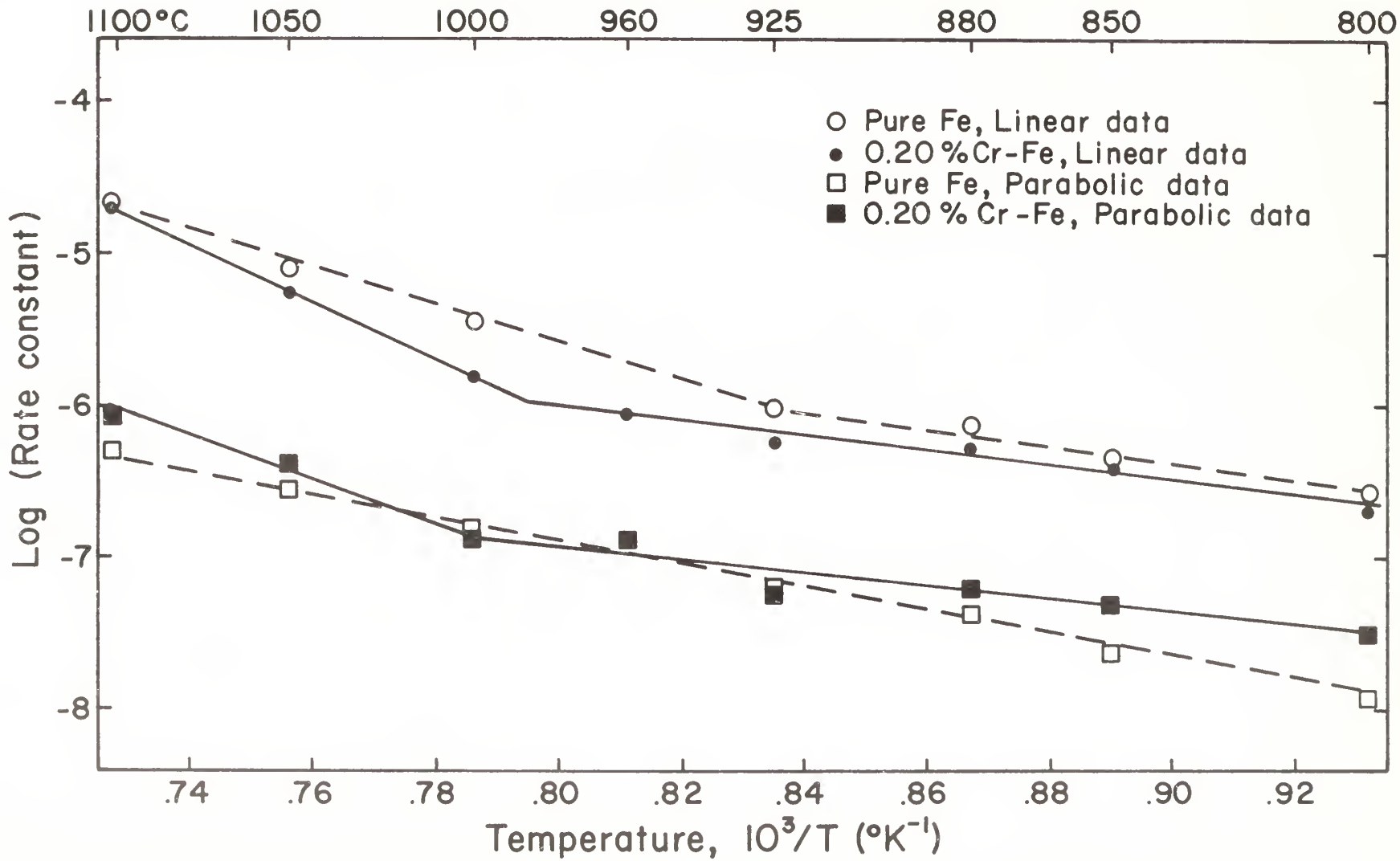

Figure 23. Temperature dependence of the linear and parabolic rate constants of oxidation of the 0.20 wt.% Cr-Fe alloy in a 60 vol.% CO_2-CO mixture.

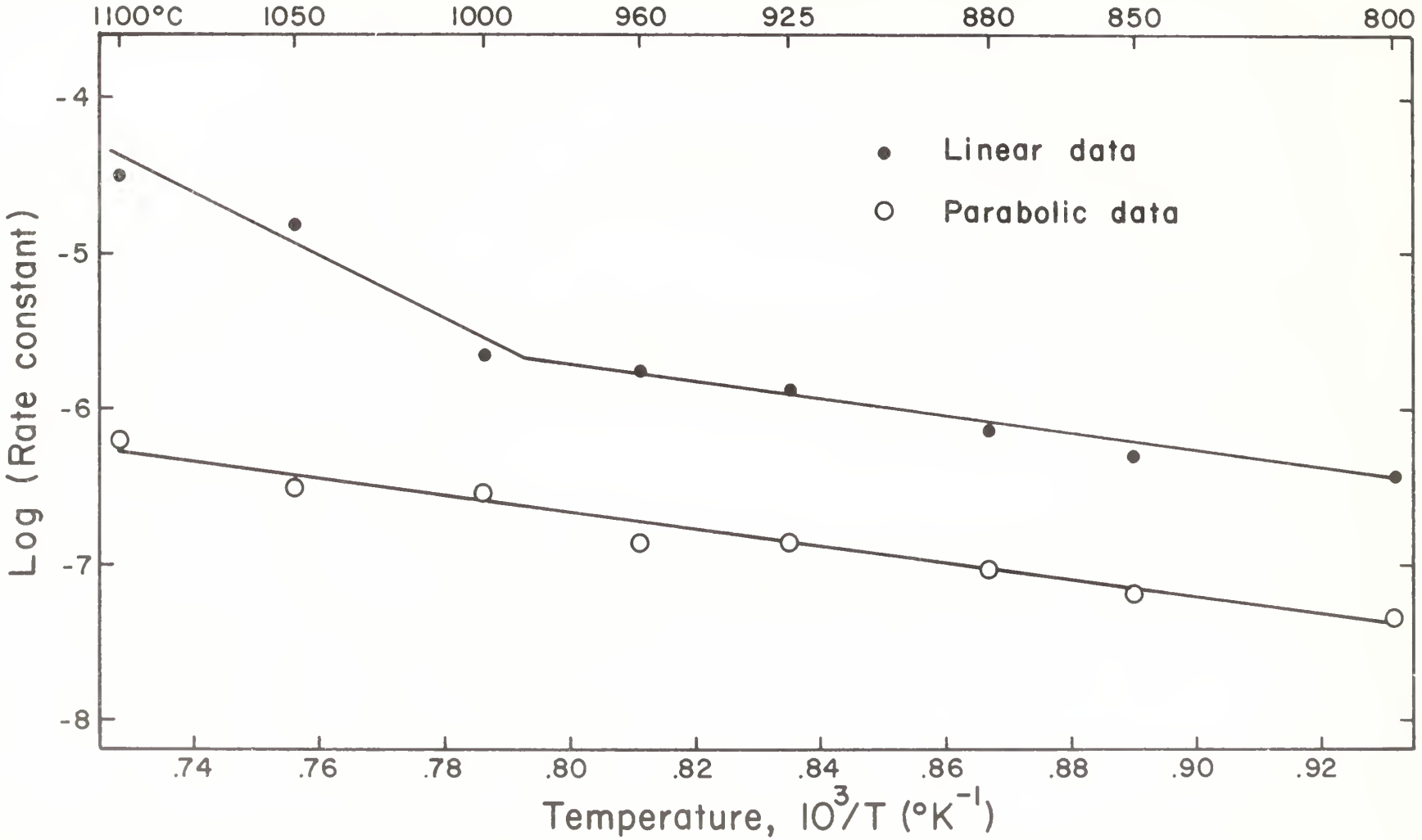

Figure 24. Temperature dependence of the linear and parabolic rate constants of oxidation of the 0.20 wt.% Cr-Fe alloy in a 70 vol.% CO_2-CO mixture.

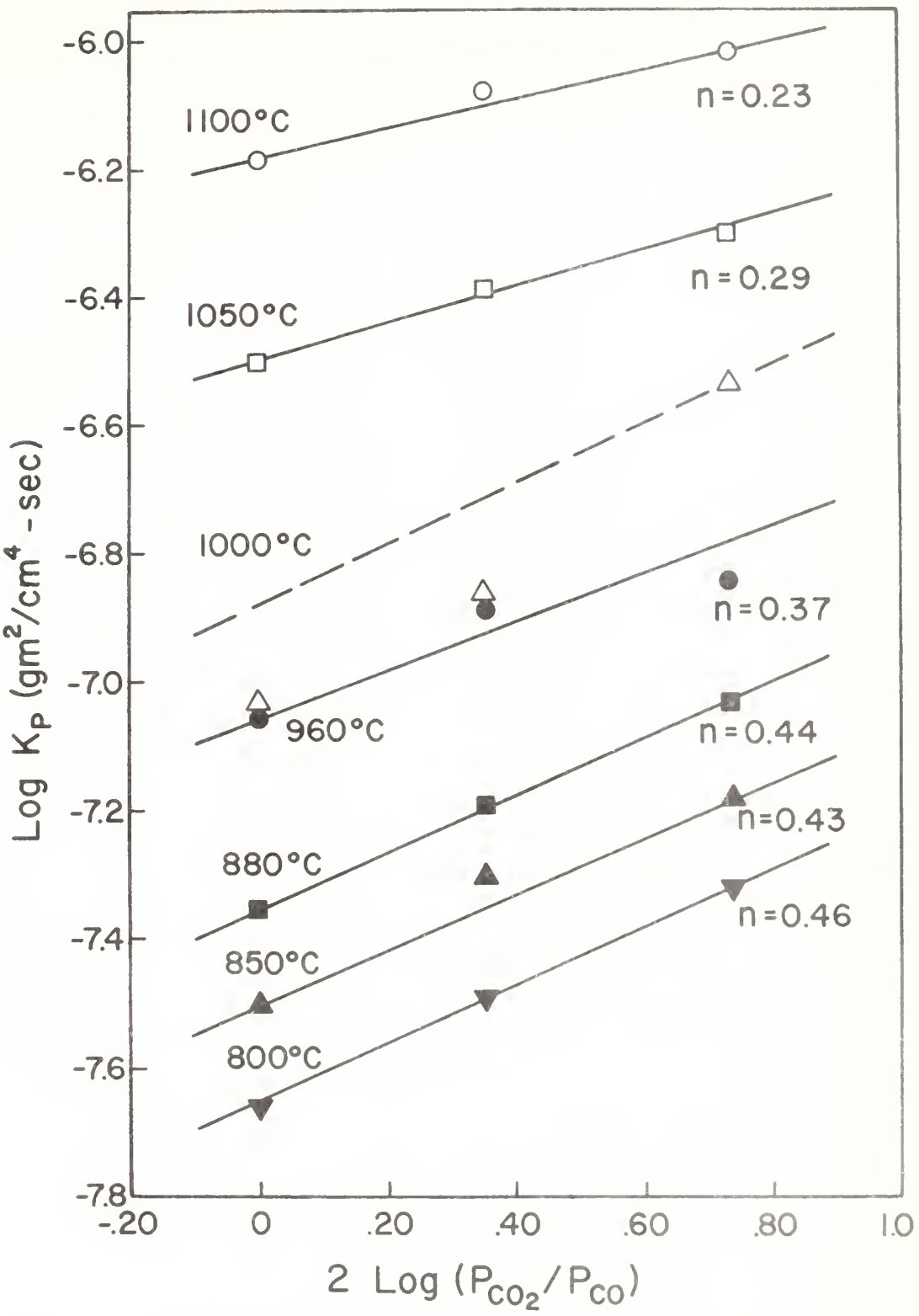

Figure 25. Pressure dependence of the parabolic rate constants of oxidation of the 0.20 wt.% Cr-Fe alloy.

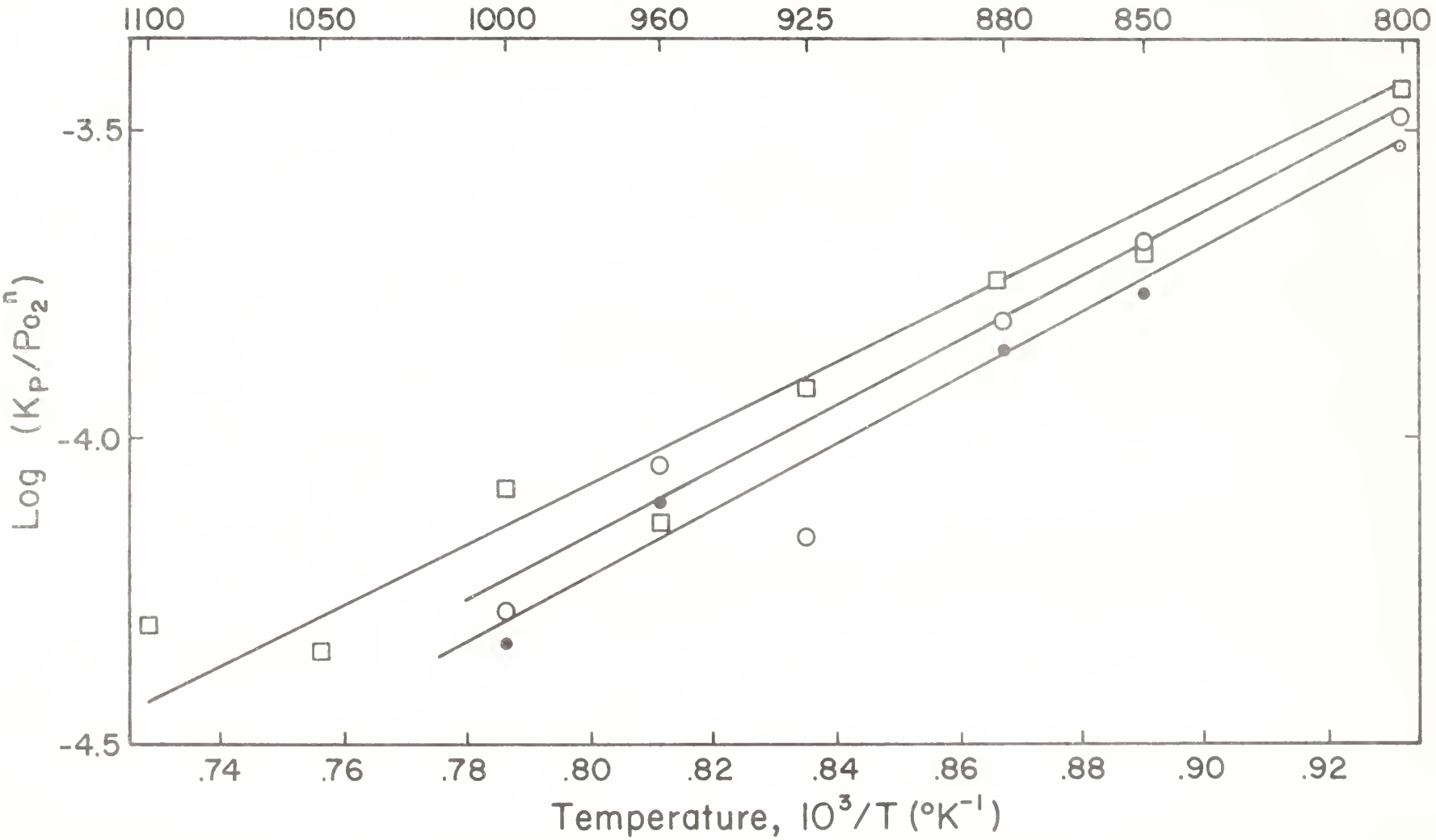

Figure 26. Temperature dependence of ($K_p/p_{O_2}^n$) where n = 1/3 for the oxidation of the 0.20 wt.% Cr-Fe alloy in various CO_2-CO mixtures. (●) N_{CO_2} = 0.500: (o) N_{CO_2} = 0.600; (□) N_{CO_2} = 0.700.

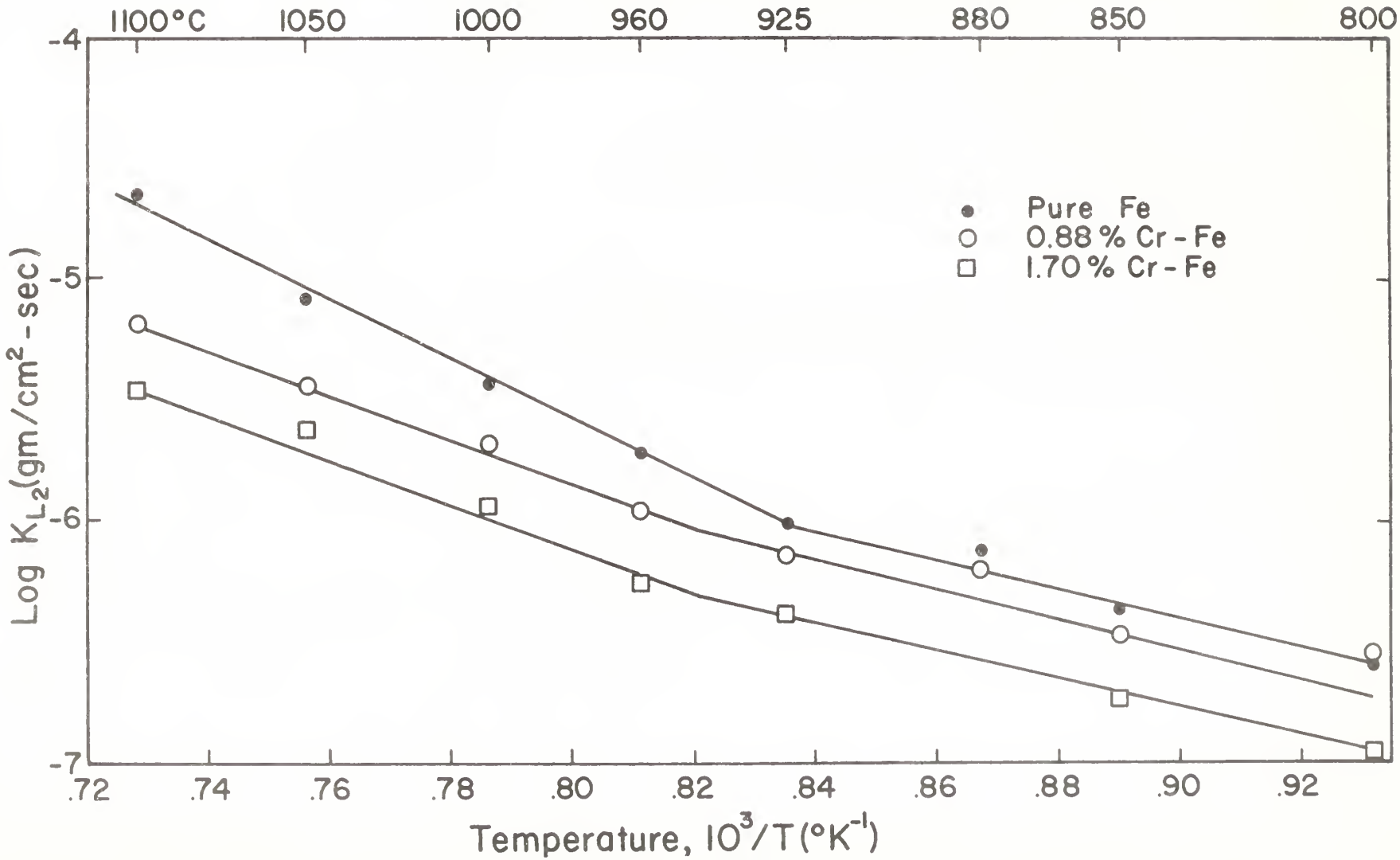

Figure 27. Temperature dependence of the linear rate constants of oxidation of pure iron (27), 0.88% Cr-Fe, and 1.70% Cr-Fe alloys in a 60 vol.% CO_2-CO mixture.

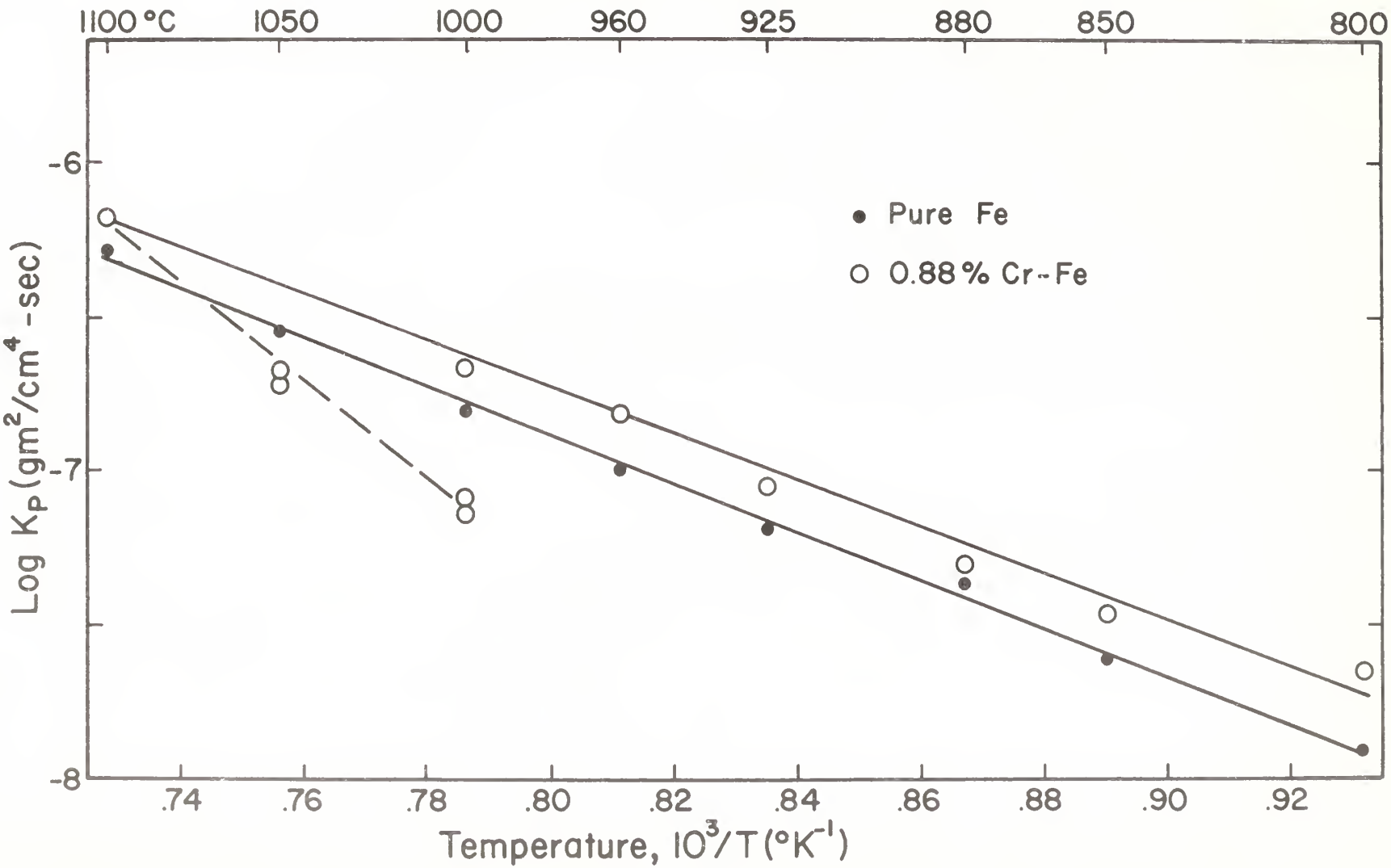

Figure 28. Temperature dependence of the parabolic rate constants of oxidation of the 0.20% Cr-Fe alloy and pure iron (27) in a 60 vol.% CO_2-CO mixture.

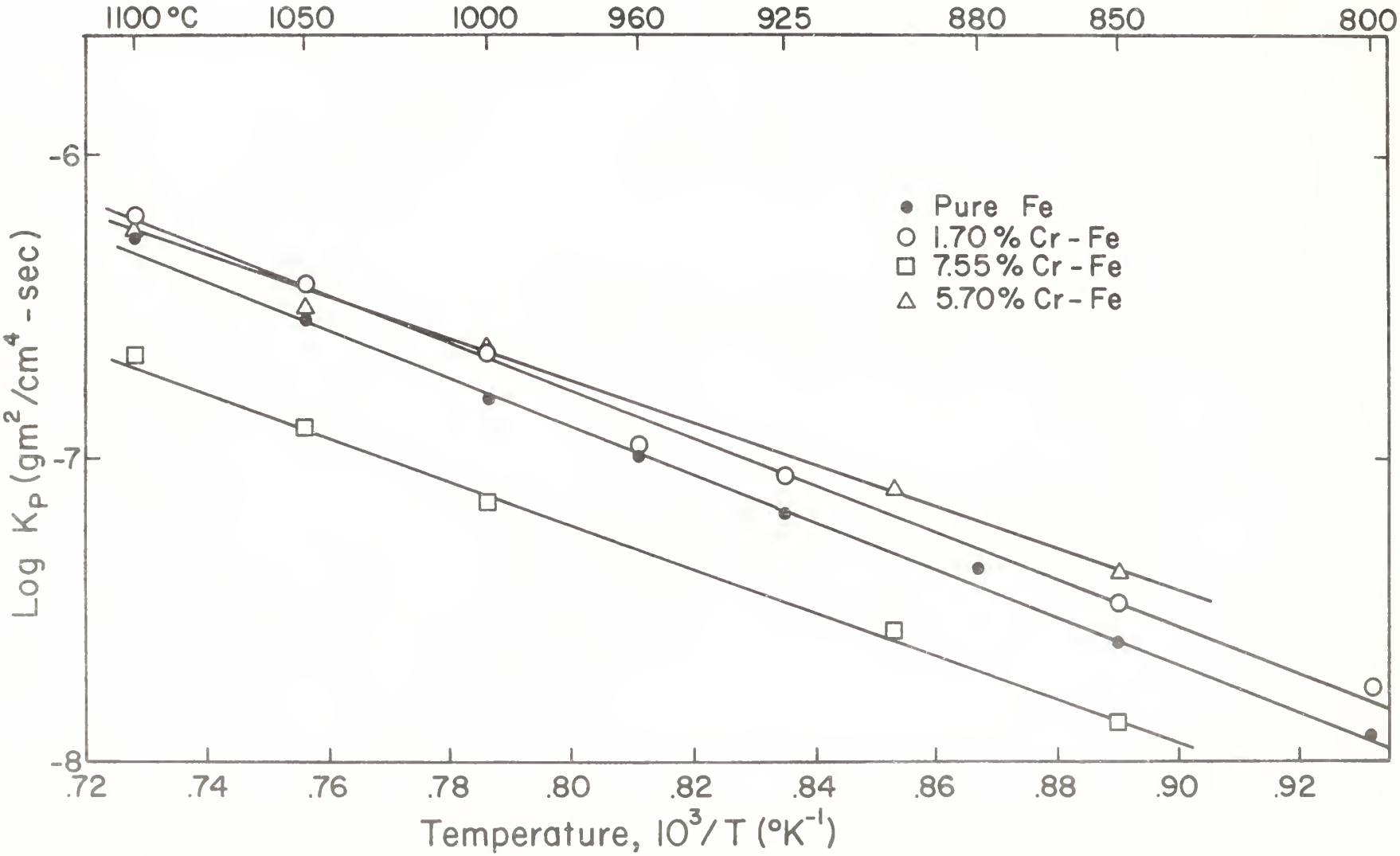

Figure 29. Temperature dependence of the parabolic rate constants of oxidation of pure iron, 1.70% Cr-Fe, 5.70% Cr-Fe and 7.55% Cr-Fe alloys in a 60 vol.% CO_2-CO mixture.

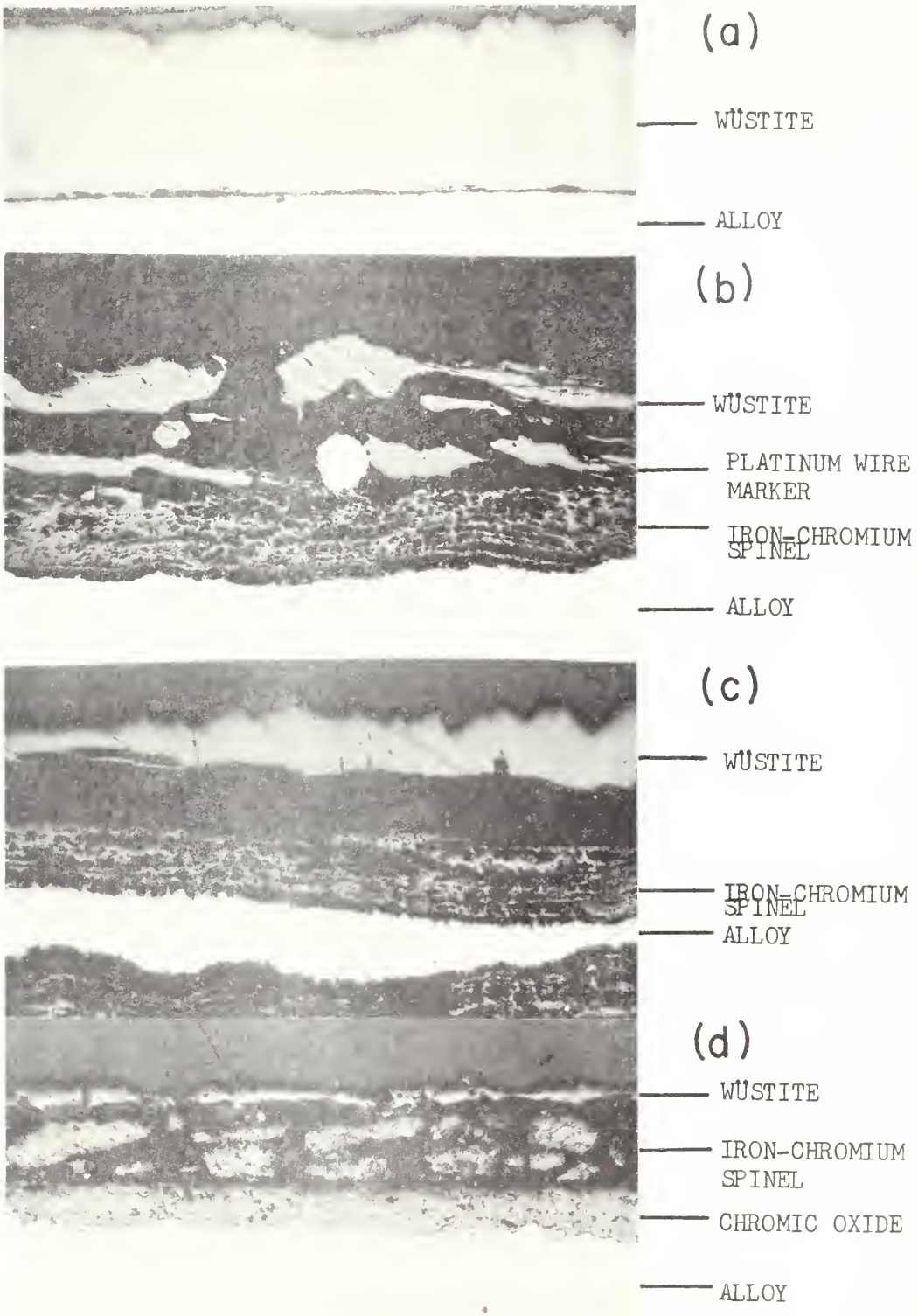

Figure 30. Cross-sections of specimens which show the oxide scale structure formed on the metal substrate at 1000°C in a 60vol % CO_2-CO mixture. a) 0.20 wt % Cr-Fe, b) 5.70 wt % Cr-Fe with Pt marker, c) 7.55 wt % Cr-Fe, d) 18.21 wt % Cr-Fe alloy.

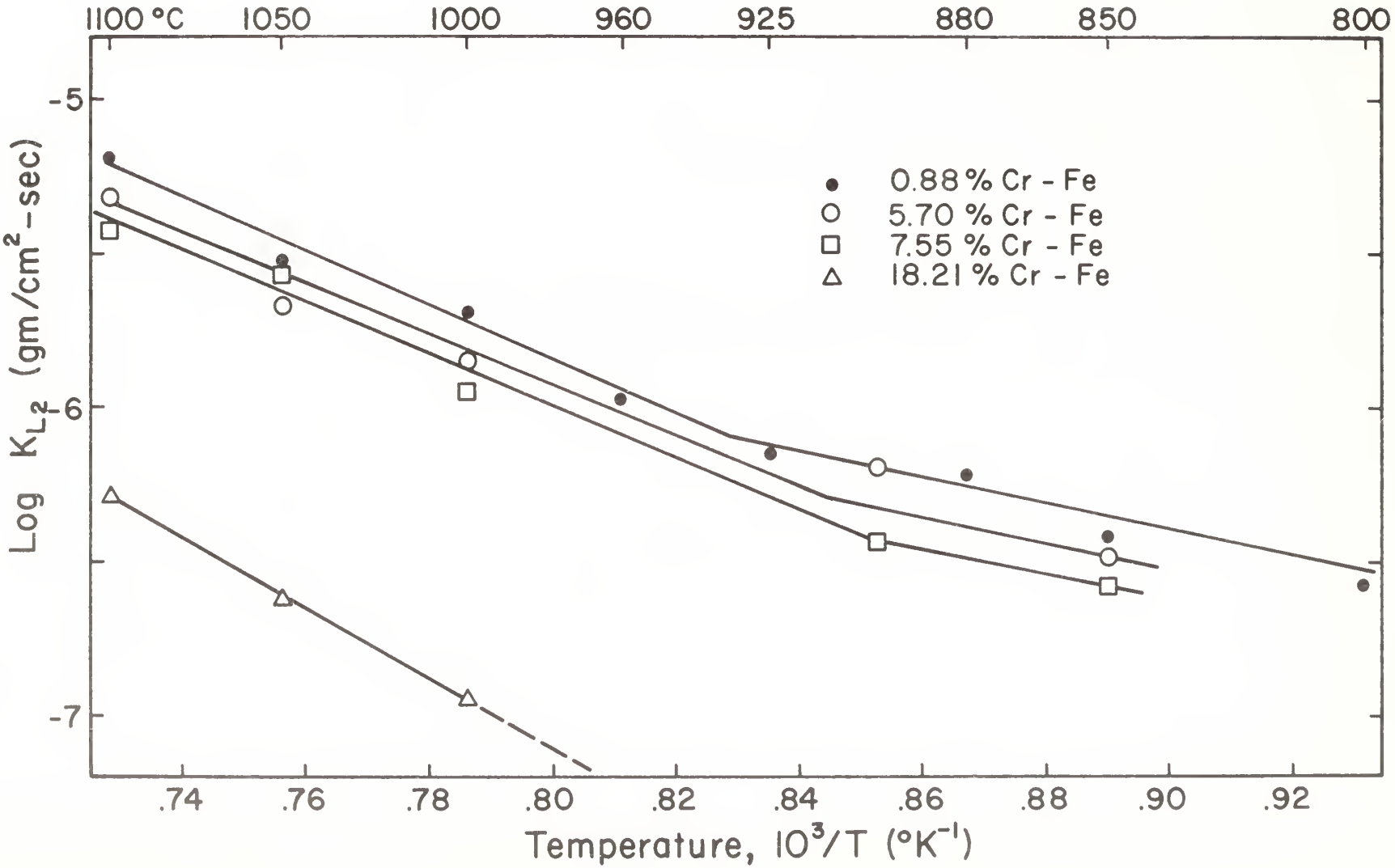

Figure 31. Temperature dependence of the linear rate constants of oxidation of various Fe-Cr alloys in a 60 vol.% CO_2-CO mixture.

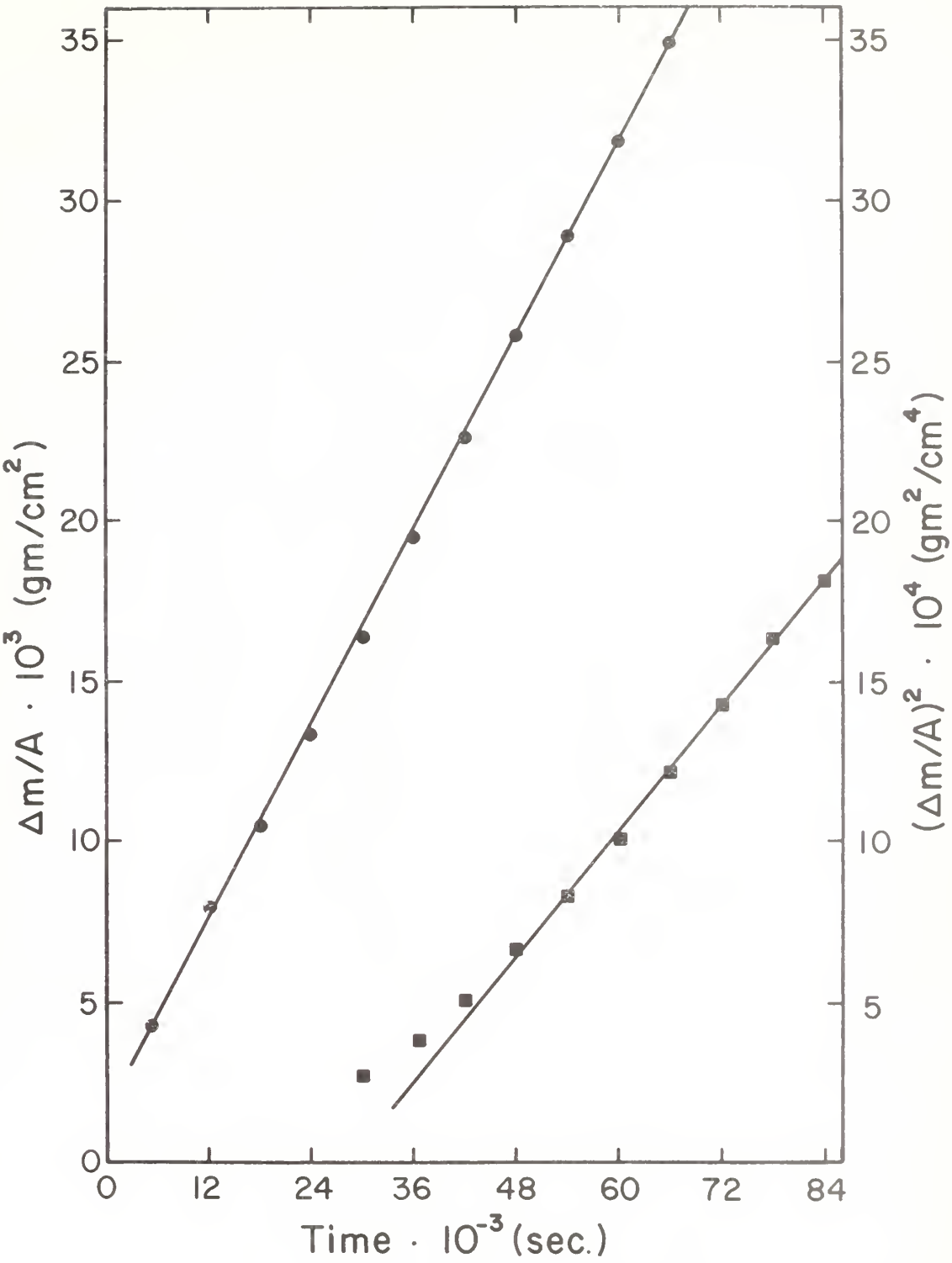

Figure 32. Typical rate curves for the oxidation of Type 430 (18.21% Cr-Fe) alloy at 1100°C in a 60 vol.% CO_2-CO mixture. (●) Linear (□) Parabolic.

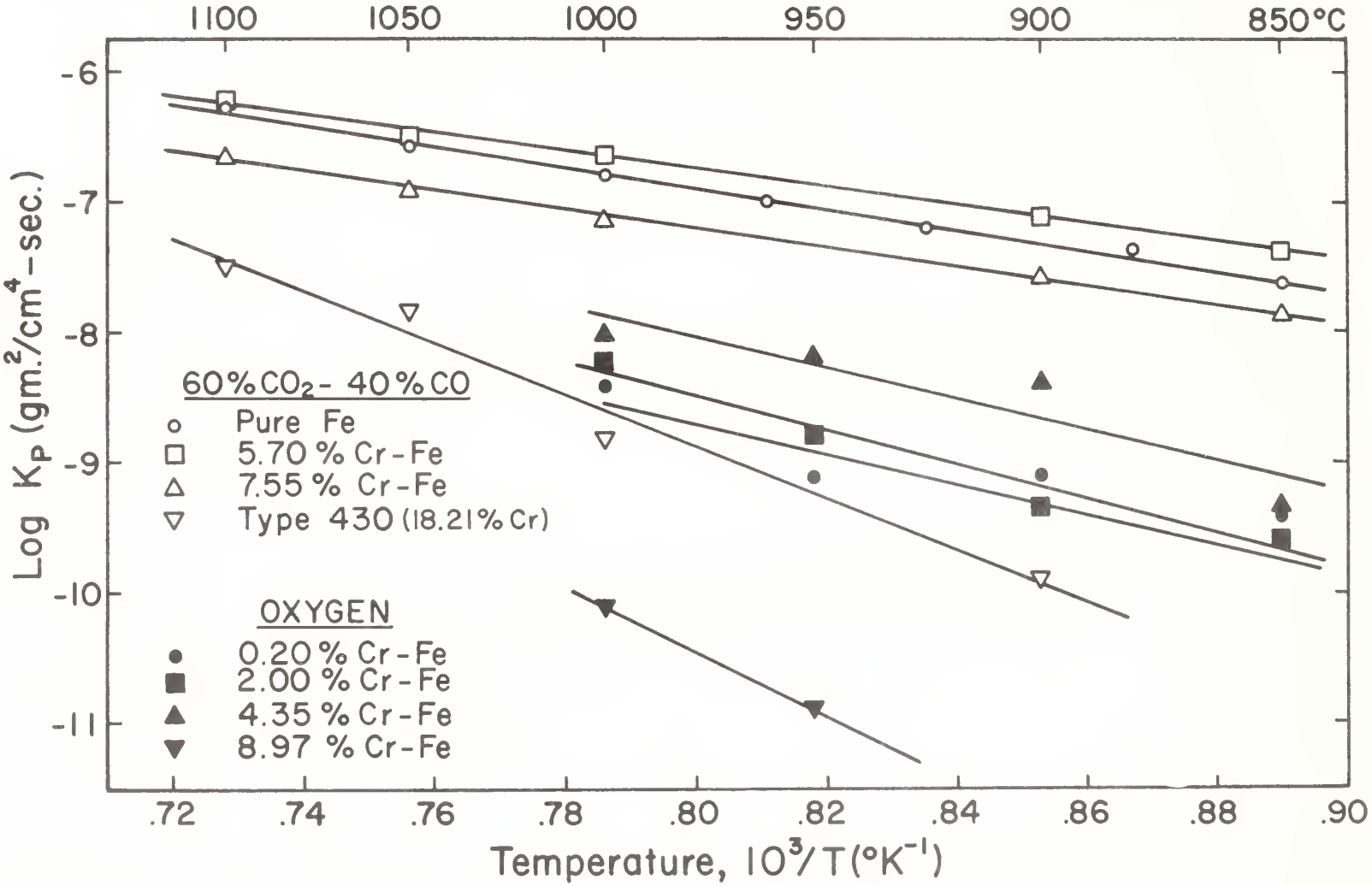

Figure 33. Temperature dependence of the parabolic rate constants of pure iron and various Fe-Cr alloys in CO_2-CO mixtures and in oxygen.

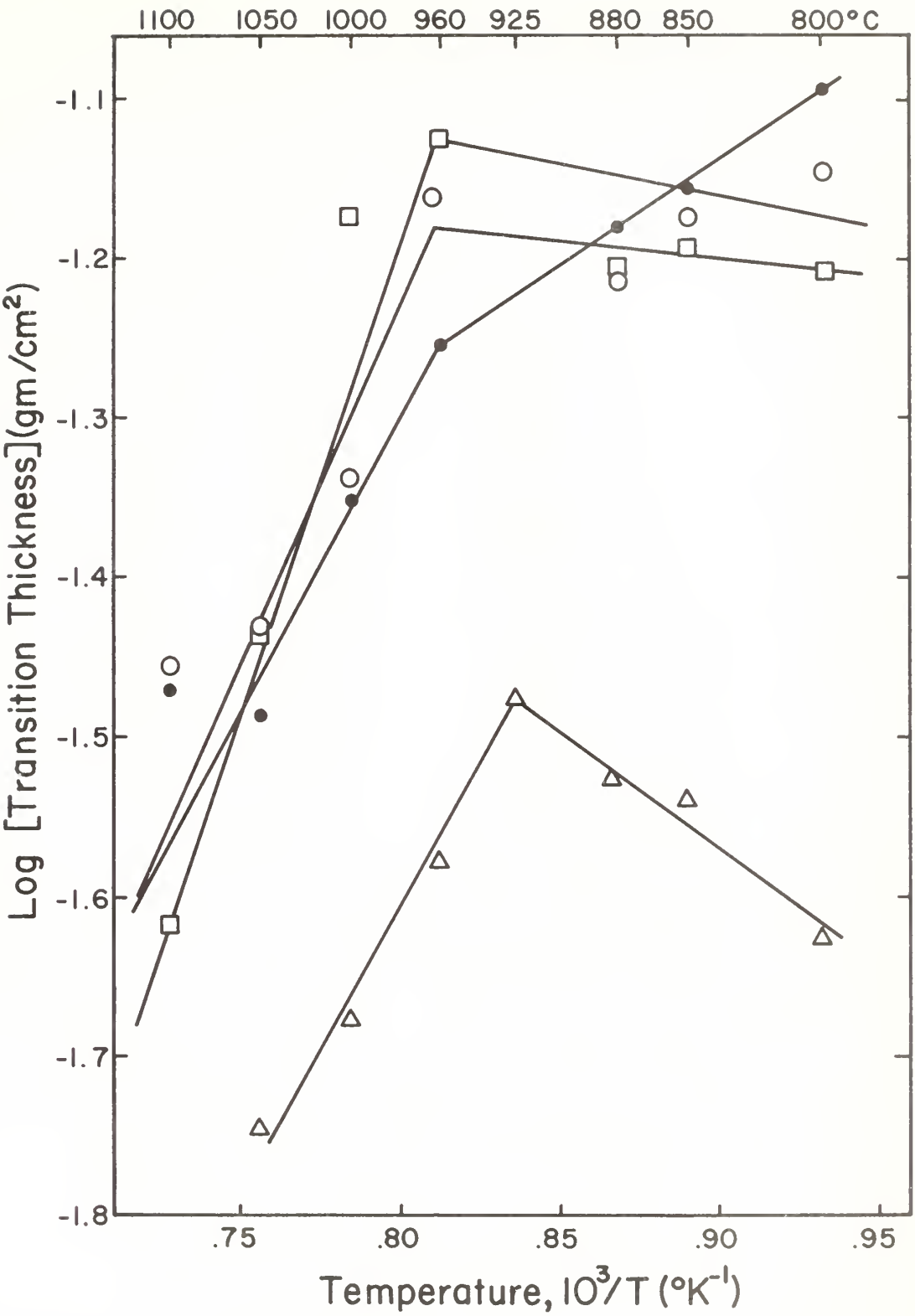

Figure 34. Temperature dependence of the transition thickness of pure iron (Δ) and 0.20% Cr-Fe alloy in various CO_2-CO mixtures. (●) N_{CO_2} = 0.500; (o,Δ) N_{CO_2} = 0.600; (□) N_{CO_2} = 0.700.

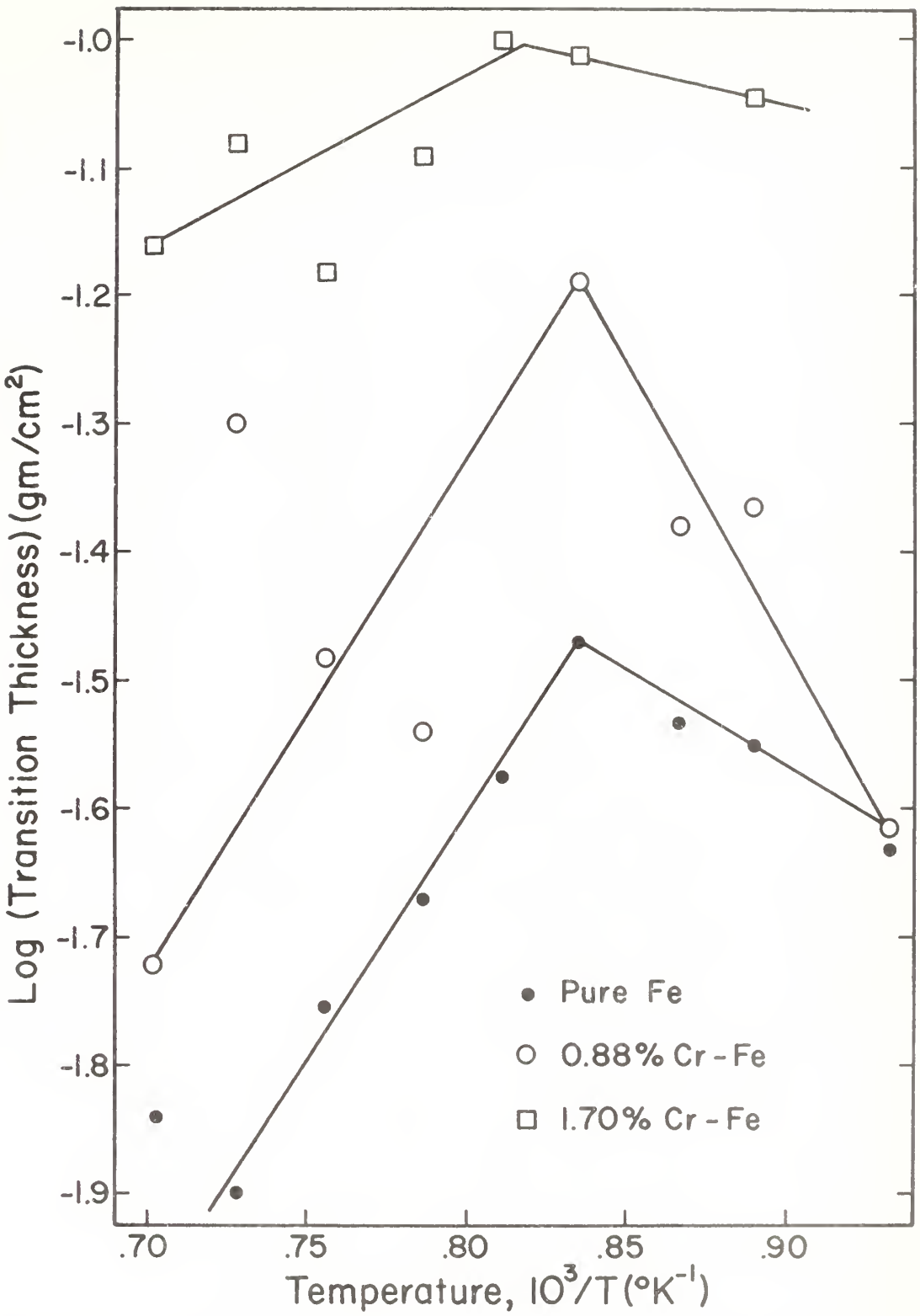

Figure 35. Temperature dependence of the transition thickness of Fe and Fe-Cr alloys in a 60 vol.% CO_2-CO mixture.

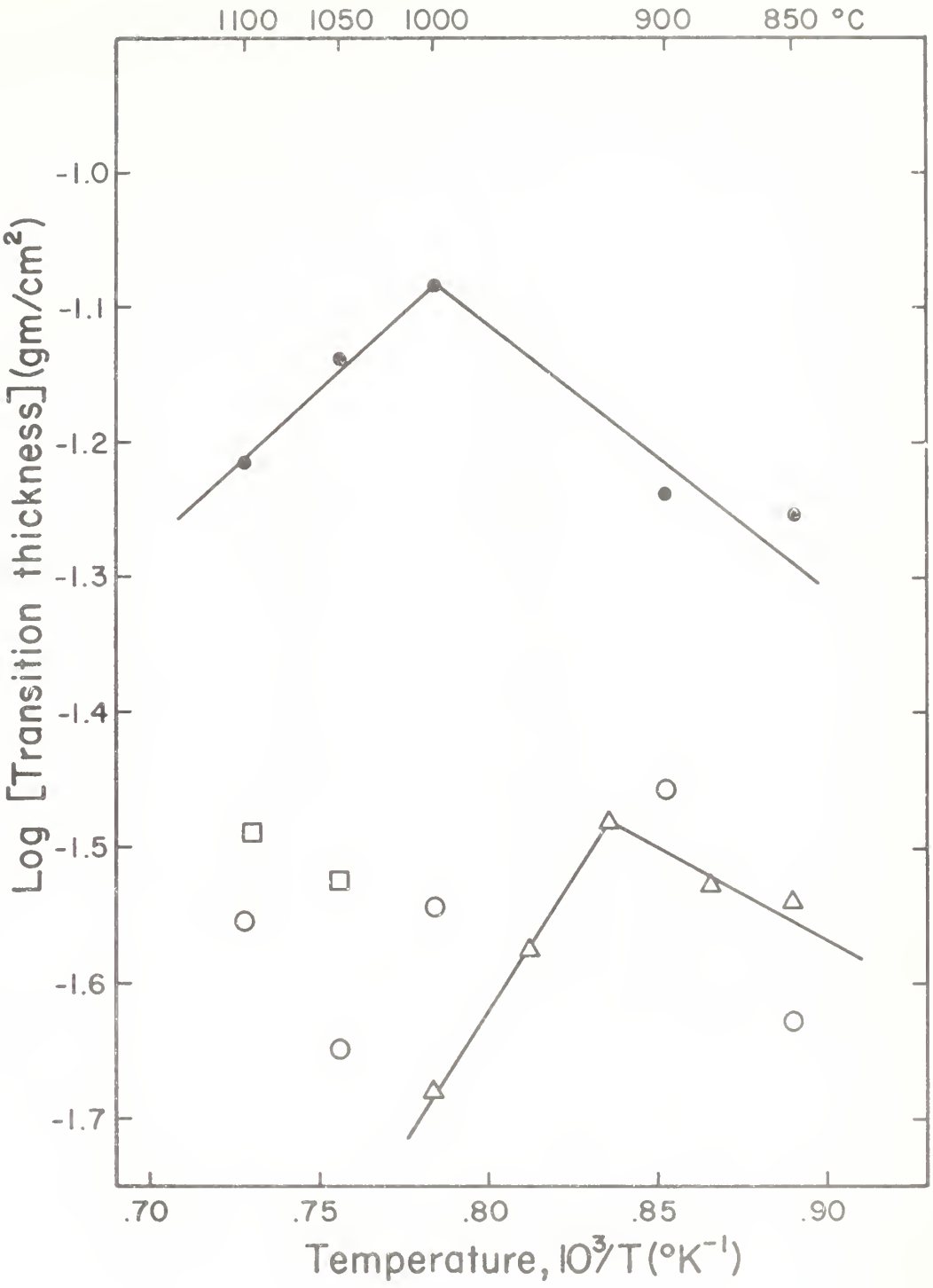

Figure 36. Temperature dependence of the transition thickness of pure iron (∧), 5.70% Cr-Fe (●), 7.55% Cr-Fe (o), and 18.21% Cr-Fe (□) in a 60 vol.% CO_2-CO mixture.

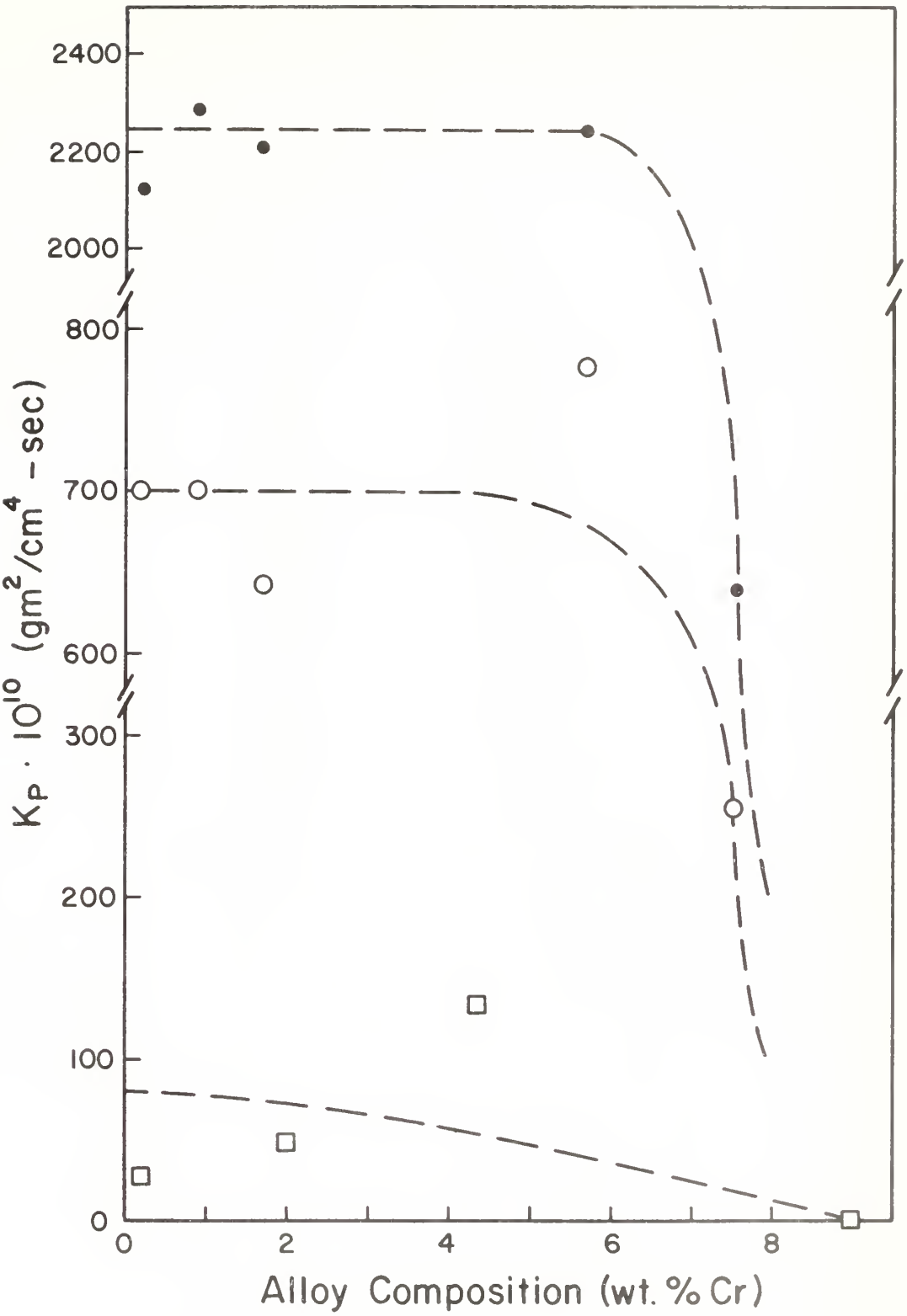

Figure 37. Rates of oxidation of various Fe-Cr alloys in carbon dioxide-carbon monoxide mixtures and in oxygen. (●) N_{CO_2} = 0.600 at 1000°C; (○) N_{CO_2} = 0.600 at 900°C; (□) pure oxygen at 1000°C.

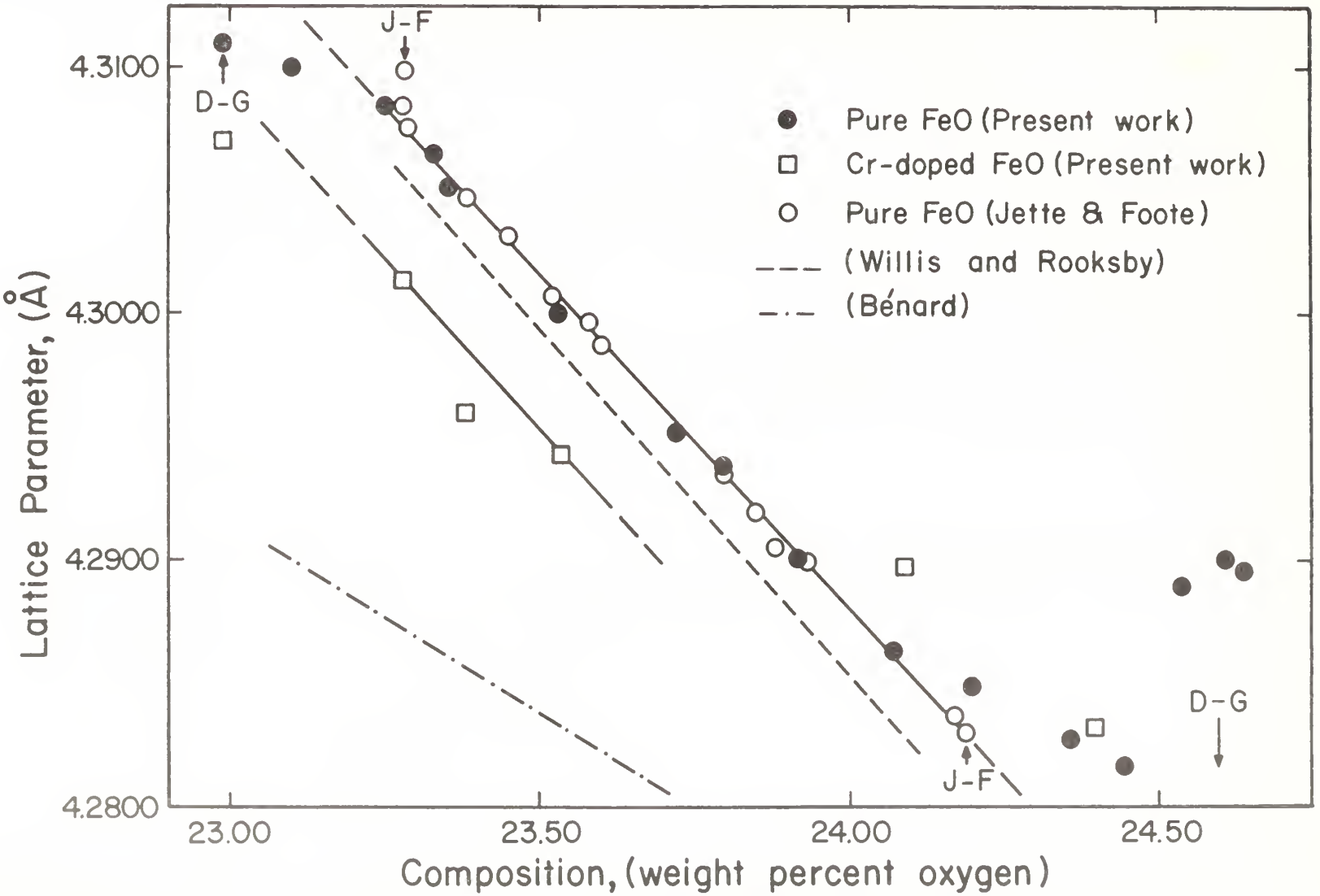

Figure 38. Lattice parameters of pure and doped wüstite as a function of oxygen content.

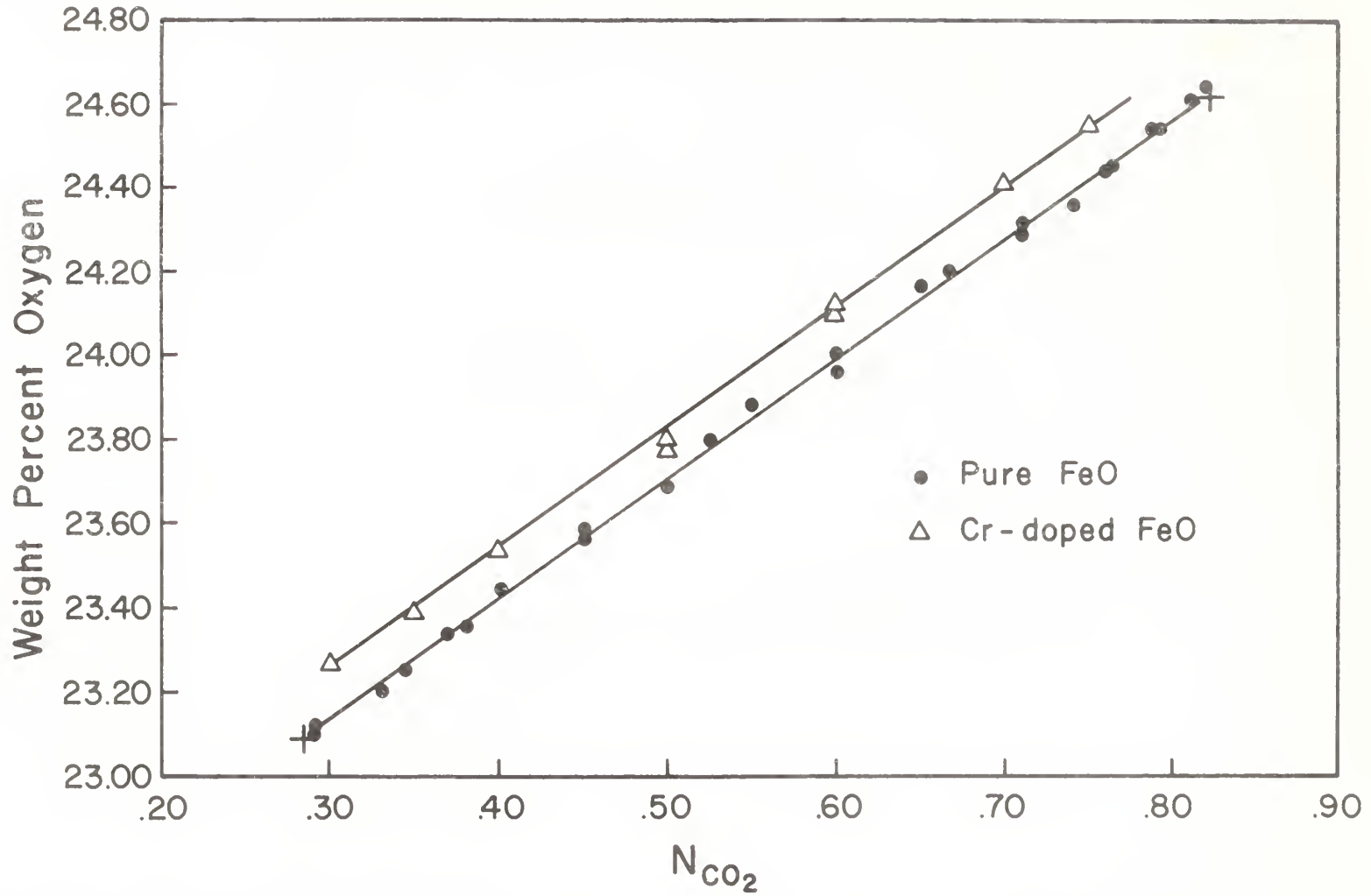

Figure 39. Equilibrium compositions of pure wüstite and wüstite containing 0.67 wt.% Cr at 1000°C in various CO_2-CO mixtures. The crosses denote the phase limits at 1000°C according to Darken and Gurry (8).

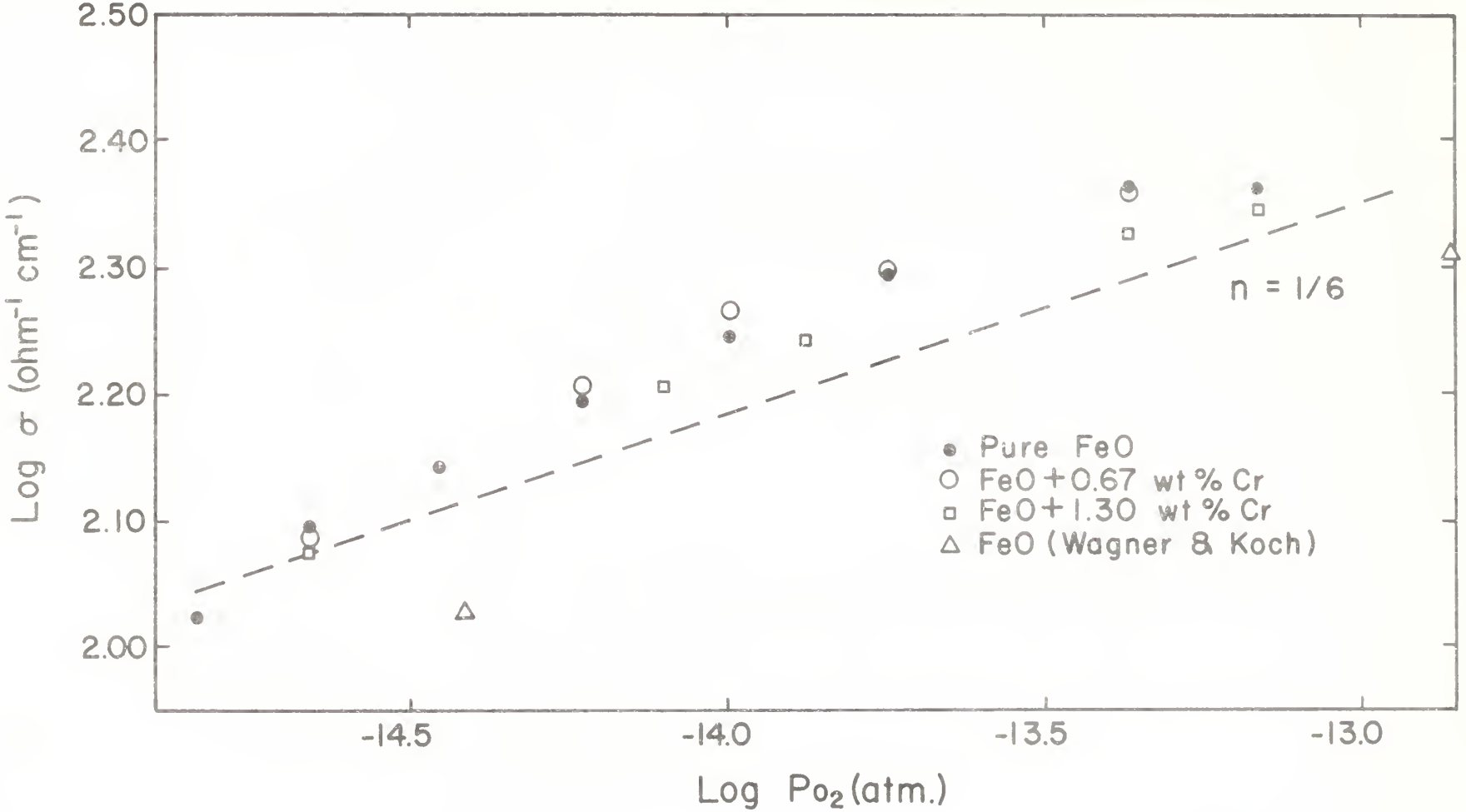

Figure 40. Electrical conductivity of pure and doped wüstite at 1000°C in various CO_2-CO mixtures.

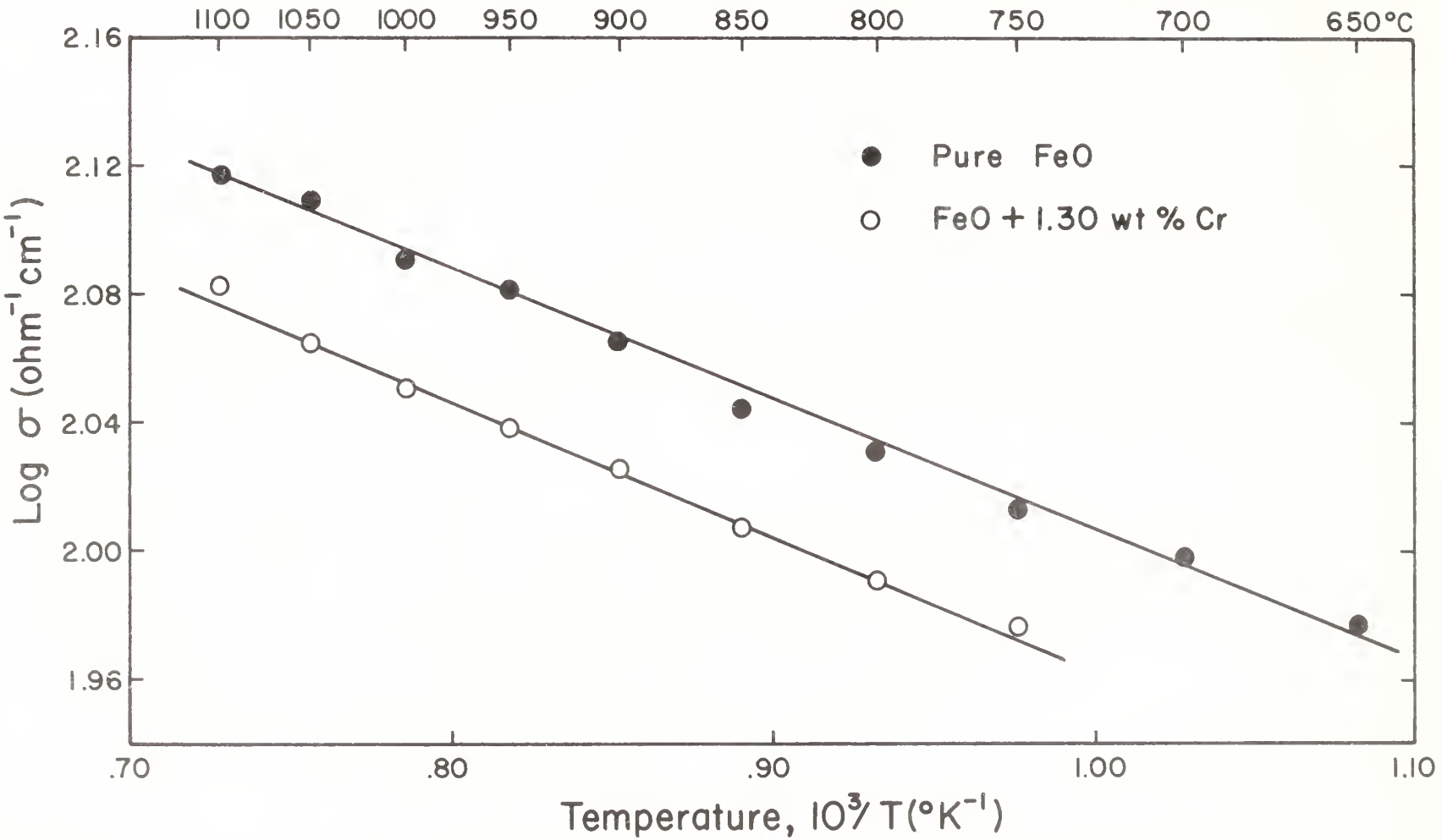

Figure 41. Temperature dependence of the electrical conductivity of pure and doped wüstite of constant composition, oxygen to metal ratio = 1.060.

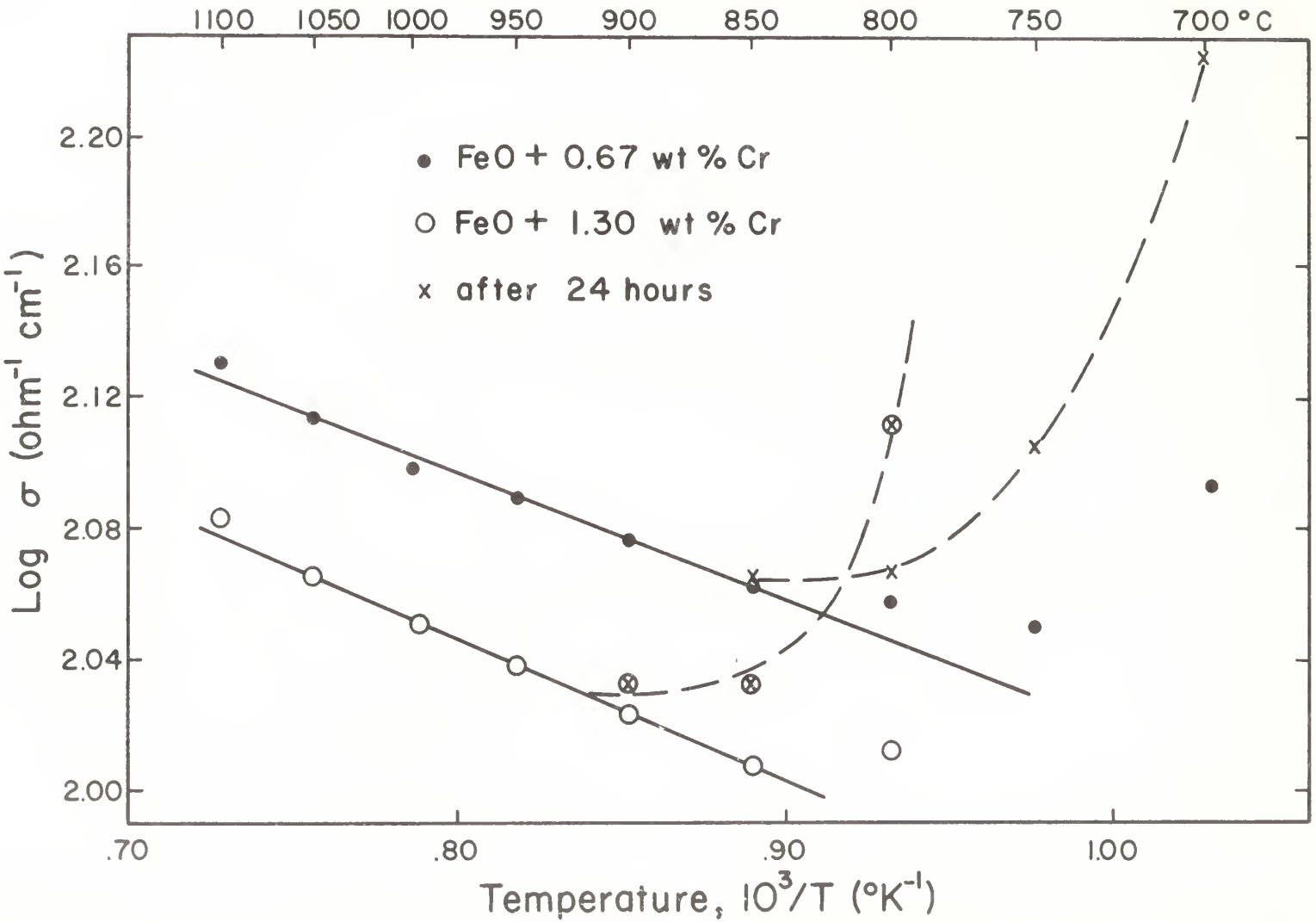

Figure 42. Temperature dependence of the electrical conductivity of doped wüstite of constant composition, oxygen/metal = 1.060. The formation of precipitated iron-chromium spinel after 24 hours causes the deviation.

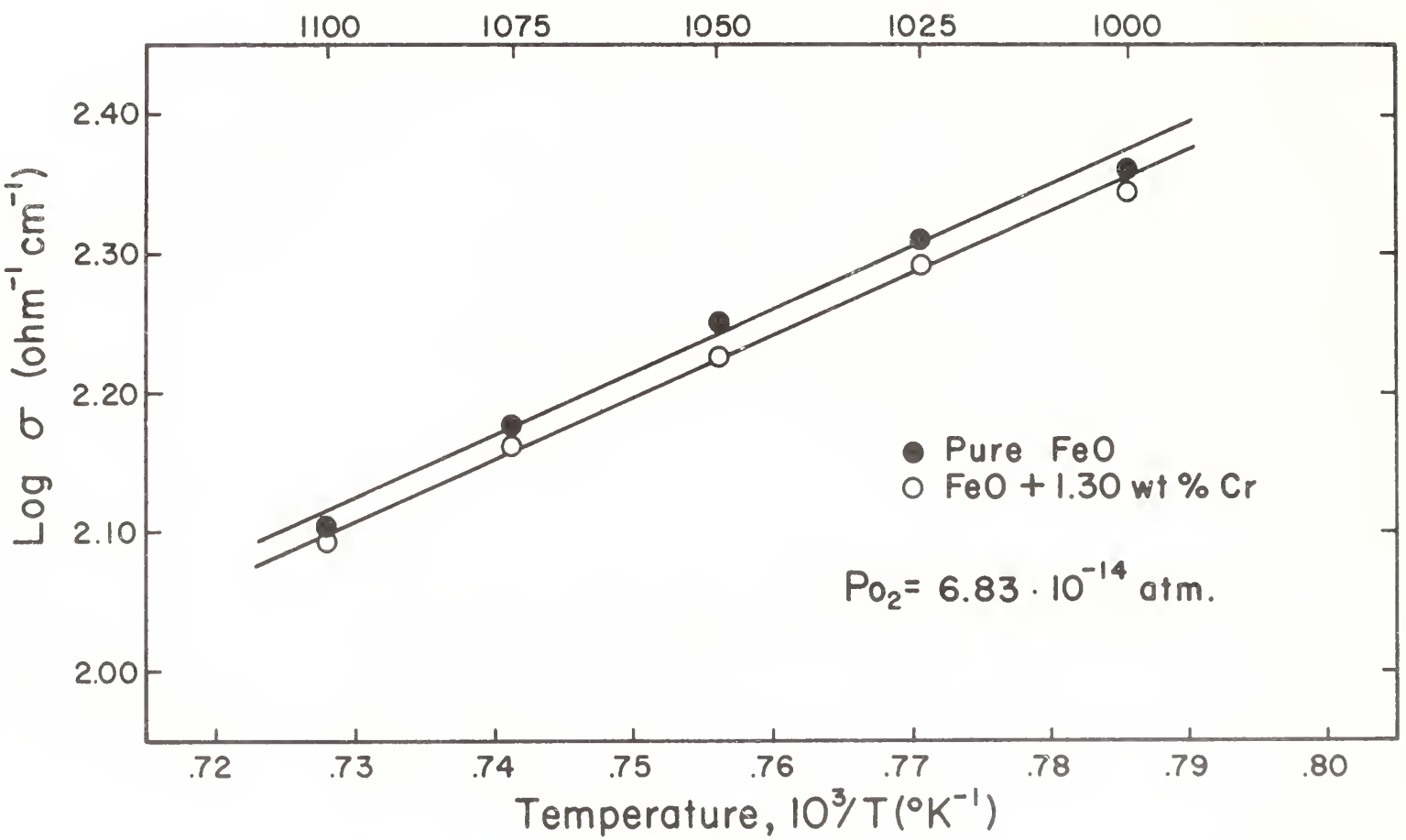

Figure 43. Temperature dependence of the electrical conductivity of pure and doped wüstite at constant oxygen pressure.

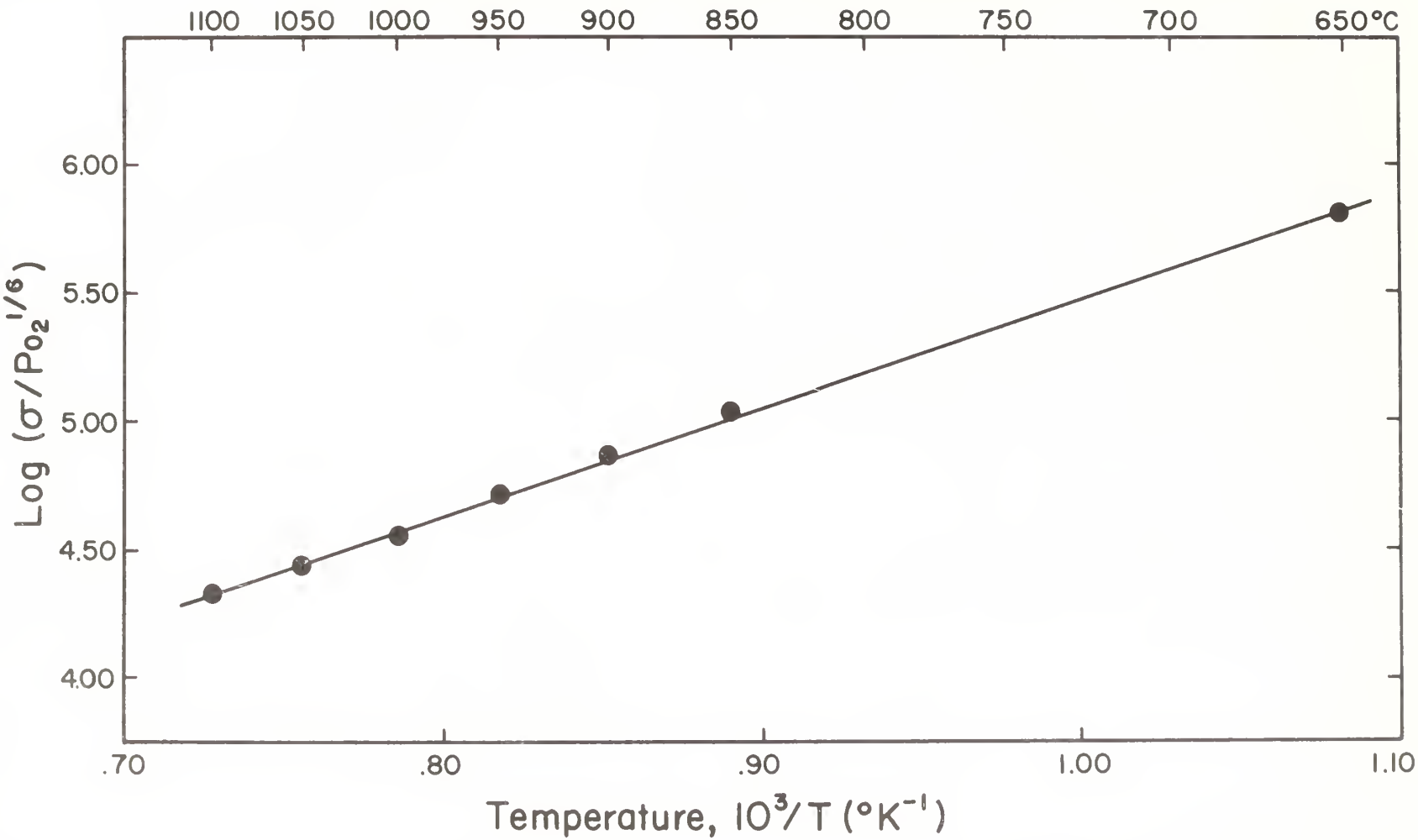

Figure 44. Temperature dependence of $(\sigma/p_{O_2}^{1/6})$ for the electrical conductivity of pure wüstite in a constant CO_2-CO mixture where $N_{CO_2} = 0.467$.

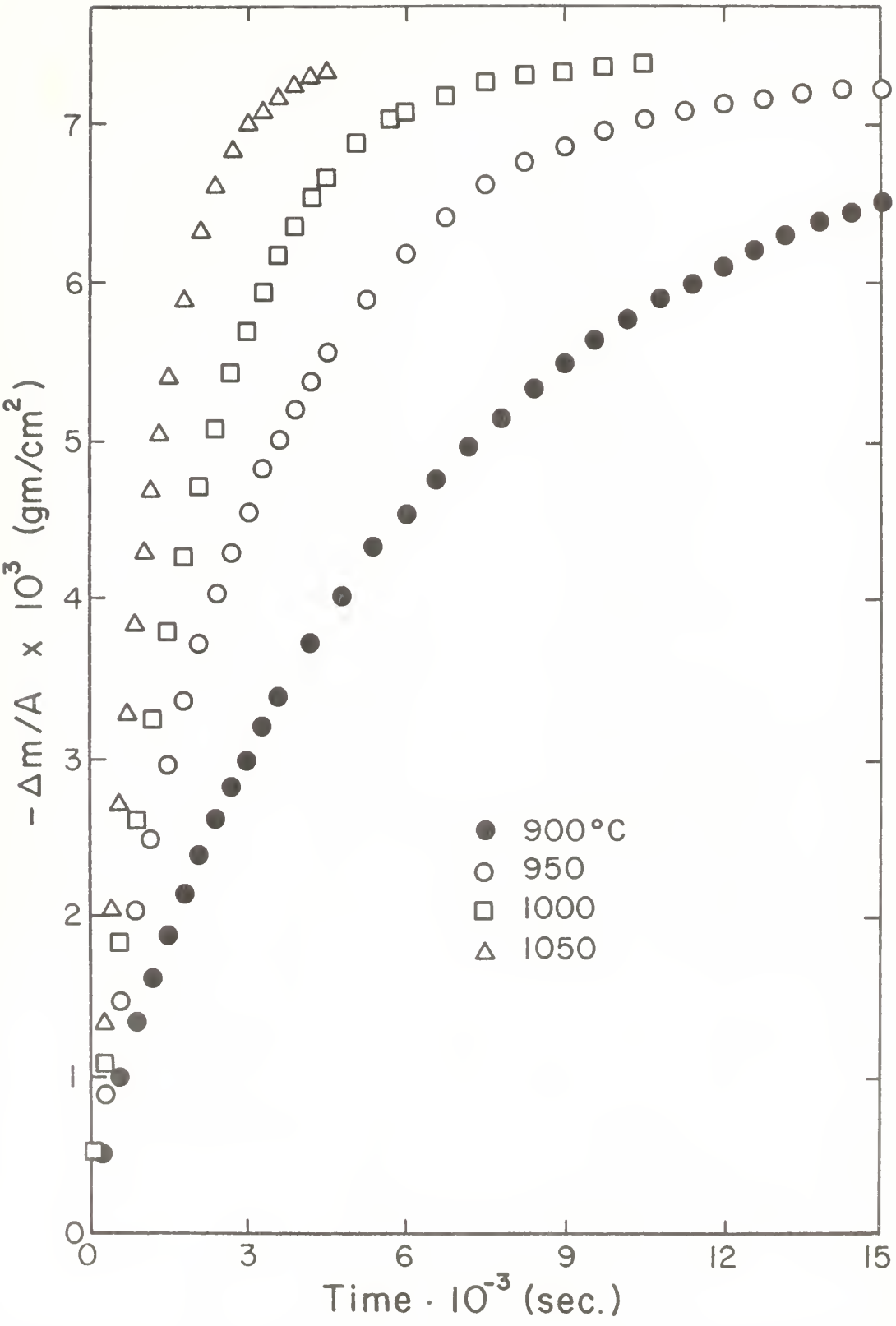

Figure 45. Typical rate curves for the reduction of pure wüstite from O/Fe = 1.125 to 1.050.

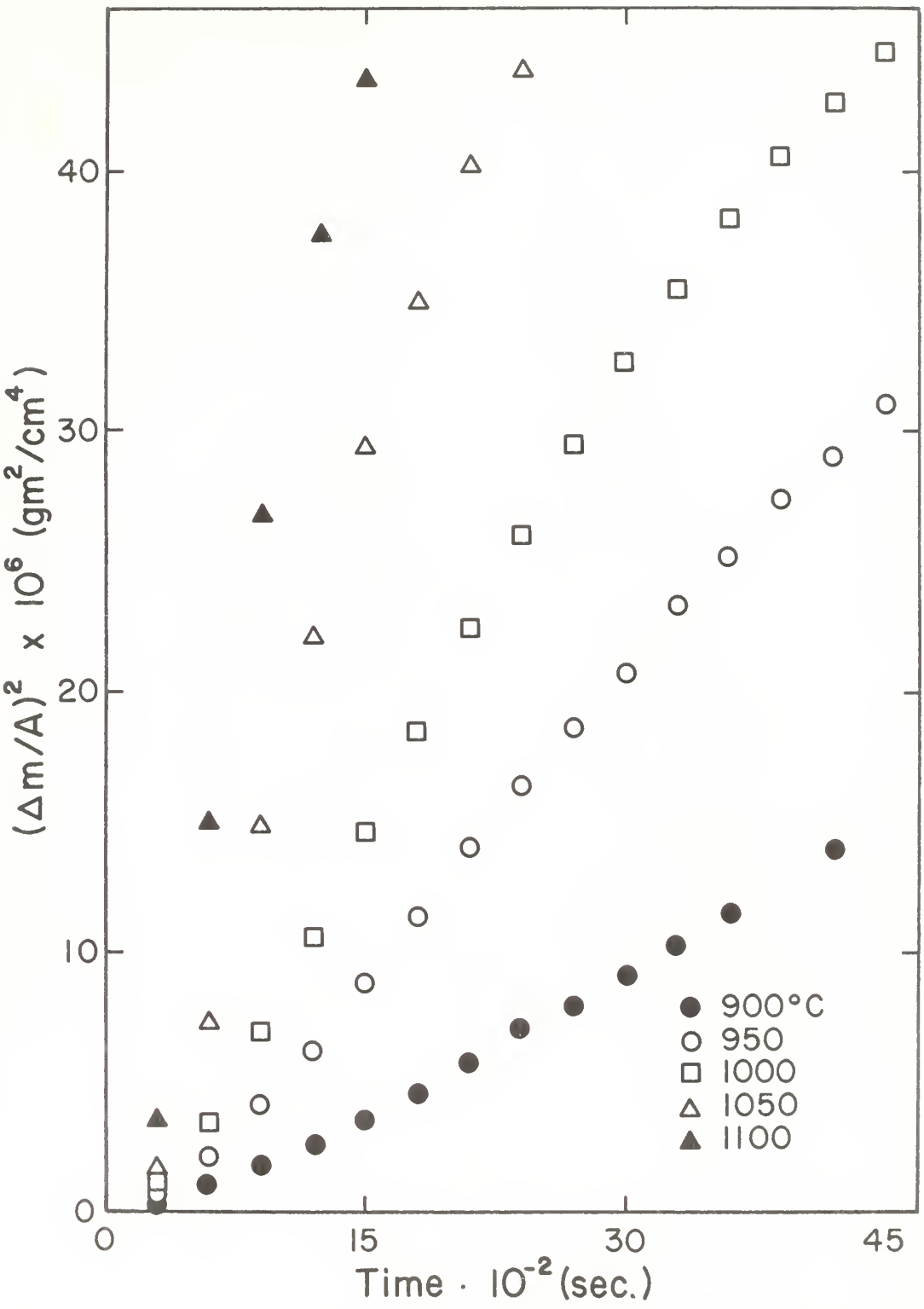

Figure 46. Parabolic rate curves for the reduction of pure wüstite from O/Fe = 1.125 to 1.050.

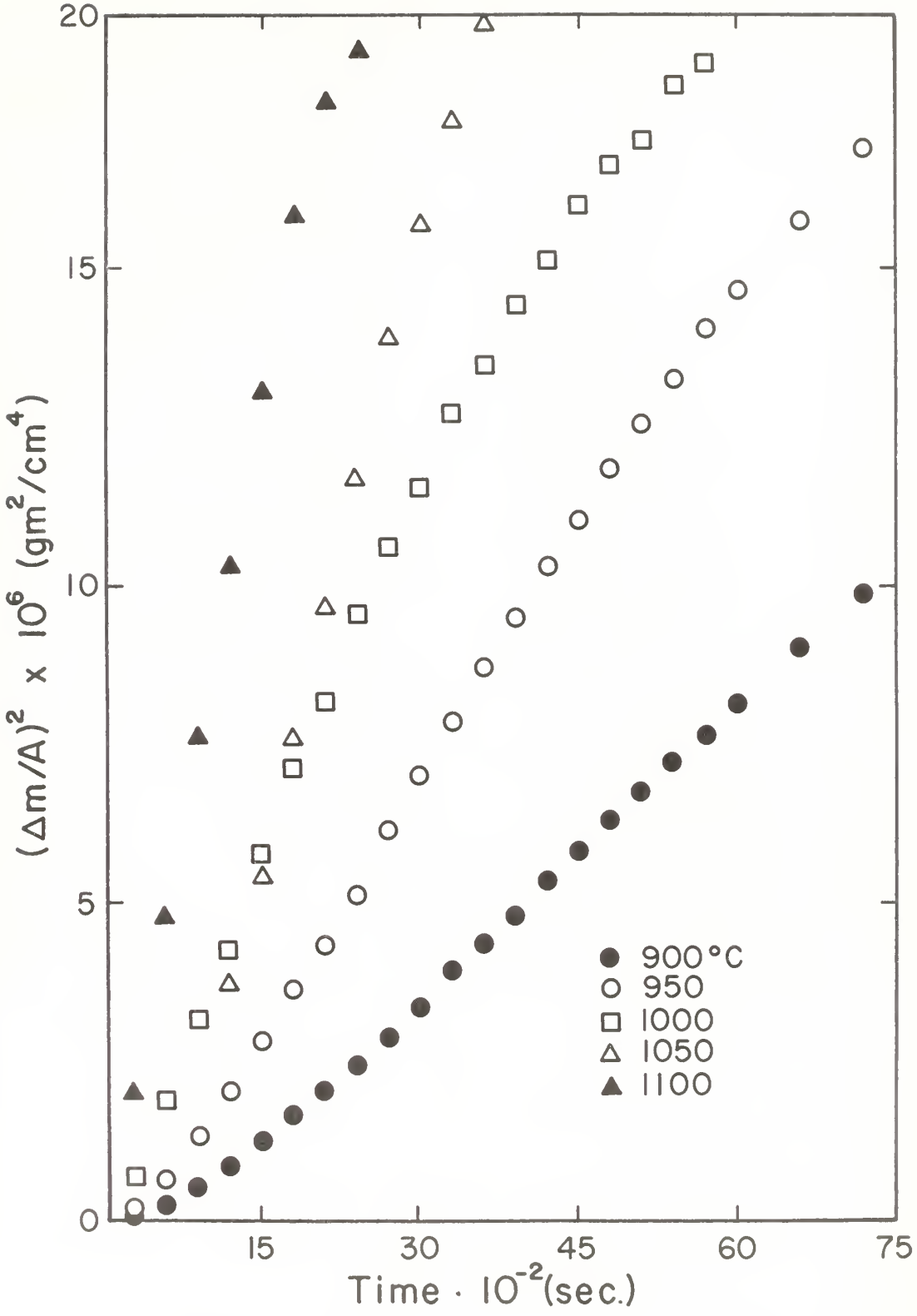

Figure 47. Parabolic rate curves for the reduction of pure wüstite from O/Fe = 1.125 to 1.075.

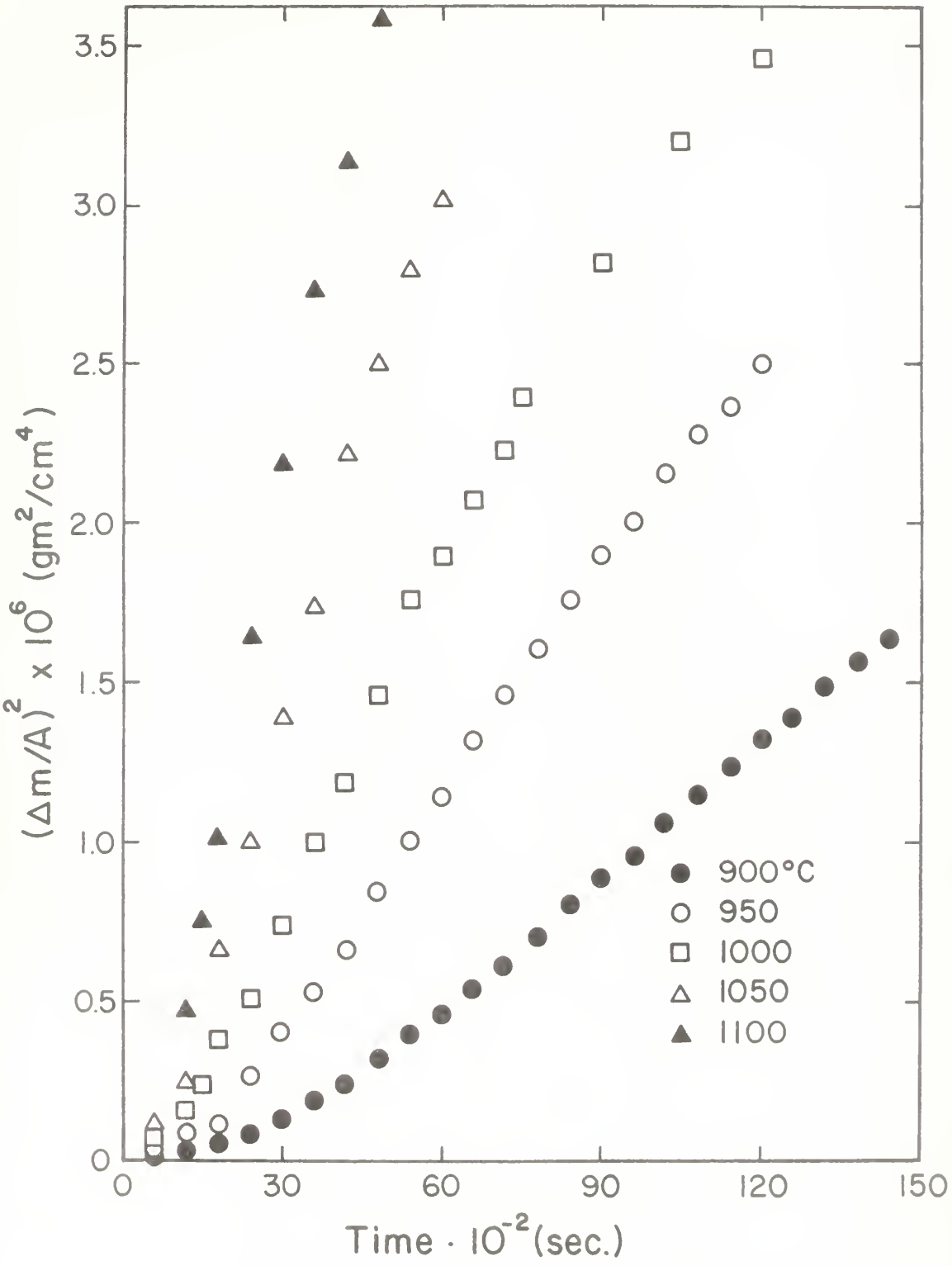

Figure 48. Parabolic rate curves for the reduction of pure wüstite from O/Fe = 1.125 to 1.100.

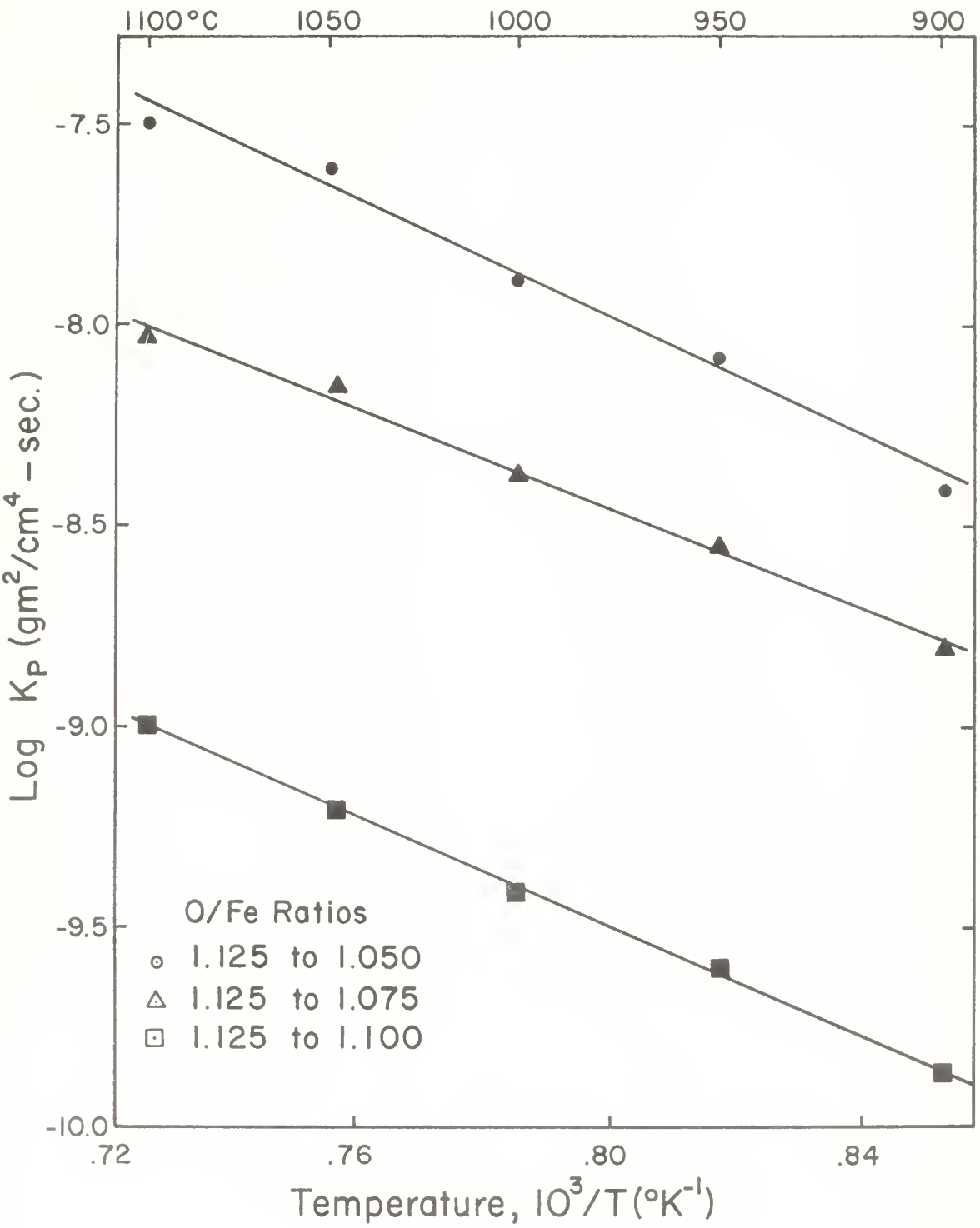

Figure 49. Temperature dependence of the parabolic rate constants of reduction of pure wüstite.

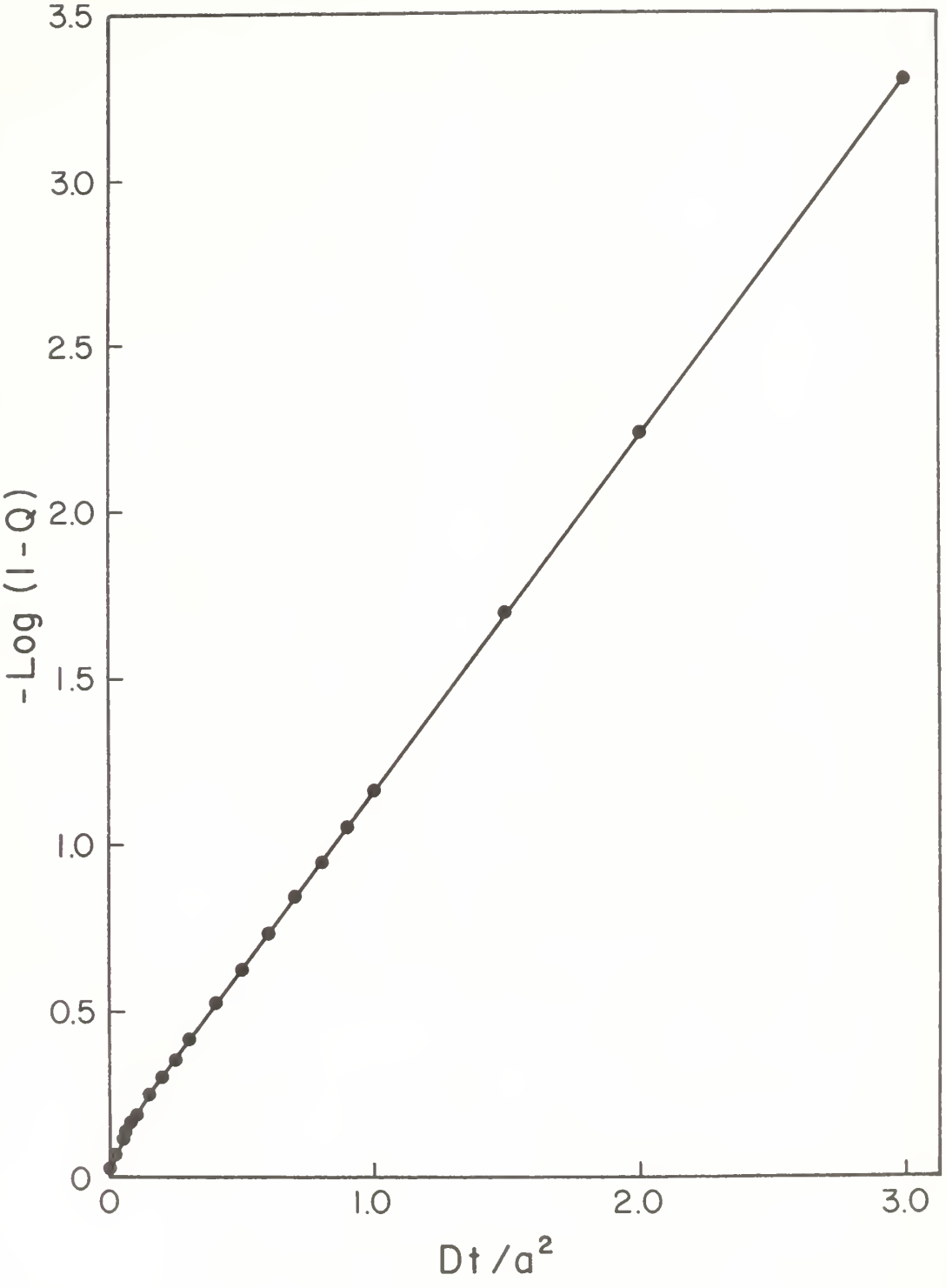

Figure 50. Theoretical curve of Equation (46) for the propagation of a concentration gradient through a wüstite slab when a diffusion process is rate-controlling.

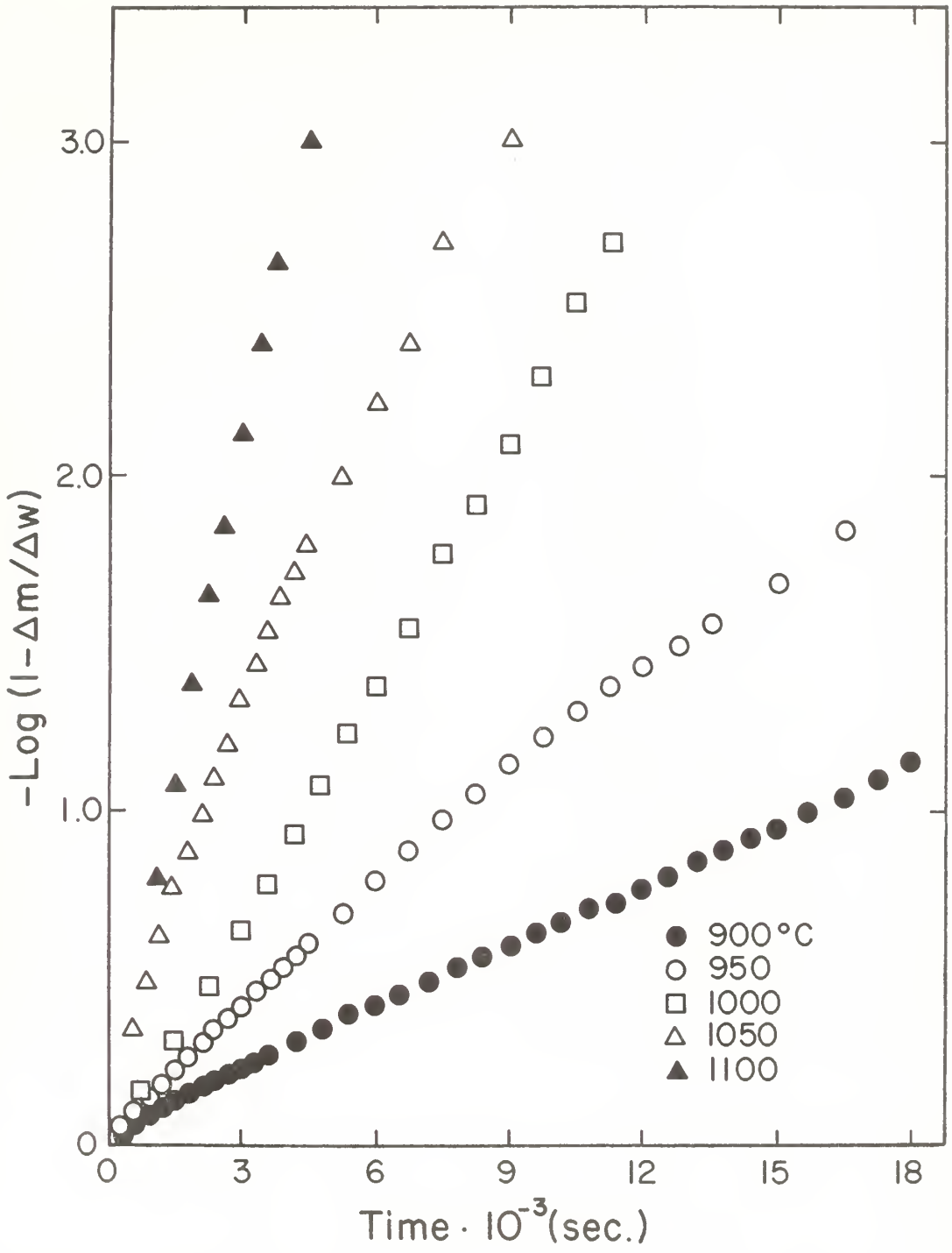

Figure 51. Experimental curve of Equation (46) for the reduction of a pure wüstite slab from O/Fe = 1.125 to 1.050 when a diffusion process is rate-controlling.

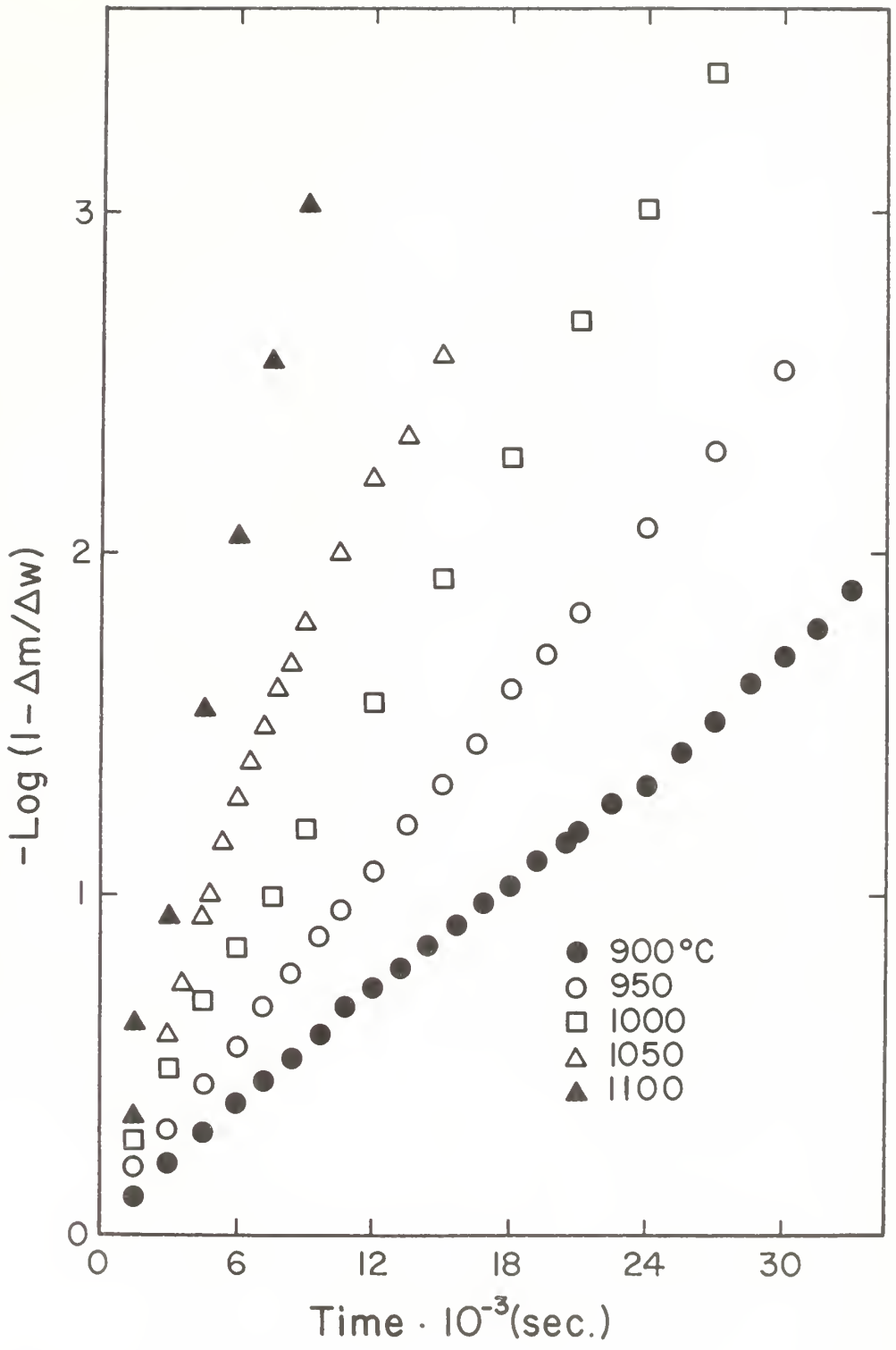

Figure 52. Experiment curve of Equation (46) for the reduction of a pure wüstite slab from O/Fe = 1.125 to 1.075 when a diffusion process is rate-controlling.

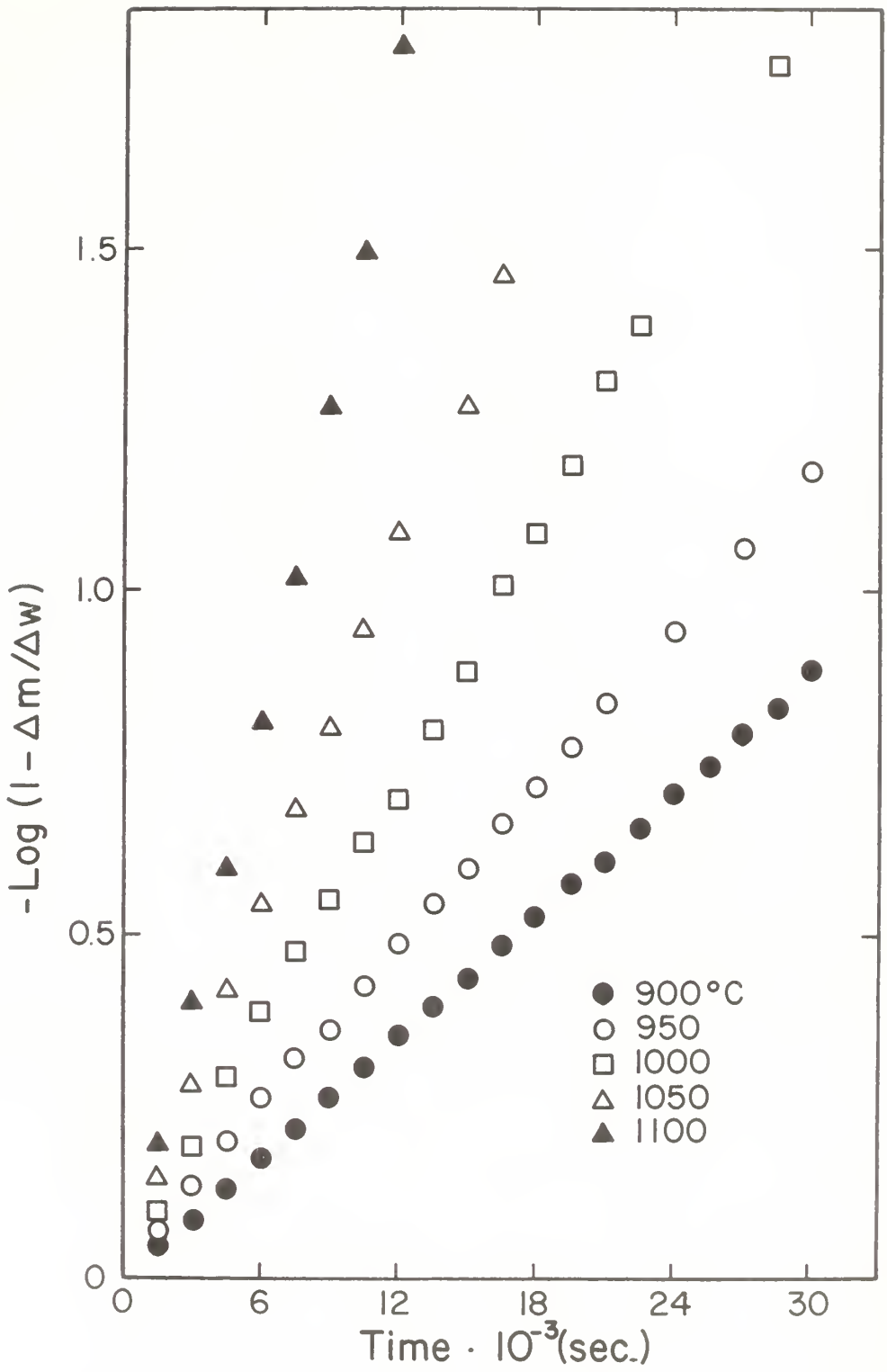

Figure 53. Experimental curve of Equation (46) for the reduction of a pure wüstite slab from O/Fe = 1.125 to 1.100 when a diffusion process is rate-controlling.

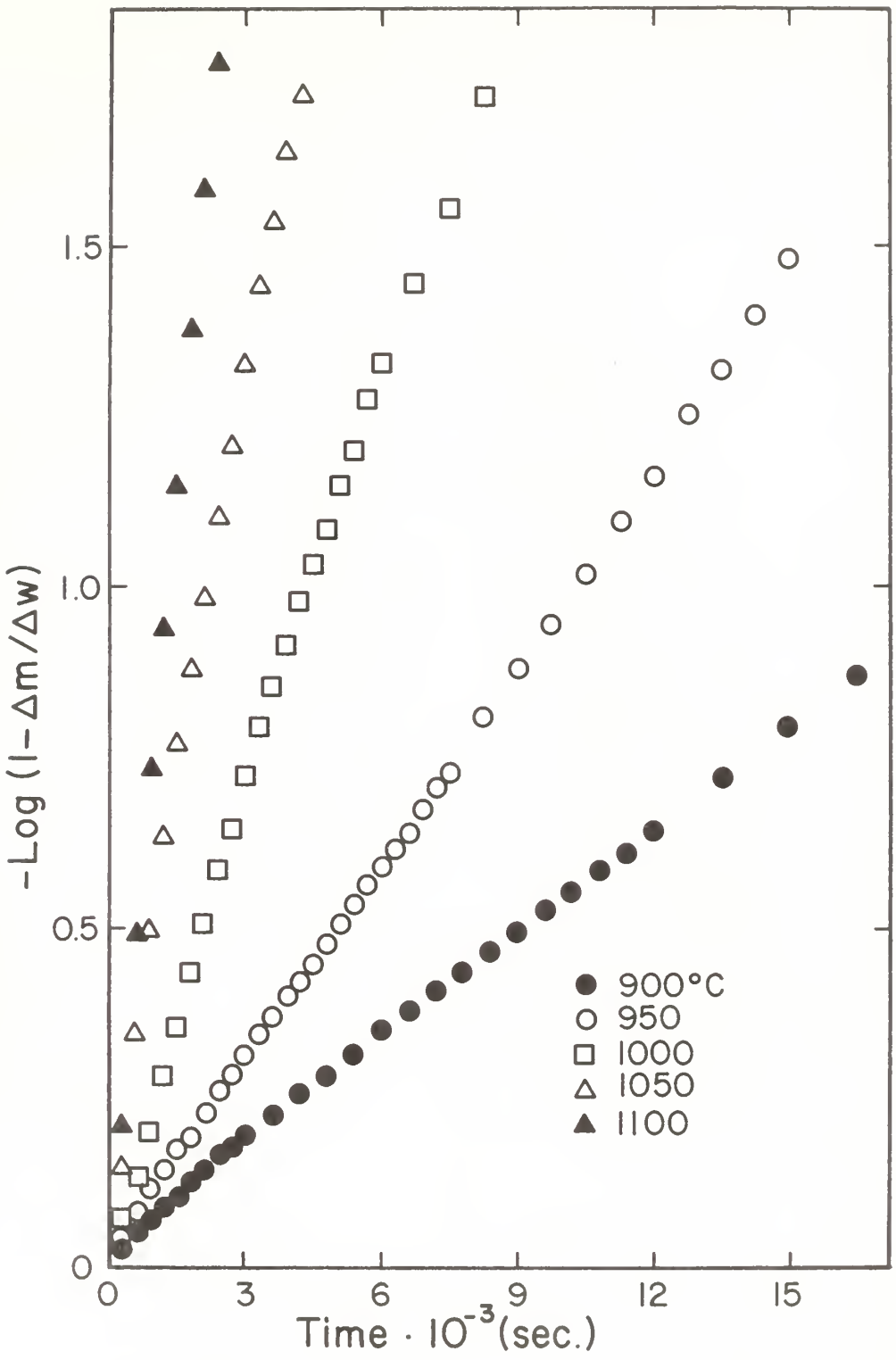

Figure 54. Experimental curve of Equation (46) for the oxidation of a pure wüstite slab from O/Fe = 1.050 to 1.125 when a diffusion process is rate-controlling.

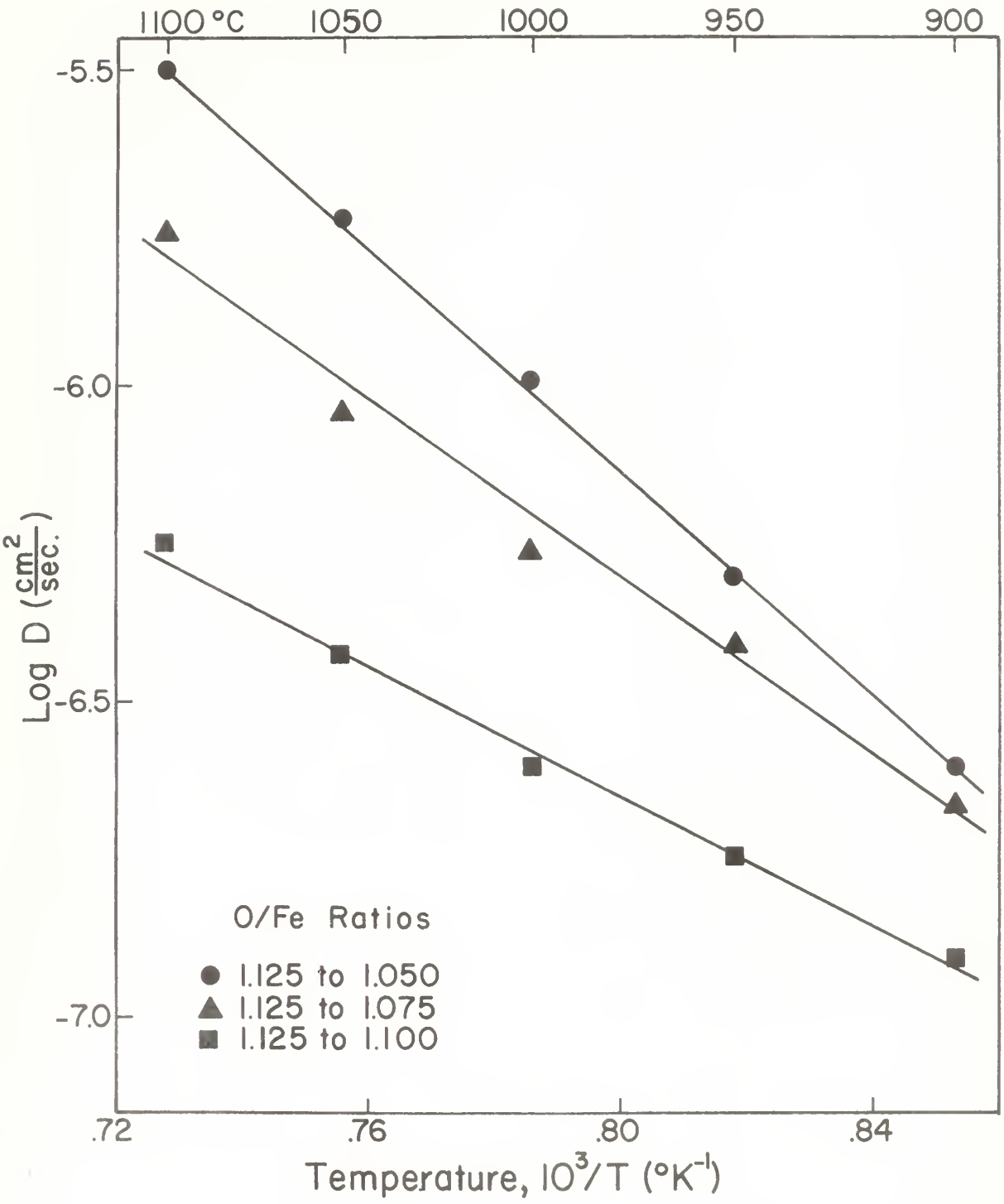

Figure 55. Temperature dependence of the chemical diffusion coefficients calculated from Equation (46) for the reduction of a pure wüstite slab.

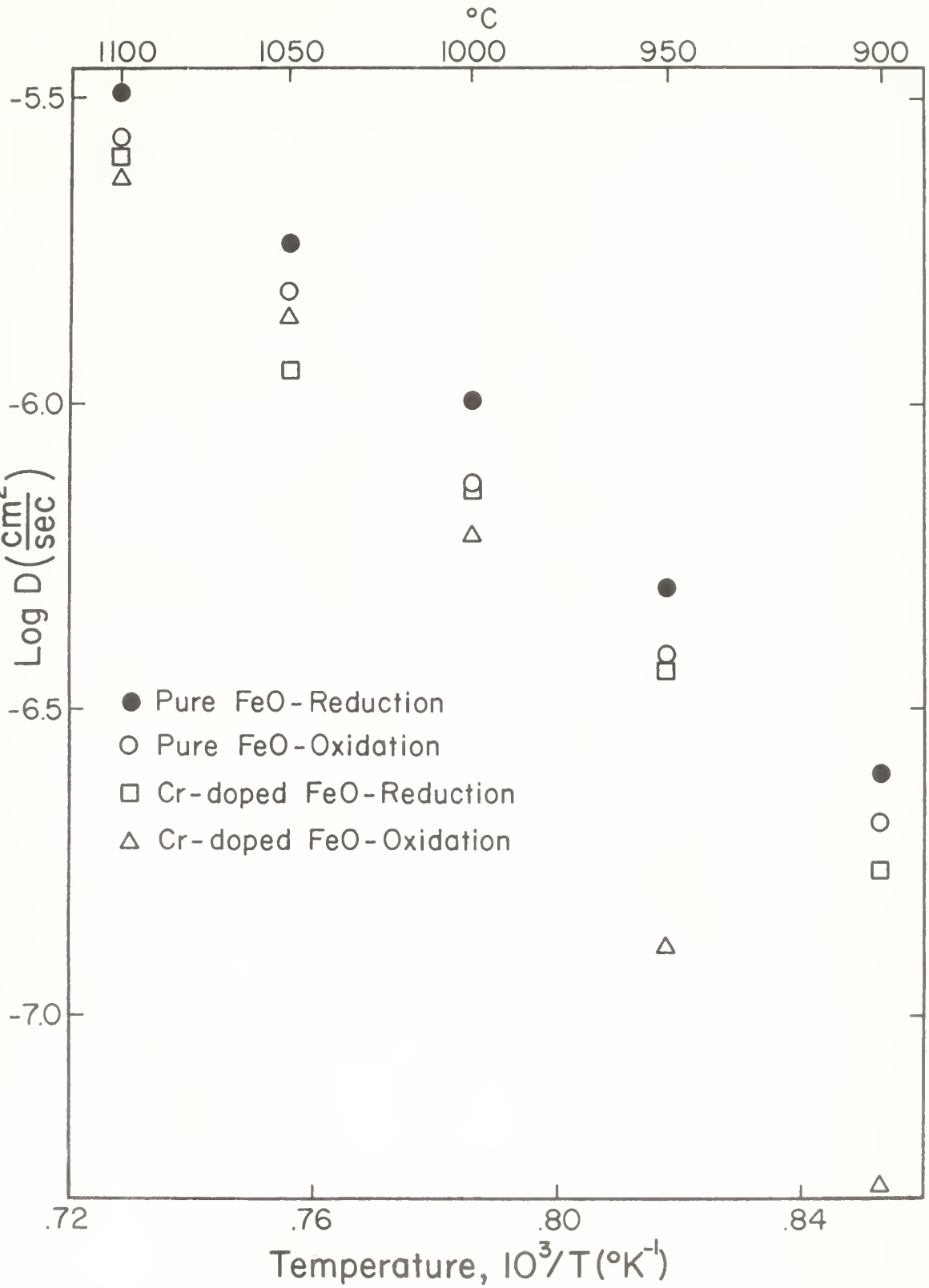

Figure 56. Temperature dependence of the chemical diffusion coefficients obtained from reduction and oxidation experiments of pure and doped wüstite between the oxygen/metal ratios of 1.050 and 1.125.

VITA

Name:	ROGER LEE LEVIN
Place of Birth:	Clearfield, Pennsylvania
Date of Birth:	March 21, 1936
Education:	The Pennsylvania State University B. S. in Metallurgy, 1958 Yale University M. Eng., 1961
Positions:	Lieutenant, United States Navy U. S. Navy Advanced Scientific Program Scholar 1959-1963
Publication:	"The Role of a Displacement Reaction in the Kinetics of Oxidation of Alloys," Roger L. Levin and J. Bruce Wagner, Jr., J. Electrochem. Soc., 108, 954 (1961).

thesL56
Kinetics of oxidation of iron-chromium a
3 2768 002 11859 8
DUDLEY KNOX LIBRARY